# Self-consistent modeling of plasma response to impurity spreading from intense localized source

Inauguraldissertation

zur Erlangung des Doktorgrades
der Mathematisch-Naturwissenschaftlichen Fakultät
der Heinrich-Heine-Universität Düsseldorf

vorgelegt von

**Mikhail Koltunov**

aus Moskau

Doktorvater und Betreuer: Prof. Dr. M. Z. Tokar

Forschungszentrum Jülich
July 2012

aus dem Institut für Energie und Klimaforschung – Plasmaphysik,
Forschungszentrum Jülich GmbH
52425, Jülich, Deutschland
E-Mail: m.koltunov@fz-juelich.de
Telefon: +49 02461 61 5387

für die Heinrich-Heine-Universität Düsseldorf

Gedruckt mit der Genehmigung der
Mathematisch-Naturwissenschaftlichen Fakultät der
Heinrich-Heine-Universität Düsseldorf

Referenten:

Prof. Dr. M. Tokar

Prof. Dr. A. Pukhov

Tag der mündlichen Prüfung:

# Kurzfassung

In heutigen Kernfusionsanlagen sind Verunreinigungen in heißen Wasserstoff-Plasmen unvermeidlich. Sie treten infolge immanenter Prozesse, wie der Wechselwirkung des Plasmas mit Gefäßwänden oder auch durch gezieltes Einblasen, auf. Üblicherweise werden Verunreinigungsteilchen beim Einblasen räumlich stark lokalisiert in das Plasma eingebracht, so dass eine signifikante Veränderung lokaler Plasmaparameter zu erwarten ist, die ihrerseits wiederum Auswirkungen auf die Verteilung der Verunreinigungen hat. Eine selbstkonsistente Modellierung der Wechselwirkung zwischen Verunreinigungen und Plasma ist deshalb nicht mit linearen Ansätzen möglich. In dieser Arbeit wird ein Modell entwickelt, das auf einer Flüssigkeitsbeschreibung der Elektronen, Wasserstoff- und Verunreinigungskomponenten basiert. Dieses Modell beschreibt den Transport der Verunreinigungen und deren Wirkung auf das Hauptplasma unter Berücksichtigung der Quasineutralität des gesamten Plasmas, der Coulomb-Stöße geladener Teilchen untereinander, der Strahlungsverluste und der Plasma-Wand-Wechselwirkung an den angrenzenden Oberflächen. Um den Effekt der Ausbreitung von Verunreinigungen und die Reaktion des Plasmas selbstkonsistent zu beschreiben, werden die Erhaltungsgleichungen der Fluid-Theorie für Teilchen, Impuls und Energie von allen beteiligten Plasmakomponenten gelöst. Die Erhaltungsgleichungen werden zu gewöhnlichen Differentialgleichungen für die zeitliche Entwicklung der Parameter reduziert, welche charakteristisch für die eigentliche Lösung sind: die Größen der Plasmadichte und Plasmatemperaturen in den Bereichen, in denen die Verunreinigungen lokalisiert sind, sowie die räumliche Ausdehnung dieser Bereiche. Die Ergebnisse aus Simulationsrechnungen mit typischen Bedingungen in Tokamak-Experimenten zur Verunreinigungsinjektion werden dargestellt und diskutiert. Ein neuer Mechanismus für das Phänomen der Kondensation und der Bildung von kalten dichten Strukturen im Plasma wird vorgeschlagen.

# Abstract

Non-hydrogen impurities unavoidably exist in hot plasmas of present fusion devices. They enter it intrinsically, due to plasma interaction with the wall of vacuum vessel, as well as are seeded for various purposes deliberately. Normally, the spots where injected particles enter the plasma are much smaller than its total surface. Under such conditions one has to expect a significant modification of local plasma parameters through various physical mechanisms, which, in turn, affect the impurity spreading. Self-consistent modeling of interaction between impurity and plasma is, therefore, not possible with linear approaches. A model based on the fluid description of electrons, main and impurity ions, and taking into account the plasma quasi-neutrality, Coulomb collisions of background and impurity charged particles, radiation losses, particle transport to bounding surfaces, is elaborated in this work. To describe the impurity spreading and the plasma response self-consistently, fluid equations for the particle, momentum and energy balances of various plasma components are solved by reducing them to ordinary differential equations for the time evolution of several parameters characterizing the solution in principal details: the magnitudes of plasma density and plasma temperatures in the regions of impurity localization and the spatial scales of these regions. The results of calculations for plasma conditions typical in tokamak experiments with impurity injection are presented. A new mechanism for the condensation phenomenon and formation of cold dense plasma structures is proposed.

# Contents


**1 Introduction** **1**

1.1 Nuclear fusion – a key for growing energy consumption demands of mankind . . . 1

1.2 Impurities in fusion devices and their impacts on plasmas . . . 3

1.2.1 Sources of impurities in tokamaks . . . 3

1.2.2 Radiation of impurities . . . 4

1.2.3 Accumulation of heavy impurities . . . 5

1.2.4 Behavior of light impurities . . . 7

1.2.5 Deliberate seeding of impurities . . . 8

1.2.6 Disruption mitigation . . . 8

1.2.7 Reactor fueling . . . 9

1.2.8 Summary of impurity impacts on fusion plasmas . . . 10

1.3 State of arts in modeling of impurity seeded plasmas . . . 10

1.3.1 Spatial and temporal requirements to models . . . 10

1.3.2 A brief survey of theoretical models and numerical codes describing interaction between impurity and plasma . . . 12

1.4 Motivation and outline of this work . . . 14

**2 Basic equations** **19**

2.1 Neutral transport . . . 20

2.2 Plasma quasi-neutrality . . . 20

2.3 Charged impurity transport . . . 20

2.4 Transport equations for main plasma components . . . 22

**3 Stationary modeling of impurity spreading and impacts on plasma of scrape-off layer and edge regions** **25**

3.1 Model . . . 26

3.1.1 Impurity neutral density . . . 26

3.1.2 Charged particle densities . . . 27

3.1.3 Heat transport . . . 28

3.1.4 Integrated particle and momentum balances . . . . . 29
3.1.5 Integrated heat balances . . . . . 32
3.2 Results of calculations and discussion . . . . . 34
3.2.1 Modification of plasma parameters with injection intensity . . . . . 35
3.2.2 Radial penetration of impurity into the plasma . . . . 37
3.2.3 Radiation energy losses from impurity cloud . . . . . 40
3.2.4 Model validation and sensitivity to input parameters . 42
3.3 Conclusions . . . . . 43

**4 Time-dependent modeling of impurity spread in hot plasma 45**
4.1 Model . . . . . 45
4.1.1 Impurity neutral transport . . . . . 45
4.1.2 Charged impurity transport in shell approximation . . 46
4.2 Numerical approach for solving of partial differential equation systems with interlaced variables . . . . . 48
4.3 Results of calculations and discussion . . . . . 50
4.3.1 Spreading of impurity ions on magnetic surfaces . . . . 50
4.3.2 Stationary characteristics of impurity ions . . . . . 54
4.3.3 Role of impurity transport in the radial direction . . . 59
4.4 Conditions for applicability of unperturbed temperature approximation . . . . . 60
4.5 Conclusions . . . . . 61

**5 The impact of plasma cooling on impurity spreading 65**
5.1 Model . . . . . 65
5.1.1 Heat transfer in main plasma components . . . . . 65
5.1.2 Integrated heat balance . . . . . 66
5.2 Results of calculations and discussion . . . . . 69
5.2.1 The impact of plasma cooling on impurity spreading . 69
5.2.2 Unstationary neutral injection . . . . . 71
5.2.3 Effect of radial transport on local plasma cooling by impurity spreading . . . . . 71
5.3 Conclusions . . . . . 74

**6 A new look on formation of cold dense structures in plasmas 75**
6.1 Model . . . . . 76
6.2 Approach to numerical solution of partial differential equation systems using “generalized” variables . . . . . 76
6.3 Results of calculations and discussion . . . . . 80

6.3.1 The roles of different mechanisms in impurity impact on plasma . . . . . 80
6.3.2 A new look on formation of cold dense structures . . . 82
6.3.3 Criterion for formation of cold dense structures . . . . 85
6.4 Conclusions . . . . . 86

**7 Summary & Outlook** **89**
7.1 Main results of this work . . . . . 89
7.2 Future developments . . . . . 91

**A Appendix** **93**
A.1 Condition of zero parallel current . . . . . 93
A.2 Calculation of the heat flux into the cloud . . . . . 93
A.3 Reduction of time-dependent model to stationary case . . . . . 95

**Bibliography** **97**

**List of publications 2009-2012** **109**

# Chapter 1

# Introduction

## 1.1 Nuclear fusion – a key for growing energy consumption demands of mankind

The growing energy demands of mankind, limited supply of fossil fuels and connected issues of pollution and climate change [1, 2] are forcing the turnarounds towards economic, sustainable and clean energy production conceptions. The number of conceivable non-fossil candidates is very limited: nuclear fission, nuclear fusion and renewables.

Natural obstacles of renewables, namely, low energy density and fluctuations in time, require energy storage that leads to the extra costs. Thus, for year-averaged natural conditions of the Middle Europe produced power per area used by the plant and supplies of wind turbines is not higher $0.001\,GW/km^2$, and for photovoltaic panels it is around $0.02\,GW/km^2$. Redistribution of peak power from off-shore electric plant to habited regions requires advanced electric network e.g. using superconducting electricity pipelines [3,4]. Another option is given by nuclear energy: fission and fusion. Fission is rather compact, power density is $0.8 - 1.0\,GW/km^2$, but highly radioactive waste is produced: $32\,tons$ of wastes per $GW$ produced energy per year. They have to be stored in a safe way or transmuted to short-living isotopes or reprocessed for reuse in reactors of new generation [5]. Also, unforeseen consequences of environmental and human impacts still represent a serious danger [6, 7].

Fusion power is one of the most ambitious and promising scientific projects of our times aiming to provide one of the most reliably available future energy sources. In nuclear fusion the binding energy of nucleons releases as kinetic energy of the reaction products. Altogether more than 80 different fusion reactions are currently known. The least difficult one to ini-

tiate on the Earth is between heavy hydrogen isotopes deuterium (${}^2_1D$) and tritium (${}^3_1T$):

$$ {}^2_1D \;+\; {}^3_1T \;\longrightarrow\; {}^4_2He\,(3.5\,MeV) \;+\; {}^1_0n\,(14.1\,MeV) $$

with production of helium (${}^4_2He$) nucleus with the energy $E_\alpha = 3.5\,MeV$ and fast neutron (${}^1_0n$). It possess of the maximum reaction rate, $R = n_D n_T \langle\sigma v\rangle$, at the temperature of the reacting components $\approx 10\,keV$. Here $n_D$ and $n_T$ denote the densities of the reacting components and $\langle\sigma v\rangle$ is the reaction cross-section averaged over Maxwell distribution of particle velocities.

Sideline interactions of D-T reaction components and products, given by

$$ \begin{aligned} {}^2_1D \;+\; {}^2_1D \;&\longrightarrow\; {}^3_2He\,(0.82\,MeV) \;+\; {}^1_0n\,(2.45\,MeV) \quad (50\%) \\ &\longrightarrow\; {}^3_1T\,(1.01\,MeV) \;+\; {}^1_1p\,(3.02\,MeV) \quad (50\%) \\ {}^2_1D \;+\; {}^3_1He \;&\longrightarrow\; {}^4_2He\,(3.6\,MeV) \;+\; {}^1_0n\,(14.7\,MeV) \end{aligned} $$

with production of light isotope of helium (${}^3_2He$) and proton (${}^1_1p$) are also exothermic, but posses of orders of magnitude lower reactivity, see e.g. [8]. Summarizing all the reactions above one gets:

$$ 6\,{}^2_1D \;\longrightarrow\; 2\,{}^4_2He \;+\; 2\,{}^1_1p \;+\; 2\,{}^1_0n \;+\; 43.3MeV $$

For comparison, reaction of chemical burning of coal releases $3.6 - 4.1\,eV$.

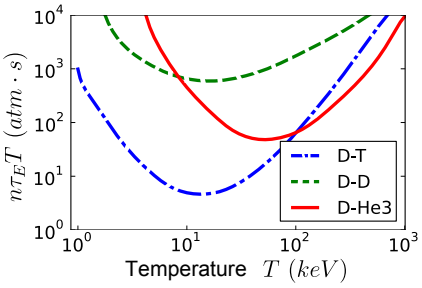


Figure 1.1: Triple product [5].

Achieving a positive energy release, i.e. obtaining more energy from fusion reactions than it is spent to maintain the hot plasma, is called break-even. The conditions are reached at the point where the plasma temperature can be maintained against the energy losses, $P_E = 3nT/\tau_E$, solely by $\alpha$-particles heating $P_\alpha = n^2\langle\sigma v\rangle E_\alpha/4$. By equating these two channels one gets the triple product of plasma density $n$, temperature $T$ and confinement time $\tau_E$ as a function of $T$. This function has a minimum $n\tau_E T = 3 \cdot 10^{21}\, m^{-3} keV s$ at $T \approx 15\,keV$ for D-T reaction, see Fig. (1.1) [5, 9].

The toroidal devices with magnetic confinement of the plasma, called tokamaks [10], are leading the competition of attaining the controlled fusion, see schematic representation in Fig. (1.2) [11]. The conditions providing the triple product necessary for the break-even have been achieved already on three tokamak machines: JET (Europe), JT-60 (Japan) and TFTR (USA) [12], ch.1-2.

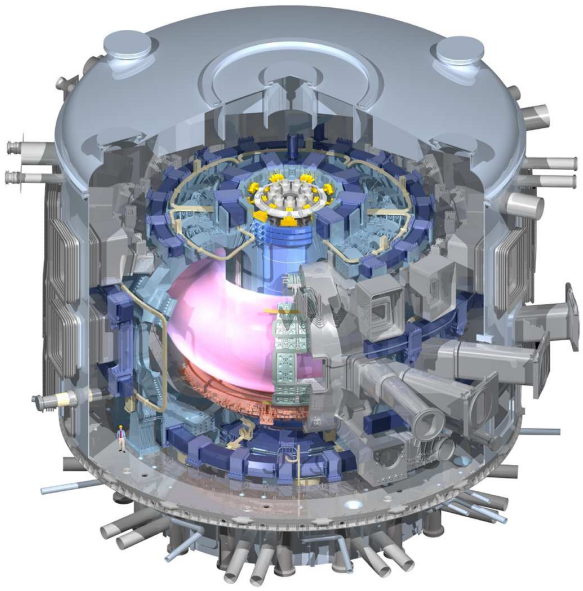

Figure 1.2: Schematic representation of the tokamak ITER [11].

The next step towards the realization of fusion power as a new primary energy source is the international tokamak ITER aimed to produce an output of $0.5\,GW$ to 2033. ITER is projected to consume $0.1\,ton$ of deuterium and $0.15\,ton$ tritium per year. To reach this ambitious goal several smaller facilities have been working towards the development of a viable scenario for ITER from physical and engineering perspectives [13]. In experiments on the JET tokamak it was possible to produce $16\,MW$ of fusion power during deuterium-tritium campaign of 1997 [14, 15].

## 1.2 Impurities in fusion devices and their impacts on plasmas

### 1.2.1 Sources of impurities in tokamaks

Impurities, i.e. molecules, atoms and ions of materials besides reacting isotopes of hydrogen and "helium ash", unavoidably present in plasmas of fusion devices. They can enter it intrinsically, due to plasma interaction with the wall of vacuum vessel, e.g. by thermal, particle or photon-induced desorption, chemical reactions, evaporation of atoms of solid surfaces, physical and chemical sputtering, arcing and blistering. In these processes both atoms of the underlying material itself (carbon, iron, tungsten, etc.) and atoms bound to their surfaces (oxygen, nitrogen, etc.) are released. With

increasing power input into fusion machines the problem of accidental uncontrollable income of impurity into the plasma has become actual. Under some conditions, in particular, when intensive heat flows hit certain wall elements, a huge amount of impurity particles can be released very locally due to melting, evaporation or even ablation of the wall material [16, 17]. In this case, impact of impurity on the plasma can be very local, but rather strong. Alternatively, certain impurities are introduced for various aims in the plasma externally by means of tiny ($2-70\,mm^3$) frozen pellets thrown into the vessel or injection of neutral gas through small outlets in vessel elements.

### 1.2.2 Radiation of impurities

The presence of impurities in plasma results in energy losses through cyclotron radiation, radiative and dielectronic recombination, line radiation and bremsstrahlung. The plasma is optically thick to cyclotron radiation at the fundamental frequency and lower harmonics of the cyclotron frequency, and radiation intensity of higher harmonics falls rapidly with increasing harmonic number, thus the plasma behaves like a black body radiating according to the Rayleigh-Jeans law. One can neglect this energy loss channel. The significant channels are bremsstrahlung and radiation which occurs through elementary processes of line excitation and recombination of strongly charged impurity ions.

The radiated power density is proportional to the electron density $n_e$ and to impurity density $n_Z$ and can be written as

$$P_{rad} = n_e n_Z L_Z \tag{1.1}$$

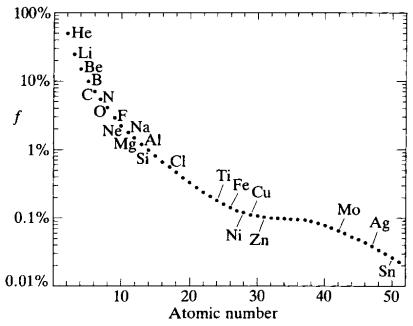


Figure 1.3: Fractional impurity level which produces a radiation power equal to 10% of the total thermonuclear power [12].

In a steady state with negligible transport effects the radiation parameter $L_Z$ is the function of the electron temperature $T_e$ and impurity element number $Z$ only. One has to specify here that impurities with low $Z$, such as lithium or beryllium, become completely ionized at temperatures of $1\,keV$ and no longer produce line radiation [18, 19], whereas high $Z$ elements, such as molybdenum or tungsten, still retain their lower orbital electrons even in regions of temperatures of $10\,keV$ as supposed to be in the core of ITER device. Bremsstrahlung radiation power rises with

increasing of charge number as $Z^2$. For sustainability of nuclear fusion, radiation power losses should be much less than produced nuclear power

$$P_{fus} = n_D n_T \langle \sigma v \rangle E_{fus} \tag{1.2}$$

where $E_{fus} = 17.6\, MeV$ is the energy released in thermonuclear reaction and $\langle \sigma v \rangle$ is the fusion cross-section averaged over Maxwellian distribution. For various elements Fig. (1.3) represents the fractional impurity level, $n_Z/n_e$, which would produce a radiated power fraction $P_{rad}/P_{fus} = 0.1$ at $T_i = T_e = 10\, keV$, see [12], ch. 4.

### 1.2.3 Accumulation of heavy impurities

The destruction of material surfaces surrounding the plasma by the impact of energetic charged particles and uncontrollable penetration of impurities produced by plasma-wall interaction into the plasma core was a subject of many concerns from the very beginning of nuclear fusion research. On the one hand, wall elements fabricated of high Z materials, such as molybdenum, tungsten and stainless steel, possess outstanding thermodynamic and mechanical properties, as well as the low level of erosion, neutron activation, and tritium retention [20]. On the other hand, radiation losses from such impurities can hinder the plasma heating to the thermonuclear temperatures ($\approx 10\, keV$) if the concentration of impurity is higher than the certain level, see Fig. (1.3) and Refs. [21, 22]. The ignition of the plasma diluted by such amount of impurity would require plasma heating up to the temperature of $\approx 65\, keV$ where even heavy impurities are almost stripped [23].

Moreover, experiments on earlier tokamak devices with wall elements of heavy metals demonstrated that instead of gradual increase of radiation, e.g. with increasing electron density, the losses could start to grow explosively when the density exceeds a certain critical level [24, 25]. This behavior is caused by uncontrollable accumulation of heavy impurity particles of high charges near the plasma axis. In ohmic discharges this led to sharply peaked radial profiles of radiation losses and flat, or even hollow, radial distributions of the plasma temperature, which resulted in discharge disruptions. On the contrary, the central radiation decreased in auxiliary heated discharges with increasing electron density. Moreover, if ion cyclotron resonance heating (ICRH) was applied when the accumulation has already happen in the ohmic stage, the plasma core relaxed to the state with a peaked temperature profile and low central radiation losses. However, with auxiliary heating by deuterium neutral beams, accumulation occurred even at high plasma density. Presence of puffed impurity under certain conditions also provoked accumulation of high-Z ions.

This behavior was understood from the analysis of radial transport of impurity and heat [26]. The density of radial impurity flux can be represented as a sum of diffusive and convective parts:

$$\Gamma_Z = -\left(D_{neo} + D_{an}\right) \partial n_Z/\partial r + V_Z n_Z \tag{1.3}$$

where neoclassical, $D_{neo}$ and anomalous, $D_{an}$, diffusivity are involved since experiments show evidence of both effects. Convective velocity $V_Z$ is governed by the gradients of the density, $n_i$, and temperature, $T_i$, of background ions:

$$V_Z = D_{neo}\left(\frac{\alpha}{n_i}\frac{dn_i}{dr} + \frac{\beta}{T_i}\frac{dT_i}{dr}\right) \tag{1.4}$$

The parameters $D_{neo}$, $\alpha$, $\beta$ are determined from kinetic theory and governed by $n_i$, $T_i$, safety factor, toroidal magnetic field and collisionality. In Pfirsch-Schlüter collision dominated regime $\alpha = Z$ and $\beta = -Z/2$. For conventional peaked profiles of plasma parameters in fusion devices, the contributions to the pinching velocity due to $dn_i/dr$ and $dT_i/dr$ are of different signs. The former is directed towards the plasma core and is responsible for peaking of impurity density. The latter provides "temperature" screening which prevents peaking.

With increasing plasma density $n_e$, impurity radiates more intensively in the center of plasma column and flattens the radial temperature profile. This decreases the screening term with $dT_i/dr$ and under certain conditions negative convective part of impurity flux can uncontrollably force the impurity to the plasma core and overcome the diffusive outflow from the core. This will lead to accumulation of the impurity in the core plasma and increase of plasma cooling by radiation and formation of flatten or even hollow radial temperature profile. Peaking of impurity density profile occurs explosively and criterion for this is derived in [26]. Additional injection of impurity increases $n_Z$ and radiative losses. Thus, it can provoke impurity peaking even at lower plasma densities. Under other conditions, e.g. in radiation improved mode, significant decrease of $D_{an}$ provokes impurity accumulation in the core plasma. ICRH, applied essentially to the core plasma, prevents the flattening of the temperature profile, rising the temperature screening term and increasing diffusive particle transport. Both mechanisms hamper impurity accumulation. Under ITER conditions the accumulative instability is supposed to be suppressed.

The deterioration of the plasma performance by metal impurities forced researchers to use light elements, such as lithium, boron, beryllium or carbon, for the wall facing components. Light impurities, such as carbon and oxigen, can be removed by baking and discharge cleaning of the vacuum vessel. Additionally, the sputtering of heavy atoms of the on-wall constructions

can be avoided by covering the metal wall by carbon tiles. Furthermore, the way of constructive thinking in attempts to reduce the amount of impurities has led to the implementation of the magnetic configuration with X-point and divertor plates. Plasma flows along the magnetic field lines and is neutralized there. Even if the material of the neutralised plate is sputtered, the atoms are ionized within the divertor region near the target plates. Since the thermal velocity of the heavy ions, $V_Z$, is smaller than the velocity of the background ions, $V_i$, directed back to the plates, arising friction force $F_{fri} \sim n_i n_Z (V_i - V_Z)$ prevents impurity penetration into the main plasma.

### 1.2.4 Behavior of light impurities

The sputtering yield of the low Z wall materials is higher than for high Z ones. The self-sputtering yields can often exceed unity when an impurity having a charge state greater than +1 is accelerated by the plasma sheath potential (at the target surface) to energies much higher than the binding energy of the target atoms. Thus, a single impurity can release multiple impurities, which, in turn, can further contaminate the core. Additionally it can be increased by chemical erosion. Moreover, carbon layers effectively accumulate tritium.

The ions of light elements radiate most intensively at relatively low temperatures ($< 1\,keV$) [18], i.e. in the edge region close to the plasma boundary. This edge radiation can play a positive role reducing the heat flows normally concentrated on the wall elements, e.g. limiters and divertor plates [27, 28]. Low melting point ($180\,^{\circ}C$) allows the application of lithium as a self-recovery and renewable wall material. And liquid lithium divertor is proposed and tested as one of the solutions for dust accumulation problem and steady state operation of fusion reactor [29–31].

However, plasma behavior in presence of light impurities does not obey simple laws also. The radiative layer attached to the plasma edge can became unstable when the plasma density rumps up above a threshold value [24]. Under some conditions it manifests itself as a detachment of the radiating shell from the edge under preserving its poloidal and toroidal homogeneity [32, 33]. The radial contraction of this shell can terminate the discharge through a disruption or lead to the formation of a quasi-stationary "detached plasma". In other cases a toroidal plasma loop of very high density and low temperature called the multi-faceted radiation from the edge (MARFE) arises first at the high field side of the tokamak and can later disappear or smear out in a detached plasma [34]. In divertor machines the processes of MARFE formation is initiated often by a plasma detachment from neutralizing plates and MARFE locates near the X-point.

Both low- and high-Z materials are under consideration for the plasma facing components in a high-power fusion devices that broadens the range of input parameters for description of interaction between plasma and impurity.

### 1.2.5 Deliberate seeding of impurities

For various purposes impurities are seeded in fusion devices deliberately. For a long time, injection of light impurities, such as helium, isotopes of lithium and carbon, is applied for diagnostic purposes by measuring local plasma parameters [35, 36]. With increasing size of fusion machines during several decades, required to increase confinement time and obtain break-even, flows of particles and energy grew as well. Estimations made for ITER [37] show that the power flux incident on the divertor plates will be $\approx 10\,MW/m^2$ and cause significant melting and/or sublimation of the plasma-wetted surfaces. Injection of light impurities is applied to increase energy losses with radiation on the plasma edge in order to redistribute the power transported from the plasma core over a large wall area, to reduce heat loads on divertor target plates and weaken plasma-wall interaction [28]. Moreover, injection of nitrogen, neon or argon allows to diminish the amplitude of edge localized modes (ELMs) by maintaining, under special conditions, still reasonable or even improved energy confinement [38–41]. Although, the nature of such conditions remains obscure and their scalability has not been demonstrated yet.

One has to note that, in spite of fewer studies, similar impacts of impurities on the edge plasma are observed in experiments on small aspect tokamaks [42] and in currentless plasmas of stellarators [43–45].

### 1.2.6 Disruption mitigation

Fast abruption of plasma discharge due to inappropriate operation or unexpected event in the fusion plasma [46], called disruption, represents a potential threat to the integrity and availability of fusion reactor. The thermal energy is released in a sub-millisecond time scale, and can lead to significant erosion of wall components. Then, the magnetic energy associated with the plasma current is dissipated in a resistive way. Since the induced currents are close to the wall, the vessel is subjected to strong forces of interaction between magnetic field and halo-currents induced in the vessel and in-vessel components causing their deformation or breakage. The electric field induced during current decay can accelerate beams of runaway electrons with energies of tens of $MeV$. A local deposition of such beams can destroy the integrity

of the vessel. The presence of impurity near the wall enhances the plasma resistivity there and decreases, therefore, halo-currents. Fast injection (within $2\,ms$) of very large amount ($> 10^{22} particles$) of highly radiating gas (neon, argon, krypton) is considered as a perspective approach to mitigate plasma disruptions. Two mitigation techniques were developed as a last resort in the case of unavoidable disruption: pellet injection [47] and massive gas injection (MGI). The latter is presently the most explored technique and is studied on many tokamaks: Alcator C-mod, ASDEX Upgrade, DIII-D, JT60-U, MAST, TEXTOR and Tore Supra by using several gases: deuterium, helium, neon and argon and deuterium-noble gas mixtures [48–51]. During the ITER lifetime disruptions and runaway electrons are expected to occur roughly 3000 times (with each having the potential to cause serious damage) and mitigation requires an injection of the order $500\,kPa\,m^3$ of helium or $100\,kPa\,m^3$ of neon [52].

The disruption caused by MGI can be divided into three phases [53–55]: pre-thermal quench (pre-TQ), thermal quench (TQ) and current quench (CQ). Pre-TQ phase begins with opening the injection valve. The jet penetrates into the plasma at approximately the sonic speed and impurity cools the edge. Radiation power increases linearly with the amount of injected atoms, and no MHD perturbations are observed at this first stage. The electron density increases by an order of magnitude in a few milliseconds. As the low temperature front reaches the surface $q = 2$, very large radiation arises from the central plasma and strong magnetic perturbations develop. The fast TQ takes place and the remaining thermal energy is released within $\approx 2\,ms$ by a soft X-ray radiation. The current decays due to high resistivity of the remaining low temperature plasma. Subsequent discharges following the gas jet injection show no indication of significant radiation from the injected impurity species.

In spite of the fact that the method of mitigation by MGI is developed, approbated on several fusion machines and accepted for use in ITER, the underlying mechanisms of impurity penetration into the plasma and impacts of spreading impurity on the plasma remain poor understood. In particular, the question of local radiation loads on the wall has to be answered yet.

### 1.2.7 Reactor fueling

Injection of a supersonic gas jet is proposed as a new technique for fueling of future fusion reactors. It is almost cheap as gas puff and much cheaper than the pellet injection. Using Laval nozzle, it is possible to achieve a well-collimated jet moving with a rather high velocity. Thus, rather dense jet remains almost neutral in spite of the energetic ambient plasma particles and

therefore is able to penetrate deep into the tokamak. The fueling efficiency is reported to be intermediate between standard gas puff and pellet injection from the high field side of the tokamak [56, 57]. One has to see that the behavior of even pure fusion plasma, consisting of deuterons and tritons, differs from a pure deuterium one [58] and should be properly taken into account in experimental and theoretical considerations. Moreover, spreading of injected fuel components in plasma should be considered individually, as an "impurity" in the main plasma, since injected neutrals and produced ions possess initially low temperature.

### 1.2.8 Summary of impurity impacts on fusion plasmas

The understanding of impurity transport in a magnetically confinement fusion plasma is one of the challenges of current fusion research. This brief introduction gives a feeling how broad is the spectrum of impurity impacts on hot plasmas of fusion devices. Impurity seeding is an essential element of power exhaust in future fusion reactors, including ITER. It extends from the troublesome phenomenon of accumulation and radiative collapse in the plasma core, through improvement of confinement under certain conditions by creation of radiating mantle, reducing the power carried by the plasma to the divertor, up to a viable method for ELM size reduction in ELMy H-mode plasmas and safe shutdown of disruptive discharges in fusion devices.

In all described cases impurities enter the plasma very locally, but their impacts can be seen both locally near the injection position and spread over the whole plasma volume. Disturbance of the electron density and plasma cooling provoked by the impurity presence affects the impurity transport itself. Interaction of the plasma and impurity is complex and highly non-linear phenomenon implying a lot of physical aspects, such as quasi-neutrality, coulomb collisions between various charged particles, etc., those should be self-consistently taken into account.

## 1.3 State of arts in modeling of impurity seeded plasmas

### 1.3.1 Spatial and temporal requirements to models

Appearance of the ionizing neutral and charged impurity causes two global modifications in the plasma, seen from the experiment: (i) additional electrons produced by ionization increase the electron density $n_e$ and (ii) radiation of impurity due to excitation and recombination leads to the heat

loss from the plasma and decrease of the electron temperature $T_e$. Decrease of the main ion temperature is frequently attributed to heat exchange with electrons and thorough consideration of this phenomena is one of the issues of this work. This task has to be treated time-dependently, because there could be no stationary solution at all or could be a stationary solution with discharge parameters inappropriate for the current fusion devices.

By neglecting transport effects one could describe the evolution of the densities of impurity charge states $n_j$ with the charge $j = 0, 1, 2, \ldots, j_{max}$ by particle balances:

$$dn_j/dt = n_e \left( k_{ion}^{j-1} n_{j-1} - k_{ion}^{j} n_j k_{rec}^{j+1} n_{j+1} - k_{ion}^{j} n_j - k_{rec}^{j} n_j \right) \tag{1.5}$$

the electron density – by plasma quasi-neutrality:

$$n_e = n_i + \sum_{j=1}^{j_{max}} j n_j \tag{1.6}$$

and the electron temperature $T_e$ through the electron heat balance:

$$d\left(n_e T_e\right)/dt = P_{heat} - n_e \sum_{j=0}^{j_{max}-1} n_j L_{rad}^{j} \tag{1.7}$$

Here $k_{ion}^{j}$, $k_{rec}^{j}$ and $L_{rad}^{j}$ are the ionization, recombination and cooling rates, respectively ($k_{rec}^{j_{max}+1} = 0$ since atoms are fully stripped at $j_{max}$); $P_{heat}$ is the power density of plasma heating. Even from such simplified description it is clear that interaction between impurity and plasma is non-linear.

In practice, impurity is injected very locally [55] in comparison with total plasma volume and then spreads. Hence, $n_j$ in Eqs. (1.5-1.7)is related with the transport of neutral and charged impurity components and with injection intensity. The model has to take into account the essentially three-dimensional geometry of impurity spreading phenomena.

Impurity neutrals enters the plasma with initially very low temperature ($< 0.05\, eV$). Impurity ions assimilate the temperature from the previous charge state and are heated by coulomb collisions with the main plasma components. The characteristic heat exchange time [59] depends on the charge and various charge states are heated up not equally. Thus, the model has to include such processes as the heat exchange through coulomb collisions between different charged components.

Even from rough estimations it is seen that the plasma with impurity includes processes with very different characteristic times. The ionization times for low charge states are $< 10^{-8}\, s$, the heat exchange times are in the

range of tens of $ms$, the time of flight of neutrals is several $ms$ and plasma discharge time is in the range of seconds. Hence, the model should perform non-stationary calculations with a time step as small as $10^{-10}\,s$ and a total number of steps of $10^8 - 10^9$.

Finally, the presence of the wall implies the constraints on the boundary conditions. The Bohm criterion requires that in plasma with a single ion charge state the ion velocity at the entrance into a Debye sheath cannot be smaller than the ion sound one [60]. In multi-species plasma it is not sufficient to define velocities of all species individually. A generalization requires that a certain relation between their velocities has to be satisfied and leads to specific approaches in numerical treatment of momentum balance equations [61].

### 1.3.2 A brief survey of theoretical models and numerical codes describing interaction between impurity and plasma

There were a lot of attempts do describe interaction of impurity and plasma. This survey describes the most recent theoretical models and computational codes dedicated to this aim and required for understanding of strong and weak sides of the approach developed in the current work.

The most rough description is done by models based on 0 D heat balances, where interaction between plasma and impurity is described by radiative loss term [62, 63] with hard stipulation of homogeneity and known impurity density, averaged over the plasma volume. With inclusion of magnetic energy these models allow to describe roughly the rump-down of tokamak plasma current, total flux of radiated power and estimate the wall temperature increase. This is useful for the tasks of disruption mitigation. In a more sophisticated approach [64] this description is fulfilled by advanced radiative loss term, taking into account the full set of impurity charge states, and by additional channel of heat transfer between charged particles through coulomb collisions. It is worth to note, looking on ahead of the current work, that this channel can be comparative or even dominant in comparison with radiation losses.

Multi-species time-dependent 1 D approach developed in the code RITM [65] and in the model [66] allow calculation of radial (the coordinate $r$) plasma profiles disturbed by the presence of impurities. They are based on fluid equations for particle, momentum and heat transport in the radial direction in each of the plasma components: electrons, main ions and various charge states of impurity ions with radially distributed sources and sinks of particles

and energy; toroidally and poloidally plasma is assumed to be homogeneous.

Another line of thinking is given in time-dependent 1 D approaches [54,67] considering local spread of impurity species along the magnetic field lines in modified plasma. Under certain assumption one can make then a transition from one magnetic line to another and reconstruct the radial penetration of the impurity. An merit of these approaches is the violation of toroidal symmetry assumption, i.e. impurity is not considered as filling the whole magnetic surface.

Several codes for impurity transport based on kinetic, mainly Monte-Carlo, approaches for 2 D radial-azimuthal case (coordinates $r\theta$), DIVIMP [68], DORIS [69] and for 3 D planar geometry (coordinates $xyz$) ERO [70] have been developed. Kinetic impurity codes use as input the parameters of the background plasma, e.g., densities, temperatures and mass velocities of electrons and main ions, and electric field. On the one hand, these parameters are normally taken from measurements performed either without impurity injection or far away from the impurity injection position [71]. Thus, their total profiles, necessary for consistent impurity modeling, have to be provided by models for the main plasma components. On the other hand, such models require as an input the electron sources due to impurity ionization, energy loss with radiation and other impurity characteristics. A final solution can be obtained only as a result of iterations between modules describing impurity and background plasma particles and by taking into account such constraints as plasma quasi-neutrality, force balances and so on. In the current "state of arts" the mentioned above Monte-Carlo codes are applied for the case of trace impurity limit. Also, they consider impurity species only stationary.

There are more advanced numerical codes using 2 D fluid approximation and developed for modeling of the plasma edge of fusion devices: B2-EIRENE [72, 73], SOLPS [74], UEDGE [75], EDGE 2D [76]. However, in spite of consideration of various charge states their temperatures are equalled to that for the main ions. This means: (i) it is considered only one channel of energy loss from the main plasma – impurity radiation with subsequent effect on the electron temperature, (ii) decrease of the main ion temperature is attributed to interaction with electrons only, (iii) heating of the impurity ions and cooling of the main ones by mutual coulomb collisions is neglected. The latter effects are taken into account in the multi-fluid code TOKES [77–79]. Another constrain concerns approximation of radial-azimuthal geometry under the assumption of toroidal symmetry. Infra-red camera and soft x-ray observations in experiments with MGI [55] show that this assumption is valid only for the higher charge states deep in the plasma core, but the lower ones are concentrated very locally near the point of injection. This constrain is removed by 3 D modeling with the Monte Carlo code EMC3-EIRENE [80]

Table 1.1: Numerical tools for modeling of plasma-impurity interaction.

| **Code name** | **Time evolution** | **Three-dimensionality** | **Plasma response to impurity** | **Several charge states** | **Ion heat exchange** | **Fast calculations** |
|---|---|---|---|---|---|---|
| KPRAD | √ | × | √ | × | × | √ |
| RITM | √ | × | √ | √ | √ | √ |
| DORIS | × | × | × | √ | √ | × |
| EDGE 2D | × | × | √ | √ | × | √ |
| B2-EIRENE | × | × | √ | √ | × | × |
| TOKES | √ | × | √ | √ | √ | √ |
| ERO | × | √ | × | √ | √ | × |
| EMC3-EIRENE | × | √ | √ | √ | × | × |

operating, however, stationary and with with identical ion temperatures. Additionally, such codes are very consumptive in respect to calculation time. This survey of existing codes is summarized in table (1.1).

## 1.4 Motivation and outline of this work

As it was seen from two previous subsections, penetration of impurity into the plasma is a complex phenomenon and none of the existent code packages includes the whole set of involved processes. Moreover, the most of research groups move on the way of spatial resolution, and the main load of simplification laid down on the physical processes, such as assumption of the the same temperatures of ion species and stationarity.

The task of disruption mitigation requires to know the depth of penetration of neutral impurity. In this case interaction between plasma and impurity is especially 3 D non-uniform and changing in time. Not always it is required to know the exact 3 D profiles of the plasma parameters. They often can be fitted by known algebraic functions such as Gaussian or parabolic ones, and those are recovered from estimations of volumes occupied by different charge states of impurity and characteristic magnitudes of their densities, temperatures and fluxes.

This thesis does not pursue the aim to describe global change in hot plasmas, including radial transport, but focuses the efforts on a description of

the local region near the entrance of impurity into the plasma. In the most of current applications (diagnostics, droplets in plasma, massive gas injection) impurity enters the plasma very locally, i.e. the area surface, through which the impurity enters the plasma, is much smaller its total area. The most approximations made in this work are build on assumption of this locality. Nevertheless, this approach allows to estimate the scale of impurity impact on the plasma, both its magnitude and spatial spread.

The locality of phenomena in question implies that characteristic distances from the position of impurity entrance are significantly smaller than device dimensions. Therefore, the particular geometry of the device should not play an essential role for the transport processes in the region under consideration. In particular, we neglect the effects of the $\nabla \mathbf{B}$ and curvature drifts, which are important in the dynamics of other scrape-off layer (SOL) phenomena such as "blobs" [81]. For higher charged impurity ions distributed more homogeneously on magnetic surfaces, these toroidal effects may be more essential. Henceforce, we use an orthogonal reference system $(x, y, z)$ with the coordinates $x$ directed across the magnetic surfaces towards the plasma core, $y$ aligned on the surface perpendicular to the magnetic field that is oriented in the direction $z$.

This thesis represents consequent development of approaches describing self-consistently interaction between impurity, in the form of neutral gas injected at some position in the periphery region, and local behavior of the plasma under the impact of impurity. The work is structured in the following manner.

Chapter (2) introduces the main equations of multi-fluid model where each sort of particles, such as neutrals, electrons, main and impurity ions of various charges are represented by appropriate fluid with corresponding set of parameters such as mass and charge of particles, their density and temperature, etc. This system is rather complex and for certain particular case can be reduced to simpler models described in chapters (3-5) with consequent discussion of the applicability range for each of them.

Chapter (3) begins with consideration of the plasma shadowed by surrounding wall elements under strong impurity injection puff. The presence of material surfaces provide sinks for charged particles. A stationary model based on a fluid description of electrons, main and singly charged impurity ions and taking into account the plasma quasi-neutrality, coulomb collisions of background and impurity charged particles, radiation losses, sinks of particles to bounding material surfaces, is elaborated. Integration of transport equations within the clouds of neutral and singly charged impurities, both inside and beyond the SOL of puffing limiter, gives particle, momentum and energy balances, which allow calculation of characteristic densities of

the plasma components in the cloud and dimension of the cloud itself. By applying this approach at various radial positions one can determine the characteristic radial scale of the region where the plasma is disturbed by impurity.

The times typical for puffing and MGI experiments, may not be enough for the impurity spread coming to any stationary state. Moreover, characteristic time scales of impurity transport can be comparable with the life-times of various lower charge states. Chapter (4) considers the spread of impurities locally injected into hot magnetized plasma on the basis of a time-dependent fluid description for electrons, impurity neutrals and ions in low charge state in the vicinity of the injection position. The elaborated model takes into account that impurity particles of different charges are localized predominantly inside nested shells whose extensions along and across the magnetic field increase with the charge. By integrating fluid equations for particle, parallel momentum and heat transfer, ordinary differential equations for the time evolution of characteristic shell dimensions, densities and temperatures of impurity ion species are deduced. The proposed approach is applied under conditions where the local impurity density can noticeably exceed the density of background plasma ions, but the effects of plasma cooling due to impurity presence are negligible. Time-dependent cooling of the plasma surrounding impurity shells is considered separately in chapter (5).

Calculations performed by using of developed "shell" model with various parameters of neutral injection and initial plasma revealed the important role of coulomb collisions in mechanisms responsible for both impurity spread and local plasma modification. It was shown that under certain conditions coulomb collisions due to the presence of impurity in plasma are more important for the for development of cooling instability and formation of cold dense structures in plasma than radiation losses. These questions are considered in chapter (6).

The set of hydrodynamic equations describing multi-component plasma with neutrals, electrons and ions of several charges and temperatures is highly non-linear. Moreover, the presence of material surfaces considered in chapter (3) and subsequent flow to them results in singularities in momentum transport equation. In chapters (4-6) the variables in time derivatives appearing by integration of transport equations are interlaced and their decoupling leads to singularities in the right hand sides. Thus, special numerical approaches for proper treatment of such systems of equations are elaborated. Chapters (3-6) are structured as follows:

(i) formulation of the problem and description of physical processes taken into account;

(ii) description of mathematical approach for solving of the equations and

elaborated numerical algorithms;

(iii) numerical calculations by using the developed model with particular physical parameters and results of the calculations;

(iv) discussion of the phenomena found through numerical simulations, studying of the model sensitivity to free parameters and applicability range of the model.

The results obtained during this study are summarised in chapter (7) and the nearest possible extensions of the model to be made in future are proposed and discussed.

# Chapter 2

# Basic equations

In this work we use fluid approximation, where every component "$a$" of a multicomponent plasma, including neutrals, electrons, and ions of various charges and masses, is described by using macroscopic parameters:

(i) the particle density, $n_a$, i.e. the number of particles of a certain sort per unit volume;

(ii) the mass velocity $\overrightarrow{V_a}$; often it is convenient to use the momentum flux density, $\overrightarrow{\Gamma_a} = n_a \overrightarrow{V_a}$;

(iii) the averaged energy or temperature, $T_a$, expressed in energetic units.

These parameters are functions of time and space coordinates, $f(t, x, y, z)$, and are governed by transport equations, see Ref. [59] and [82] (pp. 277–357), for continuity of particles, momentum and energy described below in this chapter.

Impurity, released in fusion devices by plasma-wall interaction or seeded deliberately, enters the plasma as neutrals, and normally their influxes are strongly concentrated at some specific locations. By ionization of neutrals with electrons, lower charge states of impurity are produced and spread in the vicinity of the neutral jet, both along and across the magnetic field, and disappear being ionized into higher charge states. The impact of these highly charged ions on local plasma behavior near the impurity injection position is neglected henceforth. The locality of the phenomena in question implies that the characteristic distances from the position of impurity entrance are significantly smaller than the device dimensions. Therefore, the particular geometry of the device does not play an essential role for the transport processes in the region under consideration and henceforth we use an orthogonal reference system $(x, y, z)$ with the coordinate $x$ directed across the magnetic surfaces towards the plasma core, $y$ – aligned on the surface perpendicular to the magnetic field that is oriented in the direction $z$. The origin of the coordinate system is attached to the center of the spot where impurity enters

the plasma. In real experiments it can be either in the shadow of the limiter or inside the last closed flux surface (LCFS), as it is schematically shown in Fig. (2.1). Here neutrals are injected trough the small outlets of the injection channels of vacuum vessel.

## 2.1 Neutral transport

Neutrals in Fig. (2.1) enter the plasma with the speed $\overrightarrow{V_0}$, which does not change inside the plasma volume. By penetrating into the plasma the impurity neutral jet widens and neutrals are ionized by electron impacts. The variation of the neutral density $n_0$ obeys the continuity equation:

$$\frac{\partial n_0}{\partial t} + \overrightarrow{V_0} \cdot \overrightarrow{\nabla} n_0 = -k^0_{ion} n_e n_0 \tag{2.1}$$

where frequency $k^0_{ion}$ is the ionization rate coefficient and $n_e$ is the electron density disturbed by ionization.

## 2.2 Plasma quasi-neutrality

In the reference state without impurity the main ion density $n_i$ coincides with the electron one. Ionization of impurity neutrals produces additional electrons and impurity ions, which are then ionized further. Disturbed electron density obeys to the plasma quasi-neutrality condition:

$$n_e = n_i + \sum_j j n_j \tag{2.2}$$

where $n_j$ are the densities of the impurity ions with the charges $j = 1, 2, \ldots, j_{max}$, respectively.

## 2.3 Charged impurity transport

The evolution with time $t$ of the density $n_j$ of impurity ions with the charge $j$ is governed by the continuity equation:

$$\begin{aligned} &\frac{\partial n_j}{\partial t} - \frac{\partial}{\partial x}\left(D_x \frac{\partial n_j}{\partial x}\right) - \frac{\partial}{\partial y}\left(D_y \frac{\partial n_j}{\partial y}\right) + \frac{\partial \Gamma_j}{\partial z} \\ &= k^{j-1}_{ion} n_e n_{j-1} - k^j_{ion} n_e n_j \end{aligned} \tag{2.3}$$

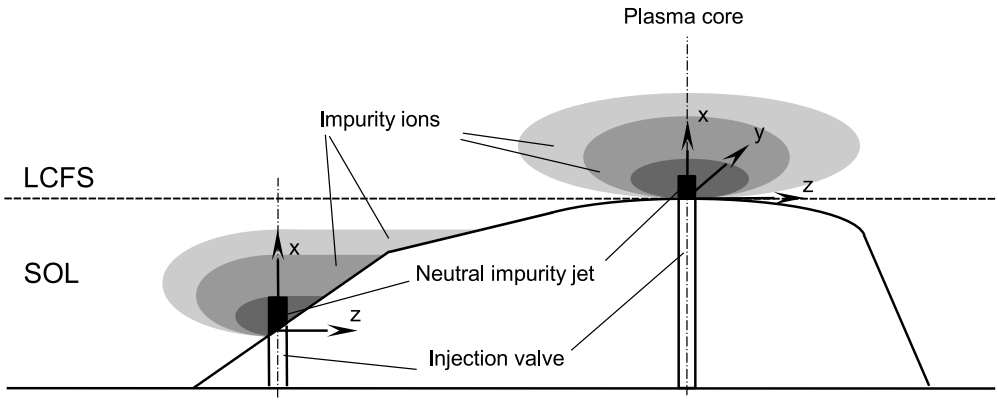


Figure 2.1: Schematic view of impurity injection into the plasma.

where $k_{ion}^{j-1}$ and $k_{ion}^{j}$ are the ionization rate coefficients; the particle transport across the magnetic field is assumed to be governed by Fick's law with corresponding diffusivity components $D_y$ and $D_x$.

The impurity motion along the magnetic field is determined by the competition of several forces. Impurity ions by their creation assimilate the momentum from $j-1$-state, are accelerated along the field lines by own pressure gradient and the parallel electric field, arising due to modification of the electron density, braked by coulomb collisions with the main ions, and disappear due to ionization into the higher charge state. The density of the impurity ion flux component $\Gamma_j$ parallel to the magnetic field is determined by the momentum balance equation:

$$\begin{aligned}
&\frac{\partial \Gamma_j}{\partial t} - \frac{\partial}{\partial x}\left(\frac{D_x}{n_j}\frac{\partial n_j}{\partial x}\Gamma_j\right) - \frac{\partial}{\partial y}\left(\frac{D_y}{n_j}\frac{\partial n_j}{\partial y}\Gamma_j\right) + \frac{\partial}{\partial z}\left(\frac{\Gamma_j^2}{n_j}\right) \\
&= k_{ion}^{j-1}\Gamma_{j-1} - k_{ion}^{j}\Gamma_j \\
&+k_{ij}\left(\Gamma_i n_j - \Gamma_j n_i\right) - \frac{\partial}{\partial z}\left(\frac{n_j T_j}{m_I}\right) \\
&+\left(jeE_z n_j - F_{th}^{ej} - F_{th}^{ij}\right)/m_I
\end{aligned} \tag{2.4}$$

where $m_I$ is the impurity ion mass; $k_{ij} = 3.34\Lambda_c j^2 e^4\sqrt{m_i}/(m_I T_i^{3/2})$ is the friction coefficient due to coulomb collisions with the background ions with the mass $m_i$, temperature $T_i$ and flux $\Gamma_i$; $\Lambda_c$ is the coulomb logarithm [59], $e$ the elementary electric charge.

Impurity ion temperature $T_j$ in the pressure gradient term of Eq. (2.4) is governed by the impurity heat transport equation taking into account that

the next charge state assimilates the temperature of the previous one and exchanges the heat in coulomb collisions with electrons and main ions. Due to high impurity transport, gained thermal energy is distributed in the impurity cloud by convection primarily, according to:

$$\begin{aligned}\frac{3}{2}n_j\frac{\partial T_j}{\partial t}+T_j\frac{\partial \Gamma_j}{\partial z} &= \frac{3}{2}\left(T_{j-1}-T_j\right)k_{ion}^{j-1}n_e n_j \\ &\quad +3n_j\left[k_{ij}n_i\left(T_i-T_j\right)+k_{ej}n_e(T_e-T_j)\right] \end{aligned} \quad (2.5)$$

where $T_e$ is the electron temperature and $k_{ej}=3.34\Lambda_c j^2e^4n_e\sqrt{m_e}/(m_I T_e^{3/2})$ heat exchange coefficient due to coulomb collisions between electrons and impurity [59].

The electric field component parallel to the magnetic field lines is determined from the force balance for the electrons by neglecting their enertia:

$$\frac{\partial}{\partial z}\left(n_eT_e\right)=-en_eE_z+F_{th}^{ei}+\sum_j F_{th}^{ej} \quad (2.6)$$

In Eqs. (2.4) and (2.6), $F_{th}^{ei}=-\alpha_{ei}n_e\partial T_e/\partial z$, $F_{th}^{ej}=-\alpha_{ej}n_e\partial T_e/\partial z$, and $F_{th}^{ij}=-\alpha_{ij}n_i\partial T_i/\partial z$ are the thermal forces arising due to coulomb collisions of particles. By assuming that the main ion mass is much smaller than the impurity one, $m_i \ll m_I$ they can be calculated for arbitrary densities of the charged particles: $\alpha_{ei}=n_i/(0.54n_e+0.87n_i)$, $\alpha_{ej}=j^2n_j/(0.54n_e+0.87j^2n_j)$, and $\alpha_{ij}=j^2n_j/(0.38n_i+0.87j^2n_j)$, see Ref. [83].

In this work we study impurity species of low enough charge allowing to consider their spread as localized in the vicinity of the injection position. For this reason equations above do not take into account recombination processes. They have to be included, however, by looking on higher charged ions penetrating into deeper plasma regions.

## 2.4 Transport equations for main plasma components

Impurity neutrals usually enter into the plasma volume through small spots, and their local density can be very high even for a relatively small absolute level of the impurity influx. Energy losses on excitation, ionization, heating of produced ions through coulomb collisions can noticeably cool down the main plasma components near the impurity entrance position. Temperature reduction near the impurity source leads to a parallel pressure gradient which drives a flow of the main ions along the magnetic field towards the

source. The consequent change of the main ion density $n_i$ is governed by the continuity equation:

$$\frac{\partial n_i}{\partial t} - \frac{\partial}{\partial x}\left(D_x \frac{\partial n_i}{\partial x}\right) - \frac{\partial}{\partial y}\left(D_y \frac{\partial n_i}{\partial y}\right) + \frac{\partial \Gamma_i}{\partial z} = 0 \tag{2.7}$$

with the density of the ion parallel flux determined by the main ion momentum transport equation:

$$\begin{aligned} &\frac{\partial \Gamma_i}{\partial t} - \frac{\partial}{\partial x}\left(\frac{D_x}{n_i}\frac{\partial n_i}{\partial x}\Gamma_i\right) - \frac{\partial}{\partial y}\left(\frac{D_y}{n_i}\frac{\partial n_i}{\partial y}\Gamma_i\right) + \frac{\partial}{\partial z}\left(\frac{\Gamma_i^2}{n_i}\right) \\ &= -m_I \sum_j k_{ij}\left(\Gamma_i n_j - \Gamma_j n_i\right) - \frac{\partial}{\partial z}\left(\frac{n_i T_i}{m_i}\right) \\ &+ \left(jeE_z n_j - F_{th}^{ej} - F_{th}^{ij}\right)/m_i \end{aligned} \tag{2.8}$$

The temperatures of the main ions and electrons are governed by the heat transport equations:

$$\begin{aligned} &\frac{3}{2} n_i \frac{\partial T_i}{\partial t} + T_i \frac{\partial \Gamma_i}{\partial z} - \frac{\partial}{\partial x}\left(\kappa_{ix}\frac{\partial T_i}{\partial x}\right) - \frac{\partial}{\partial y}\left(\kappa_{iy}\frac{\partial T_i}{\partial y}\right) - \frac{\partial}{\partial z}\left(\kappa_{iz}\frac{\partial T_i}{\partial z}\right) \\ &= 3n_i\left[k_{ei} n_e (T_e - T_i) + \sum_j k_{ij} n_j \left(T_j - T_i\right)\right] \end{aligned} \tag{2.9}$$

$$\begin{aligned} &\frac{3}{2} n_e \frac{\partial T_e}{\partial t} + T_e \frac{\partial \Gamma_e}{\partial z} - \frac{\partial}{\partial x}\left(\kappa_{ex}\frac{\partial T_e}{\partial x}\right) - \frac{\partial}{\partial y}\left(\kappa_{ey}\frac{\partial T_e}{\partial y}\right) - \frac{\partial}{\partial z}\left(\kappa_{ez}\frac{\partial T_e}{\partial z}\right) \\ &= n_e\Bigg(\sum_j n_j\left[3k_{ej}(T_e - T_j) - k_{ion}^j\left(I_j + \frac{3}{2}T_e\right) - L_j\right] \\ &+ 3n_i k_{ei}\left(T_i - T_e\right)\Bigg) \end{aligned} \tag{2.10}$$

where $\kappa_{ix}$, $\kappa_{ex}$, $\kappa_{iy}$, $\kappa_{ey}$, $\kappa_{iz}$ and $\kappa_{ez}$ are the components of heat conductions, $I_j$ and $L_j$ – the ionization energy and cooling rates of impurity ions, respectively. The densities of the main ion and electron particle fluxes along the magnetic field, $\Gamma_i$ and $\Gamma_e$, are interrelated by charge conservation law:

$$\Gamma_e = \Gamma_i + \sum_j j\Gamma_j \tag{2.11}$$

The system of Eqs. (2.1)-(2.11) describes self-consistently interaction between neutral and ionized impurity and disturbed plasma. It represents the set of strongly non-linearly coupled partial differential equations (PDEs) and requires a proper treatment. In particular cases, however, it can be reduced to simpler models, which are described in the next chapters.

# Chapter 3

# Stationary modeling of impurity spreading and impacts on plasma of scrape-off layer and edge regions

We begin consideration of interaction between impurity and plasma with consideration of impurity transport parallel to the magnetic field and impurity impact on the plasma shadowed by the puffing limiter.

Development of models for a self-consistent description of plasma mixtures with several ion species is interfered with many challenges. In particular, in plasma domains where charged particles can escape to material surfaces the Bohm criterion set constraints on the ion velocities at the entrance of the Debye sheath near the surface. In a multi-species plasma this results in singularities in the ion momentum balance equations inside the computational domain and a proper treatment of such complexities is a challenging numerical task [84].

With reasonable approximations the difficulties outlined above can be, however, evaded without disregard to the most important physical processes in question. By integrating stationary transport equations along the magnetic field within the clouds of impurity neutrals and singly charged ions a stationary zero-dimensional model is elaborated in this chapter.

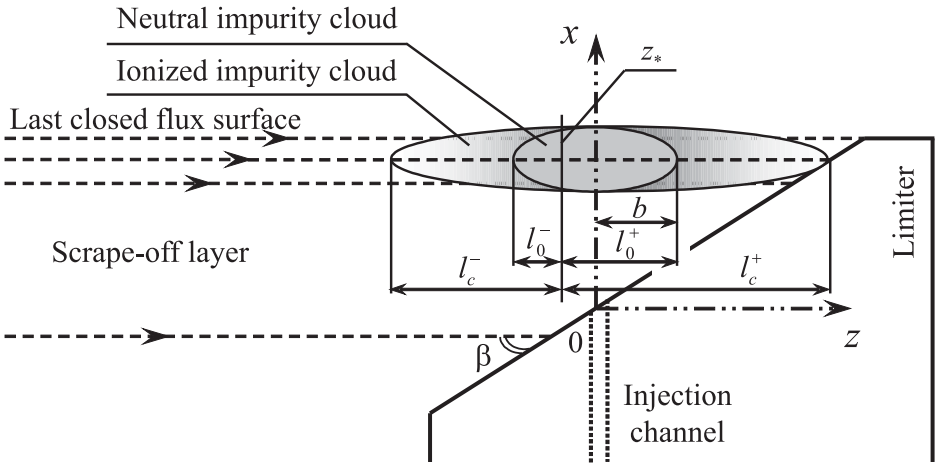


Figure 3.1: Clouds of impurity neutrals and singly ionized ions near the injection position.

# 3.1 Model

## 3.1.1 Impurity neutral density

Fig. (3.1) shows schematically the cloud of impurity neutrals injected into the plasma through the outlet in the puffing limiter surface and the cloud of singly ionized impurity particles. The origin of the Cartesian coordinate system $(x, y, z)$ is placed in the outlet center. The limiter surface is assumed to be inclined at the small angle $\beta$ to the magnetic field direction $z$ and neutrals move predominantly in the direction $x$ across the magnetic surfaces, with the speed $V_0$. In addition, the cloud spreads both along the magnetic field and perpendicular to the $(z, x)$-plane, in the direction $y$, with the spreading angle $\alpha$. Henceforth, we assume that the jet of injected neutrals has a square cross-section in the $(y, z)$-plane with the half-width increasing as $b(x) = b_0 + x \tan\alpha$, where $b_0$ is the outlet half-width. For a given $x$ the neutral density $n_0$ is assumed to be constant for $|y| \le b(x), |z| \le b(x)$ and zero outside the jet cross-section. Due to ionization by electrons the total flux of impurity neutrals, $\Phi_0 = 4b^2 n_0 V_0$, decays with $x$. This behavior is described by the integral of continuity equation (2.1) over the cloud cross-section in the $(y, z)$-plane that in stationary case gives:

$$\frac{d\Phi_0}{dx} = -\frac{n_e k^0_{ion}}{V_0}\Phi_0 \tag{3.1}$$

where $n_e$ is the electron density and $k^0_{ion}$ the ionization rate coefficient which are assumed as changing weakly with $y$ and $z$ inside the cloud. Integration

of Eq. (3.1) gives the variation of the neutral density in the direction perpendicular to the magnetic surfaces:

$$n_0(x) = \frac{n_0(0)}{(1 + x\tan\alpha/b_0)^2} \exp\left( - \int_0^x \frac{k_{ion}^0 n_e}{V_0} dx \right) \tag{3.2}$$

The presence of impurity itself disturbs both the plasma density, through the production of additional electrons by its ionization, and the electron temperature $T_e$ owing to the energy losses on excitation and ionization of impurity neutral and charged particles. The ionization rate coefficient is a function of $T_e$ and, thus, both channels are of importance for the neutral penetration process, see the exponential factor in Eq. (3.2). It is clear that impurity ions are essentially involved into this phenomenon and a description of charged impurity has to complement the equations for the transport of neutrals.

In this study we neglect other sources of neutrals such as recycling from the limiter surface of impurity ions produced in the scrape-off layer(SOL). On the one hand, this is still an unresolved issue being under comprehensive examinations [71]. On the other hand, even if the majority of impurity ions reaching the limiter returns into the plasma as neutrals, their influx density is much lower than that of the primary jet, because of the smallness of the surface inclination angle $\beta$. Therefore, we expect local effects from recycling impurity particles to be weaker than those from the impurity jet. Nevertheless, these effects have to be included in a future more sophisticated analysis.

### 3.1.2 Charged particle densities

Consider a bunch of field lines crossing the neutral impurity cloud at a certain position $x$. Impurity ions, generated through ionization of neutrals, are pushed along the field line by their pressure gradient and by the parallel electric field modified due to increased electron density. Coulomb collisions between main and impurity ions results in a friction force [59] hampering this spreading of the impurity cloud. Particle and momentum transport equations (2.3) and (2.4) averaged over the bunch width, $|y| \le b(x)$, provide the variation of the particle and parallel flux densities of singly charged impurity ions, $n_I$ and $\Gamma_I$, respectively:

$$\partial\Gamma_I/\partial z = k_{ion}^0 n_0 n_e - \nu_I n_I \tag{3.3}$$

$$\partial\left(m_I n_I V_I^2 + n_I T_I\right)/\partial z = eE_\parallel n_I - m_i k_{iI} n_i n_I (V_I - V_i) - m_I \nu_I \Gamma_I \tag{3.4}$$

Here $\nu_I = k^1_{ion} n_e + \nu^I_\perp$ with $k^1_{ion}$ being the ionization rate coefficient of singly ionized ions. The value $\nu^I_\perp$ characterizes the losses of impurity ions with perpendicular transport in the direction $y$ to the plasma regions where field lines do not pierce the neutral cloud. The contribution from the transport in the radial direction $x$ is neglected because for a typical radial diffusivity of $0.1 - 1\, m^2 s^{-1}$ it is small compared with the first source term in the r.h.s. of Eq. (3.3). In this chapter we use for $\nu^I_\perp$ a prescribed value and consider how its variation affects the results. In Eq. (3.4) $m_I$, $V_I = \Gamma_I / n_I$ and $T_I$ are the mass, parallel velocity and temperature of impurity ions; $e$ is the elementary electric charge; $k_{iI} = 3.34 \Lambda_c e^4 / (\sqrt{m_i} T_i^{3/2})$ is the friction coefficient due to coulomb collisions with the main ions, $\Lambda_c$ is the Coulomb logarithm [59]; $m_i$, $n_i$, $V_i$ and $T_i$ are the mass, density, velocity and temperature of the main ions. Parallel electric field is calculated from Eq. (2.6):

$$\partial \left( n_e T_e \right) / \partial z = - e n_e E_\parallel \tag{3.5}$$

where $T_e$ is the electron temperature. Thermal forces are absent here for the reasons that become clear by integration of the balances above in the next subsection. The electron density $n_e$ obeys quasi-neutrality condition, Eq. (2.2), that in this consideration takes from:

$$n_e = n_i + n_I \tag{3.6}$$

Beyond the impurity cloud $n_e = n_i = n$ and in stationary case the latter is governed by the plasma pressure balance:

$$n \left( T_e + T_i \right) = n_\infty \left( T_e^\infty + T_i^\infty \right) \tag{3.7}$$

where $n_\infty (x)$, $T_e^\infty (x)$ and $T_i^\infty (x)$ are the plasma density, electron and main ion temperatures on the magnetic surface in question far from the cloud. These parameters are considered as prescribed in this study.

### 3.1.3 Heat transport

To obtain the temperatures of charged plasma components, $T_e$, $T_i$ and $T_I$, inside and beyond the impurity cloud, we averaged the heat transport equations (2.10), (2.9) and (2.5) in the direction $y$ as in the case of particle and momentum balances above:

$$\partial q_e / \partial z = Q_{e\perp} - Q_{ei} - Q_{eI} - R \tag{3.8}$$

$$\partial q_i / \partial z = Q_{i\perp} + Q_{ei} - Q_{iI} \tag{3.9}$$

$$\partial q_I / \partial z = Q_0 + Q_{eI} + Q_{iI} - Q_{I\perp} \tag{3.10}$$

Here $q_{e,i,I} = -\kappa_{||}^{e,i,I}\partial T_{e,i,I}/\partial z + 2.5\Gamma_{e,i,I}T_{e,i,I}$ are the densities of the heat fluxes in the plasma components along the field line, $\kappa_{||}^{e,i,I}$ the parallel heat conductivity, the electron flux density is governed by the condition of zero parallel current, $\Gamma_e = \Gamma_i + \Gamma_I$ (see Appendix), with $\Gamma_i = n_i V_i$ being the flux density of the main ions; $Q_{e,i\perp} = 1.5k_\perp^{e,i}\left(T_{e,i}^\infty - T_{e,i}\right)n_{e,i}$ are the heat sources due to transfer perpendicular to the magnetic field in the direction $y$ from regions undisturbed by impurity injection; $Q_{kh} = 3\left(m_k/m_h\right)n_k n_h k_{kh}\left(T_k - T_h\right)$ with $k_{ei} \approx k_{eI} \approx 3.34\Lambda_c e^4/(\sqrt{m_e}T_e^{3/2})$ due to heat exchange between light, subscript $k$, and heavy, subscript $h$, charged particles [59]; $R = \left(L_0 n_0 + L_I n_I\right)n_e$ is the density of the power spent by electrons on excitation and ionization of the neutral and singly ionized impurity, $L_{0,I}$ are the corresponding cooling rates [65]; $Q_0 = 1.5k_{ion}^0 n_0 n_e T_0$ is the heat accumulated by ionized impurity from injected neutrals having the temperature $T_0$; $Q_{I\perp} = 1.5\nu_I n_I T_I$ is the power lost by impurity ions with perpendicular transport and ionization to higher charged states. In Eqs. (3.8) and (3.9) we neglect contributions due to transport in the radial direction $x$ because for typical radial heat conductivities of $10^{19} - 10^{20}\,m^{-1}s^{-1}$ they are small compared to the sink terms $R$ and $Q_{iI}$, respectively.

Normally, the Spitzer-Härm formula is used for parallel heat conductivities: $\kappa_{||} = \sigma n T\tau/m$ with $\sigma \approx 3$ and $\tau \sim T^{3/2}$ being the time between coulomb collisions. However, it has been deduced in the limit of a very small mean free path between collisions, $\lambda \approx \tau\sqrt{T/m}$, compared to the characteristic dimension for the temperature change along the field line, $l_T = 1/|\nabla_{||} lnT|$. For plasmas under consideration it has to be reduced by a factor $\sigma \sim 0.1$ for electrons and $\sigma \sim 0.3$ for ions because of (i) nonlocal effects leading to a reduction in the perturbation caused by the temperature gradient [85] and (ii) deceleration of electrons by ambipolar electric field [86]. In this chapter we use for $\nu_\perp^{e,i}$ prescribed values for characterisation of perpendicular heat transport and consider how their variation affects the results in discussion of calculations.

### 3.1.4 Integrated particle and momentum balances

First, we consider the situation in the SOL where field lines hit the surface of the puffing limiter. The impurity ions created by the ionization of injected neutrals spread along the line towards both the limiter surface and the distant plasma. At any radial position $x$ there is a point in the cloud, $z = z_*$, where the ion mass velocity $V_I$ reduces to zero, see Fig. (3.1). The parallel velocity of ions outcoming from the neutral cloud towards the limiter, $V_I^+$, can be estimated from the following consideration. Similar to Ref. [87] one can

reduce Eqs. (3.3-3.5) to an equation for the impurity ion density gradient:

$$\partial n_I/\partial z = -W/D \tag{3.11}$$

where

$$W = 2k^0_{ion} n_0 n_e V_I - m_i k_{iI} n_i n_I \left(V_i - V_I\right)/m_I - \nu_I \Gamma_I$$
$$D = \left(T_I + T_e n_I/n_e\right)/m_I - V_I^2$$

The impurity ion density decreases in the region between the point $z_*$, where $V_I = 0$, and the limiter surface. Thus, here $\partial n_I/\partial z < 0$ and the terms $W$ and $D$ should be of the same sign. In the neutral cloud, $|z| \le b(x)$, $W > 0$ due to the large positive contribution $k^0_{ion} n_0 n_e$ from the ionization source. Close to $z_*$ impurity velocity is small and, thus, $D > 0$. Right to the cloud, $z > b(x)$, $n_0(x) = 0$ and $W < 0$ because the second contribution from the friction force is negative since lighter main ions move to the limiter faster than heavier impurity ones. Therefore, $D$ has to change its sign at the right boundary of the neutral cloud, $z = b(x)$, i.e., here:

$$V_I = V_I^+ \equiv \sqrt{\left(T_I + T_e n_I/n_e\right)/m_I} \tag{3.12}$$

The presence of the point where $D = 0$ causes a singularity in Eq. (3.11) and requires special approaches to integrate it numerically [84]. We do not pursue here calculations of exact profiles of the parameters, but try to determine their characteristic values in the clouds of neutral and singly ionized impurity, $n^c_{e,i,I}$ and $T^c_{e,i,I}$, being functions of the radial coordinate $x$ only. For this purpose at the given $x$ the transport equations are integrated along the magnetic field, in the direction $z$, under the assumption that $n_{e,i,I} = n^c_{e,i,I}$ and $T_{e,i,I} = T^c_{e,i,I}$ within the ionized impurity cloud, $-l_c^- \le z - z_* \le l_c^+$, and $n_I = 0$ outside the cloud.

First, perform the integration of Eq. (3.3) from the stagnation point $z = z_*$ to the boundaries of the neutral cloud, $|z| = b(x)$. This results in:

$$\Gamma_I^{\pm} = \pm\left[k^0_{ion} n_0 n^c_e - \nu_I n^c_I\right] l_0^{\pm} \tag{3.13}$$

where $n^c_e = n^c_i + n^c_I$ and $\Gamma_I^-$ and $\Gamma_I^+$ are the densities of the impurity ion fluxes at the left and right neutral cloud boundaries, correspondingly. These boundaries, located at the distances $l_0^-$ and $l_0^+$ from the point $z_*$, satisfy the condition:

$$l_0^- + l_0^+ = l_0 \equiv 2b(x) \tag{3.14}$$

Next, by integrating Eq. (3.3) over the left part of the ionized impurity cloud, $z_* - l_c^- \le z \le z_*$, one gets:

$$k^0_{ion} n_0 n^c_e l_0^- = \nu_I n^c_I l_c^- \tag{3.15}$$

where it is taken into account that the ion source exists only within the neutral cloud and $\Gamma_I = 0$ both at $z_*$ and beyond the singly ionized impurity cloud.

To integrate the impurity momentum balance, Eq. (3.4), we assume a piecewise-linear dependence of the impurity flux density $\Gamma_I$ on $z$, with the boundary conditions above. Since the impurity ion pressure reduces to zero at the left boundary of the cloud, this procedure results in:

$$T_I^c n_I^c = -\int\limits_{z_*-l_c^-}^{z_*} eE_\parallel n_I dz + \left[m_i k_{iI} n_I^c \Gamma_i - \left(m_I \nu_I + m_i k_{iI} n_i^c\right) \frac{\Gamma_I^-}{2}\right] l_c^- \quad (3.16)$$

To compute the work of the electric field, the first term on the r.h.s. of Eq. (3.16), we express $E_\parallel$ from Eq. (3.5) and proceed from the integration over $z$ to the integration over $n_I$, by taking into account that $n_I = 0$ beyond the impurity cloud. As a consequence, the result is independent of a particular $z$-profile of $n_I$:

$$\int\limits_{z_*-l_c^-}^{z_*} eE_\parallel n_I dz = T_e^c \int\limits_0^{n_I^c} \frac{n_I}{n_i^c + n_I} dn_I = T_e^c \left[n_I^c - n_i^c \ln\left(n_e^c/n_i^c\right)\right]$$

From Eqs. (3.13) and (3.15) one can express $l_c^-$ through $n_I^c$ and $\Gamma_I^-$ and substitute into Eq. (3.16). This gives a quadratic equation for the outflow velocity of impurity ions from the source towards the distant plasma, $V_I^- \equiv \Gamma_I^-/n_I^c$:

$$\xi \left(V_I^-\right)^2 - \frac{\Gamma_i}{n_i^c} V_I^- - \frac{2U}{m_I} (\xi - 1)\, \zeta = 0 \quad (3.17)$$

where $\xi = 1 + m_I \nu_I / \left(m_i k_{iI} n_i^c\right)$, $U = T_I^c + T_e^c \left[1 - \left(n_i^c/n_I^c\right) \ln\left(1 + n_I^c/n_i^c\right)\right]$, and $\zeta = 1 - n_I^c \nu_I / \left[k_{ion}^0 n_0 \left(n_i^c + n_I^c\right)\right]$. From two real roots we have to choose the negative one corresponding to the impurity ion movement outward the limiter:

$$V_I^- = -\left[\sqrt{\left(\Gamma_i/n_i^c\right)^2 + 8U\xi\,(\xi - 1)\,\zeta/m_I} - \Gamma_i/n_i^c\right] / (2\xi) \quad (3.18)$$

The difference of Eqs. (3.13) for the signs "+" and "−" provides:

$$\Gamma_I^+ - \Gamma_I^- = \left[k_{ion}^0 n_0 \left(n_i^c + n_I^c\right) - \nu_I n_I^c\right] \left(l_0^- + l_0^+\right) \quad (3.19)$$

According to the boundary condition at the right boundary of the neutral impurity cloud:

$$\Gamma_I^+ = n_I^c V_I^+ \quad (3.20)$$

with $V_I^+$ given by Eq. (3.12) where $n_{e,I}^c$ and $T_{e,I}^c$ have to be used. Finally, by using Eq. (3.14), we get an algebraic transcendent equation for the characteristic impurity ion density in the cloud, $n_I^c$:

$$k_{ion}^0 n_0 l_0 \zeta = n_I^c \left(V_I^+ - V_I^-\right) / \left(n_i^c + n_I^c\right) \tag{3.21}$$

This equation has a single positive solution for any other parameters involved. Indeed, both sides of Eq. (3.21) are positive and with growing $n_I^c$ the r.h.s. increases from zero to maximum value $2\sqrt{\left(T_I^c + T_e^c\right)/m_I}$. Physically it means that at a high enough injection rate the pressure gradient and electric field accelerate impurity ions up to their ion sound speed at the boundaries of the neutral cloud. The l.h.s. of Eq. (3.21) decreases with $n_I^c$ down to zero when the ionization of neutrals is completely compensated by the losses of singly charged particles with perpendicular transport and ionization into higher states. It results in the constraint $\zeta \geq 0$ that limits $n_I^c$ from above.

From Eq. (3.13) and the definition of the coefficient $\zeta$ we find the lengths of the regions in the neutral cloud where generated impurity ions move towards the limiter and distant plasma, respectively:

$$l_0^{\pm} = \pm n_I^c V_I^{\pm} / \left(k_{ion}^0 n_0 n_e^c \zeta\right) \tag{3.22}$$

It is easy to check that the sum of $l_0^{\pm}$ given by these expressions satisfies Eq. (3.14). Note that generally $l_0^+ \neq l_0^-$. For example, if the flux of the main ions $\Gamma_i$ is very high and the friction force exceeds significantly the pressure gradient and electric field forces, all impurity ions are pushed to the limiter. Indeed, for $\Gamma_i \to \infty$ Eq. (3.18) results in $V_I^- \to 0$ and Eqs. (3.21) and (3.22) – in $l_0^+ = l_0$ and $l_0^- = 0$. With $l_0^+$ found one can define the position of the stagnation point $z_* = b(x) - l_0^+$ and the extension of the right part of the ionized impurity cloud, where ions move to the limiter, see Fig. (3.1):

$$l_c^+ = l_0^+ - b(x) + x/tan\beta \tag{3.23}$$

By substituting $l_0^-$ into Eq. (3.15), we get the extension of the left part of the ionized impurity cloud, where impurity ions move towards the distant plasma:

$$l_c^- = -V_I^- / \left(\nu_I \zeta\right) \tag{3.24}$$

### 3.1.5 Integrated heat balances

Consider field lines crossing the impurity cloud at a certain radial position $x$. Beyond the ionized cloud the electron and main ion temperatures change from $T_{e,i}^c$ at the cloud boundary to the unperturbed values $T_{e,i}^\infty$ in the

distant plasma. Here we neglect the energy losses on impurity excitation and radiation $R$, as well as the terms due to heat exchange between electrons and ions, $Q_{eI}$, $Q_{iI}$, $Q_{ei} \sim T_e^{-3/2}$, because of high enough electron temperature. Moreover, due to the same reason we keep in the heat flux densities $q_{e,i}$ only the heat conduction contributions since $\kappa_{||}^k = A_{||}^k T_k^{2.5}$. By multiplying both sides of Eqs. (3.8) and (3.9) by $q_k = -\kappa_{||}^k \partial T_k/\partial z$ and using the pressure balance, Eq. (3.7), one gets:

$$dq_k^2 = -3A_{||}^k T_k^{2.5} \nu_\perp^k \left(T_k{}^\infty - T_k\right) n_\infty \frac{T_e{}^\infty + T_i{}^\infty}{T_e + T_i} dT_k \tag{3.25}$$

To integrate this we have to make an assumption on the interrelation between the temperatures of electrons and main ions beyond the cloud. As the simplest possibility we assume a linear dependence:

$$T_e \left(T_i^\infty - T_i^c\right) + T_e^\infty T_i^c = T_i \left(T_e^\infty - T_e^c\right) + T_e^c T_i^\infty \tag{3.26}$$

On the one hand, this relation describes two important limit situations. Thus, for high electron temperature and weak heat exchange between plasma components $T_e$ and $T_i$ are decoupled and do not change a lot along the field lines, i.e. $T_{e,i} \approx T_{e,i}^c \approx T_{e,i}^\infty$, and Eq. (3.26) holds. If, however, $T_e$ is strongly reduced by impurity injection, often coulomb collisions between electrons and ions lead to $T_i \approx T_e$, also reproduced by Eq. (3.26). On the other hand, in an intermediate case it is not of extreme importance to know the exact relation between $T_e$ and $T_i$ since even in both limits considered above the magnitudes of $q_k$ differ by a factor of $\sqrt{2}$ only. This is a consequence of the fact that such a relation is needed just for the temperature dependence of the density in Eq. (3.25). This is, however, in any case, much weaker than that for the parallel heat conduction. With Eq. (3.26) one can find analytically from Eq. (3.25) the densities of the parallel heat fluxes into the cloud, $q_k^c$, see Appendix for details:

$$q_k^c = \sqrt{\frac{6A_{||}^k \nu_\perp^k n_\infty \left(T_k^\infty + T_h^\infty\right) \left(T_k^\infty\right)^{3.5}}{1 + \left(T_h^\infty - T_h^c\right) / \left(T_k^\infty - T_k^c\right)}} \Psi_k \tag{3.27}$$

where $k = (e, i)$, $h = (i, e)$ and the explicit form of the factor $\Psi_k$ is given in Appendix.

By integrating Eqs. (3.8-3.10) over the extension of singly charged impurity cloud, $-l_c^- + z_* \leq z \leq l_c^+ + z_*$, the loss terms in the r.h.s are assumed constant and computed for the characteristic parameter values. The result is represented in the form of the heat balances of plasma components in the

cloud with the total length $l_c = l_c^+ + l_c^-$:

$$q_e^c + Q_{e\perp}^c l_c = \left(Q_{eI}^c + Q_{ei}^c\right) l_c + \left(n_I^c L_I l_c + n_0 L_0 l_0\right) n_e^c + q_e^{lim} \quad (3.28)$$

$$q_i^c + Q_{i\perp}^c l_c = \left(Q_{iI}^c - Q_{ei}^c\right) l_c + q_i^{lim} \quad (3.29)$$

$$1.5 k_{ion}^0 n_0 T_0 n_e^c l_0 + \left(Q_{eI}^c + Q_{iI}^c\right) l_c = Q_{I\perp}^c l_c + q_I^{lim} \quad (3.30)$$

where $Q_{e,i,I\perp}^c$ and $Q_{kh}^c$ are $Q_{e,i,I\perp}$ and $Q_{kh}$, respectively, computed with $n_{e,i,I}^c$ and $T_{e,i,I}^c$; $q_{e,i,I}^{lim} = \gamma_{e,i,I} \Gamma_{e,i,I}^{lim} T_{e,i,I}^c$ with $\gamma_e = 5.5$ and $\gamma_{i,I} = 2.5$ are the densities of heat outflows to the limiter surface, see Ref. [82], p. 94; the densities of the charged particle outflows are estimated as $\Gamma_I^{lim} = \Gamma_I^+$, $\Gamma_e^{lim} = \Gamma_i^{lim} + \Gamma_I^{lim}$ and $\Gamma_i^{lim} = 0.5 n_\infty \sqrt{\left(T_e^\infty + T_i^\infty\right)/m_i}$. Note that the latter estimate corresponds to the case of a SOL plasma undisturbed by impurities [82]; in the case of a strong impurity influence the absolute level of $\Gamma_i^{lim}$ is of minor importance because $q_i^{lim}$ is small compared with other loss channels.

Equations (3.28) and (3.29) mean that the heat brought into the impurity cloud by electrons and main ions with parallel and perpendicular heat transport is spent by coulomb collisions with the impurity ions, excitation of impurity neutral and ionized particles and is lost to the limiter. Impurity ions gain initially the temperature of impurity neutrals, the first term in Eq. (3.30), and are heated up in collisions with electrons and main ions. This energy is lost as singly charged impurities are ionized into the higher charge states, leave the cloud due to perpendicular transport or escape to the limiter. In the core plasma, inside the last closed flux surface (LCFS), the impurity cloud is considered as symmetrical, i.e., $\Gamma_i = 0$, $V_I^- = -V_I^+$ and $q_{e,i,I}^{lim} = 0$ in the equations above.

A numerical solution of integral balance equations is carried out as follows. Calculations are started from the field line crossing the outlet of the injection channel, $x = 0$, where the density of impurity neutrals, $n_0(0)$, is given by the injection intensity. Non-linear algebraic equations (3.21–3.24, 3.28–3.30) for the quantities $T_{e,i,I}^c$, $n_{e,i,I}^c$, $l_c$ are solved by iterations and the set of physically reasonable positive solutions turns out to be unique. By using these characteristics in Eq. (3.2) one can calculate the neutral density deeper in the plasma, $x > 0$, and the whole procedure is repeated further.

## 3.2 Results of calculations and discussion

As an example of the model application we present here the results of calculations done for the conditions of experiments with puffing of methane into the tokamak TEXTOR [36, 88]. Instead of a consideration of the whole family of neutral molecules generated by the disintegration of $CH_4$, such as

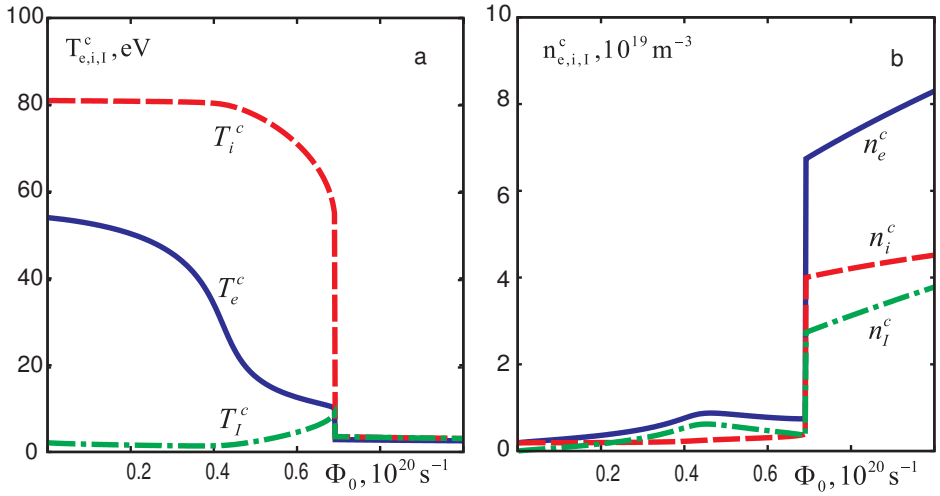


Figure 3.2: Temperatures (a) and densities (b) of plasma components in the impurity cloud vs the influx of impurity neutrals in the core plasma close to the LCFS.

$CH_{1-3}$, only carbon atoms, arising at the end of the reaction chain [89], are taken into account. In the course of decay reactions they acquire a characteristic "temperature" $T_0 \approx 0.8\,eV$ [89], corresponding to the radial velocity $V_0 = 2800\,ms^{-1}$ and a divergence angle $\alpha = 45°$.

### 3.2.1 Modification of plasma parameters with injection intensity

First, consider the modification of the plasma parameters in the impurity cloud at a position slightly closer to the plasma center than the LCFS of the puffing limiter at $x_s = 0.017\,m$ as a function of the total flux $\Phi_0$ of carbon neutrals there. The impurity cloud is symmetric with an extent of the carbon neutral jet $l_0$ of $0.07\,m$ [36]. The plasma parameters far away from the injection position $n_\infty = n_{LCFS} = 1.9 \cdot 10^{18}\,m^{-3}$, $T_e^\infty = T_e^{LCFS} = 54\,eV$ and $T_i^\infty = T_i^{LCFS} = 81\,eV$; the empirical frequencies for perpendicular transport, $\nu_\perp^I = \nu_\perp^{e,i} = 2 \cdot 10^3\,s^{-1}$, were estimated by assuming a particle diffusivity of $1\,m^2 s^{-1}$.

The plasma parameters in the impurity cloud computed as functions of $\Phi_0$ are shown in Fig. (3.2). One can see that for $\Phi_0$ below a level of $4 \cdot 10^{19}\,s^{-1}$ the electron and main ion temperatures are close to $T_{e,i}^\infty$. With increasing $\Phi_0$ the energy losses on ionization and excitation of impurity begin to play a role and $T_e^c$ decreases. When it reduces to a half of $T_e^\infty$, the temperature of main ions starts also to decline due to heat exchange by coulomb collisions

with impurity ions. Because of collisions with the background plasma components the temperature of impurity ions significantly exceeds that of impurity neutrals, but remains noticeably smaller than $T_e$ and $T_i$. This heating up of impurity ions enhances their pressure gradient that spreads the cloud to some extend. The decrease of the electron and main ion temperatures leads to higher heat fluxes into the impurity cloud from the surrounding plasma and results in some increase of the impurity ion temperature at higher injection rates. Both the electron source due to ionization of impurity neutrals and the rise of the main ion density due to pressure equilibration contribute to the increase of the electron density in the cloud, $n_e^c$. At low injection rates the former factor is more important. As the electron temperature decreases at high injection, the ionization rate drops and the latter mechanism becomes dominant, the density of ionized impurity decreases and that of the main ions increases. The critical level of $\Phi_0$ of $4 \cdot 10^{19}\, s^{-1}$ at which a strong cooling of the impurity cloud is initiated agrees well with observations in Ref. [88]. There a significant reduction of the local electron temperature was found for a $CH_4$ puffing rate of $6 \cdot 10^{19}\, s^{-1}$. The discrepancy of 50% can be explained well by the attenuation of carbon atoms in the SOL of puffing limiter.

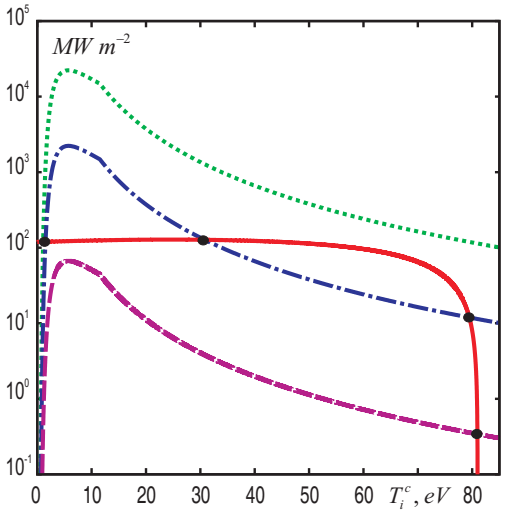


Figure 3.3: $T_i^c$-dependence of the main ion heat influx into the cloud (solid curve) and the heat loss due to collisions with impurity ions for different magnitudes of the neutral puffing rate: $\Phi_0 = 3 \cdot 10^{17}\, s^{-1}$ (dashed curve), $10^{19}\, s^{-1}$ (dash-dotted curve), and $10^{20}\, s^{-1}$ (dotted curve).

There are the sharp abrupt drop of the temperatures and rise of the densities of all plasma components at the neutral influx $\Phi_0 \sim 7 \cdot 10^{19}\, s^{-1}$. This bifurcation like behavior is triggered by the reduction of $T_i$ due to the heat loss by coulomb collisions with impurity ions. The latter increases as $k_{iI} \sim T_i^{-3/2}$ and overcomes the heat source due to the parallel heat conduction from undisturbed plasma. If $T_i$ becomes lower than $T_e$, collisions between the main plasma components lead to the drop of the latter. As a result, the neutral ionization rate is reduced and a new steady state is reached due to the decrease of the impurity ion temperature. This behavior is illustrated in Fig. (3.3). Here solid curve displays the $T_i^c$-dependence of the main ion heat influx into the cloud, $q_i^c$. It is reducing to zero at $T_i^c = T_i^\infty$ but is

nearly constant for $T_i^c < T_i^\infty$. Other curves in Fig. (3.3) show the heat loss from the main ions due to collisions with impurity ones found for different puffing rates $\Phi_0$.

For a very low $\Phi_0 = 3 \cdot 10^{17}\, s^{-1}$, see dashed curve, there is an unique stationary solution with $T_i^c \approx T_i^\infty$ corresponding to the balance between the heat source and loss. If $\Phi_0$ exceeds a critical level of $5.5 \cdot 10^{17}\, s^{-1}$ a bifurcation to three stationary states takes place. Only two of them, those with the highest and lowest magnitudes of $T_i^c$, are stable. This is easy to realize by considering small deviations from stationary temperature values. For stable steady states the difference between source and loss becomes negative (positive) for a positive (negative) deviation and the stationary state is restored. In the intermediate unstable state this difference is of the opposite sign and the initial perturbation is enhanced. For a $\Phi_0$ increasing steadily over the critical level the impurity cloud remains in the state with $T_i^c \approx T_i^\infty$ as, e.g., in the case of the dash-dotted curve found for $\Phi_0 = 10^{19}\, s^{-1}$. This state vanishes abruptly if $\Phi_0$ exceeds the second critical level of $5 \cdot 10^{19}\, s^{-1}$ and the cloud makes a jump-like transition in a state of a very low $T_i^c$ of $2\, eV$, see the dotted curve for $\Phi_0 = 10^{20}\, s^{-1}$. Namely, this jump corresponds to the transition at $\Phi_0 \approx 7 \cdot 10^{19}\, s^{-1}$ in Fig. (3.2).

### 3.2.2 Radial penetration of impurity into the plasma

It is of interest to consider the radial variation of the neutral density and parameters of charged plasma components in the case where impurity jet is intensive enough to induce significant changes in the plasma. Henceforth, the results of calculations for the neutral injection rate $\Phi_0\,(0) = 1.2 \cdot 10^{20}\, s^{-1}$ are presented. In this study the radial profiles of the plasma parameters far from the injection position were approximated by analytical formulas. In the SOL region,

$$\begin{aligned} n_\infty\,(x \le x_s) &= n_{LCFS} \cdot \exp\left[(x - x_s)/\lambda_n\right] \\ T_{e,i}^\infty\,(x \le x_s) &= T_{e,i}^{LCFS} \cdot \exp\left[(x - x_s)/\lambda_T\right] \end{aligned}$$

with the same parameters at the LCFS, $n_{LCFS}$ and $T_{e,i}^{LCFS}$, as in the previous section and the $e$-folding lengths $\lambda_n = 0.022\, m$ and $\lambda_T = 0.04\, m$. In the confined plasma region,

$$\begin{aligned} n_\infty\,(x \ge x_s) &= n_{core} - \left[n_{core} - n_{LCFS}\right] \cdot r^4/a^4 \\ T_{e,i}^\infty\,(x \ge x_s) &= T_{core} \cdot \left(T_{e,i}^{LCFS}/T_{core}\right)^{r^2/a^2} \end{aligned}$$

where $a = 0.46\, m$ is the minor radius of the LCFS, $r = a + x_s - x$, $n_{core} = 3 \cdot 10^{19}\, m^{-3}$ and $T_{core} = 1.2\, keV$ are the central plasma parameters.

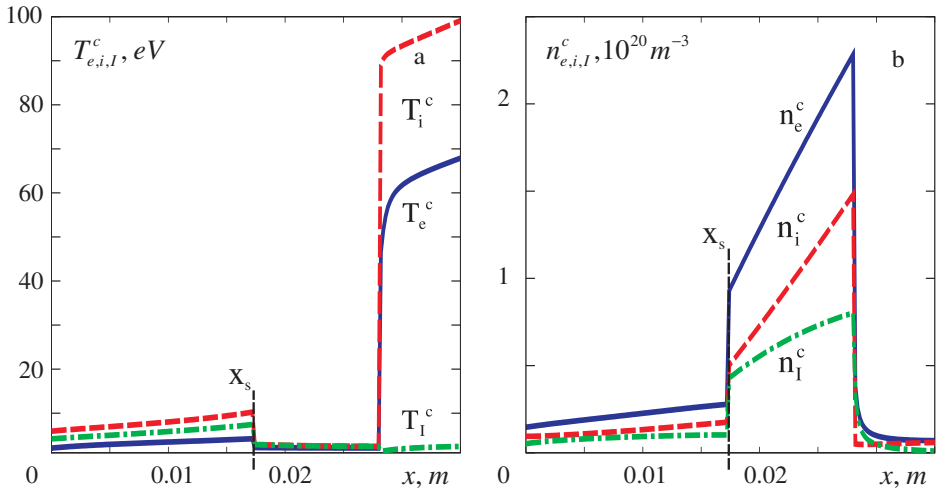


Figure 3.4: Temperatures (a) and densities (b) of plasma components in the impurity cloud vs radial distance from the injection outlet.

Fig. (3.4) represents the temperatures (a) and densities (b) of plasma components in the impurity cloud as functions of the radial distance $x$ from the injection outlet. One can distinguish 4 characteristic regions: two where impurity significantly affects the plasma, within, $x \lesssim 0.017\,m$, and beyond, $0.017\,m \lesssim x \lesssim 0.027\,m$, the SOL; the region with the very sharp variation of the parameters, $0.027\,m \lesssim x \lesssim 0.028\,m$, and the unperturbed plasma, $x \gtrsim 0.028\,m$. In the former two regions the electron temperature is much less than it would be without impurity because of the energy losses on ionization and excitation of impurity neutrals and ions. The main ions are cooled down through coulomb collisions with electrons and impurities. On the contrary, collisions with electrons and main ions heat up heavy impurity ions to several $eV$ from their initial temperature equal to that of neutrals, $T_0$. Inside the SOL the flux of the main ions to the limiter makes a strong contribution to the friction force that restrains the spreading of impurity ions towards the distant plasma. In the opposite direction the impurity cloud is bounded by the limiter surface. Therefore, the total cloud extension, $l_c$, is noticeably smaller inside the SOL than outside. As a result, the total energy losses are lower and temperatures are higher for $x \leq 0.017\,m$ than for $0.017\,m \lesssim x \lesssim 0.027\,m$. This effect is enhanced by approaching to the LCFS since $\Gamma_i$ increases with $x$. Outside the SOL the sink of impurity ions at the limiter vanishes and their density and radiation losses increase. Consequently, the charged particle temperatures drop even lower than in the SOL. Due to the pressure equilibration the main ion density in the impurity cloud rises also. In the region $0.027\,m \lesssim x \lesssim 0.028\,m$ the plasma parameters have very sharp

radial gradients, so that $n^c_{e,i}$ and $T^c_{e,i}$ are restored to their unperturbed values for $x \gtrsim 0.028\,m$. This occurs because the neutral density is reduced here to such a low level, see Fig. (3.5), at which the energy losses do not disturb the plasma. The electron temperature increase leads to a very non-linear growth of the ionization rate coefficient, as $\exp(-I_0/T_e)$, where $I_0$ is the neutral ionization energy; the transition layer between regions of low and high temperatures is very narrow.

The thin interfaces located at $x = 0.017\,m$ and $0.028\,m$ in Fig. (3.4) and separating the plasma regions with strongly different parameters are swelled out in a real plasma with a strong radial transport that arises due to sharp gradients. In the vicinity of these interfaces the zero-dimensional description for perpendicular transport, through introducing the characteristic frequencies $\nu_\perp$, is questionable. Let us estimate to what extent the interfaces can be broaden by considering, e.g., the electron heat balance inside them. By assuming that the contribution to the heat flux divergence from the radial component is comparable to that from the parallel one, i.e. $\kappa^e_x T_e/\delta^2 \approx q^c_e/l_c$, where $\kappa^e_x$ is the radial component of electron heat conductivity, one gets for the characteristic thickness $\delta$ of the interfaces:

$$\delta \approx \sqrt{\kappa^e_x T_e l_c / q^c_e}$$

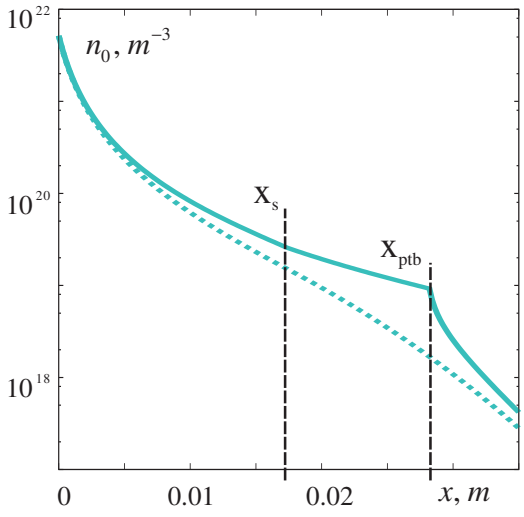


Figure 3.5: Radial profile of the impurity neutral density computed with (solid line) and without (dashed line) taking into account the modifications of local plasma parameters.

For typical values $\kappa^e_x \approx 10^{19} - 10^{20}\,m^{-1}s^{-1}$, $T_e \approx 50\,eV$, $l_c \approx 0.1\,m$ and $q^c_e \approx 100\,MW m^{-2}$, see Fig. (3.3), we obtain $\delta \approx 0.0003 - 0.001\,m$. This is much smaller than the characteristic radial width of $0.01\,m$ of the plasma regions in question. Thus, the present idealized picture with thin interfaces should not be violated significantly with the radial transport explicitly taken into consideration.

Fig. (3.5) presents the calculated radial profile of neutral density. For comparison the profile computed with undisturbed plasma parameters is given by the dashed curve. One can see that all plasma regions described above are characterized by their own e-folding length for the

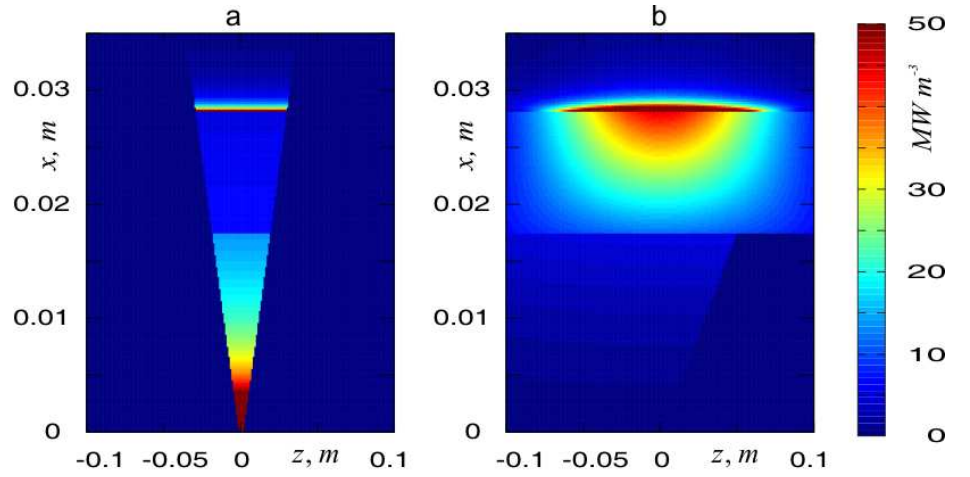


Figure 3.6: Density of radiation emitted by impurity neutrals (a) and singly charged ions (b).

neutral density, $x_0 = -dx/d\ln n_0$. The standard definition for the penetration depth of impurity neutrals as a distance where $n_0$ is reduced by a certain factor with respect to its value at the outlet is not informative any more. It is more instructive to talk about the width $x_{ptb}$ of the plasma region with strongly perturbed parameters. In the case under consideration $x_{ptb} = 0.028\,m$ and to this point $n_0$ decays by a factor of $50 - 100$, see Fig. (3.5). Due to the strong reduction of the electron temperature and of the ionization rate coefficient in the disturbed regions, neutrals penetrate deeper into the plasma core, in spite of the immensely increased $n_e$ in these regions.

The calculations show that the radial extension of the strongly cooled plasma, $x_{ptb}$, increases with $\Phi_0(0)$ and it is of $3\,cm$ for $\Phi_0(0) = 10^{20}\,s^{-1}$. This is comparable with the results of experimental measurements in Ref. [88] where the temperature profile was noticeably disturbed over $5\,cm$ by a methane puffing rate of $8 \cdot 10^{19}\,s^{-1}$.

### 3.2.3 Radiation energy losses from impurity cloud

The density of radiated power is one of the most straightforward characteristics for comparison of numerical results with experimental observations. By using calculated above characteristic values of the electron and impurity ion densities, electron temperature and the lengths of neutral and ionized impurity clouds, one can roughly built up a two-dimensional distribution of

the density of the power radiated by neutrals and singly charged ions,

$$J_0(z,x) = n_0 L_0 n_e^c, \;\; J_I(z,x) = n_I^c L_I n_e^c f_I(z),$$

respectively. Here the parameters $n_0, n_{e,I}^c, L_{0,I}, f_I$ depend on the distance from the injection outlet, $x$. As the impurity neutral density itself, $J_0$ is assumed to be zero outside the neutral cloud, $|z| > b(x)$. The ion radiation profile function $f_I$ is chosen to reproduce experimentally continuous Gaussian-like patterns of the impurity radiation observed experimentally [36]. Beyond the SOL, $f_I = \exp(-z^2/s_I^2)$, with $s_I = l_c/\sqrt{\pi}$ preserving the total amount of impurity ions in the cloud equal to $n_I^c l_c$. Inside the SOL, $x \leq x_s$, a bell-shaped profile is used left to the stagnation point $z_*$ and $f_I = 1$ in the right part of the cloud. A sophisticated consideration of multi-species plasmas, Ref. [87], shows that $n_I$ and, thus, $f_I$ decay by approaching to the limiter surface, but not more than $20 - 30\%$.

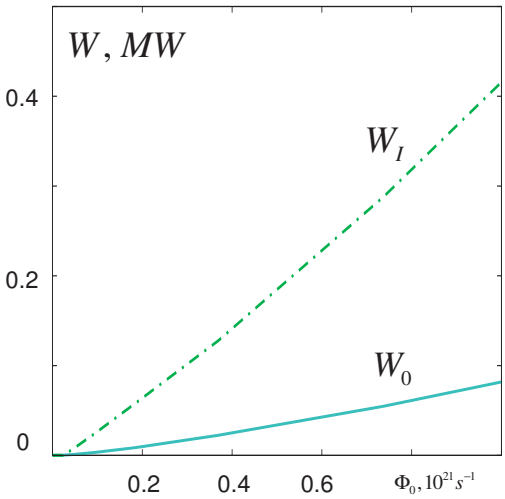


Figure 3.7: Total power radiated by puffed impurity neutrals, $W_0$, and singly charged ions, $W_I$, vs the injection rate.

The result of such a reconstruction is presented in Fig. (3.6). It gives a graphic information about the shape of the impurity cloud, and together with the profiles in Fig. (3.4) allows to consider the role of physical mechanisms involved into the process of impurity penetration both along and across the magnetic field. In the SOL plasma region impurity ions escape fast along field lines to the limiter surface and their density and radiation are low. Beyond the SOL mostly the competition between the friction with the main ions and the impurity ion pressure gradient determines the cloud extent $l_c$. For $T_I \approx T_e$, see Fig. (3.4), the contribution from the electric field to the drag force is by a factor of 3 smaller. This can be seen by analysing the factor $U$ in Eq. (3.18). As soon as the transition region is passed, the cloud shrinks shortly before the neutral jet is completely exhausted.

In Fig. (3.7) the contributions from impurity neutrals and ions to the total radiation power, $W_0$ and $W_I$, respectively, are shown as functions of the injection rate $\Phi_0\,(0)$. Both dependences are close to linear ones. Most easily this can be explained in the case of the neutral radiation. By using

the definition of the neutral flux $\Phi_0$, Eq. (3.1), and the fact that $n_e$ and $L_0$ are assumed constant inside the jet for a given $x$, we obtain:

$$W_0 = \int_0^\infty dx \int_{-b(x)}^{b(x)} dy \int_{-b(x)}^{b(x)} n_e L_0 n_0 dz = \int_0^\infty n_e^c L_0 \frac{\Phi_0}{V_0} dx = \int_0^{\Phi_0(0)} \frac{L_0}{k_{ion}^0} d\Phi_0$$

Both the cooling rate $L_0$ and the ionization rate coefficient $k_{ion}^0$ are functions of $T_e$. However, in the range $20\,eV \leq T_e \leq 10\,keV$ the ratio $L_0/k_{ion}^0$ is about $10\,eV$ and changes by less than 40% [65]. In the region with strongly modified plasma parameters $T_e$ can be noticeably lower and $L_0/k_{ion}^0$ is larger. Nonetheless, the main contribution to $W_0$ is given by the subregion beyond the SOL, $x_s \lesssim x \lesssim x_{ptb}$ where the electron temperature is fixed at a level of $2\,eV$, practically independent of $\Phi_0\,(0)$. Thus, $W_0 \sim \Phi_0(0)$, in principal agreement with data from puffing experiments on the tokamak TEXTOR.

### 3.2.4 Model validation and sensitivity to input parameters

In the present calculations the plasma parameters far from the impurity injection position, $n_\infty$ and $T_{e,i}^\infty$, are assumed as given and undisturbed by impurities. This can be justified for injection rates $\Phi_0\,(0)$ not exceeding significantly $10^{20}\,s^{-1}$. Indeed, the total radiation losses are estimated as $W_{rad} = E_A \Phi_0\,(0)$, where $E_A$ is the impurity radiation potential [33]. Under the conditions in question $E_A \approx 2\,keV$ for carbon and $W_{rad}$ does not exceed 10% of a heating power of $340\,kW$ transported to the plasma edge in TEXTOR ohmic discharges. Thus, impurities should not affect the plasma behavior globally. In additionally heated plasmas this is valid even for significantly higher injection rates.

Another constraint is the consideration of singly charged impurity only. The rate with which higher charge states are generated is characterized by the frequency $\nu_{ion}^1 \equiv k_{ion}^1 n_e$. For $\Phi_0(0) \lesssim 10^{20}\,s^{-1}$ the electron temperature and density are $T_e \approx 1$–$2\,eV$ and $n_e \lesssim 2 \cdot 10^{20}\,m^{-3}$ in the most important region of the impurity cloud, $x_s \lesssim x \lesssim x_{ptb}$. Therefore, $\nu_{ion}^1$ does not exceed $20\,s^{-1}$. This is much less than the frequency $\nu_\perp^I$ characterizing the losses of impurity ions with perpendicular transport. Thus, singly ionized impurities leave the bunch of field lines, piercing the neutral jet, before they are ionized to higher charge states and the latter do not contribute noticeably to energy losses from the cloud.

The examination above demonstrates that $\nu_\perp^I$ is one of the important input parameters for our model. Here we consider how the magnitude of

$\nu_\perp^I$ affects the results. The increase of $\nu_\perp^I$ by a factor of 2 with respect to the assumed above $2 \cdot 10^3\, s^{-1}$ results in the increase of the impurity cloud extension $l_c$ at the beginning of the transition region, $x \gtrsim 0.027\, m$, from 0.054 to $0.058\, m$. A similar reduction of $\nu_\perp^I$ — in the decrease of $l_c$ by a factor of 1.1. At first sight such a behavior seems to be surprising since the smaller $\nu_\perp^I$, i.e., the longer the time $\tau_\perp^I$ that a particle spends at magnetic field lines crossing the cloud, the larger the distance they may travel. However, this distance is determined by the particle velocity $V_I$ too, see Eq. (3.15). The increase of $\tau_\perp^I$ leads to larger energy losses, the temperatures are decreased and impurity friction with the main ions is enhanced. As a result, $V_I$ and, hence, $l_c$ are reduced. The temperature drop makes the ionization of impurity neutrals less effective and they penetrate deeper into the plasma in the radial direction.

The heat influxes into the cloud from undisturbed plasma are proportional to $\sqrt{A_{||}^{e,i}\nu_\perp^{e,i}}$, see Eq. (3.27). One can expect that the lower $q_k^c$ and, thus, the temperatures of charged particles in the cloud, the deeper the penetration of impurity neutrals. This has been confirmed in calculations with different $\nu_\perp^{e,i}$ and $A_{||}^{e,i}$, however, the results are more sensitive to the electron heat transport. Thus, the characteristics of perpendicular transport of charged particles and energy impact noticeably the results of our calculations. A future development of the model has to include a more sophisticated description of these physical processes, taking into account, e.g., the radial transport, which is very different in the edge region in the L- and H- confinement modes.

The temperature of impurity neutrals, $T_0$, is the input parameter whose impact on the results was also studied. An increase of it results in the rise of the neutral velocity. For the same influx the neutral density at the outlet changes as $n_0\,(0) \sim 1/V_0 \sim 1/\sqrt{T_0}$. In spite of this, the region with strongly perturbed plasma extends in the radial direction always up to the position where $n_0 l_0$ drops to the same critical level of $10^{18}\, m^{-2}$ for the conditions discussed in the previous subsection. This is in a qualitative agreement with Fig. (3.2) where a sharp change in the electron temperature and density occurs at a critical $\Phi_0$. For the temperature of impurity ions the magnitude of $T_0$ does not play a noticeable role because $T_I > T_0$ due to collisions with electrons and main ions. As we have already seen, this effect is of importance for the transport of impurity ions along the magnetic field.

## 3.3 Conclusions

In this chapter we considered in stationary zero-dimensional approximation the modifications of plasma parameters in the cloud of neutral and singly

ionized impurity particles close to the injection position. Higher charge states are neglected in the model since their source inside the impurity cloud is too weak, for the corresponding range of of parameters discussed above. Developed approach allows to integrate the fluid transport equations within the regions where the plasma is significantly affected by impurity neutrals and singly charged ions. The initial system of differential equations is reduced to a set of non-linear algebraic equations for the characteristic densities and temperatures of the plasma components and for the cloud dimensions.

The spreading of charged impurity along the magnetic field is demonstrated to be determined, on the one hand, by the competition between the electric force and the pressure gradient and, on the other hand, the friction with the main ions and finite, due to perpendicular transport, lifetime on the field line. The temperature of impurity ions is found by taking into account the heat exchange between charged particles and exceeds significantly the temperature of impurity neutrals. This enhances strongly the impurity pressure gradient. Produced force, pushing impurity ions out of the cloud, under conditions in question overcomes the drugging force from parallel electric field. This has to be accounted in further development of approaches to modeling of impurity injection.

At high puffing rates the radial variation of plasma parameters in the impurity cloud has a complex pattern. The radial extension of the region with a perturbed plasma is determined by the decrease of the product of the neutral density and the neutral cloud dimension to a certain critical level. In considered range of injection rates the total radiated power does not exceed 10% of the heating power transported to the plasma edge. Therefore, impurity does not affect the plasma behavior globally and the model assumption of undisturbed plasma parameters far from the injection position is valid. In spite of strong changes in the local electron density and temperature the local radiation losses grow up roughly linear with the injection rate, in agreement with observations in puffing experiments on the tokamak TEXTOR.

# Chapter 4

# Time-dependent modeling of impurity spread in hot plasma

Calculations performed with stationary model have shown that a significant disturbance of the electron density occurs already at injection rates noticeably lower than those provoking an appreciable reduction of the electron and main ion temperatures in the impurity cloud. On the other side, the times typical for puffing and MGI experiments, may not be enough for the impurity spread coming to any stationary state. Moreover, characteristic time scales of impurity transport can be comparable with the life-times of low charge states. The time dynamics of the spreading of neutral and charged impurity species from the injection position under such conditions, with strongly perturbed density, but weakly affected temperatures of electrons and main ions, is considered in this chapter.

## 4.1 Model

### 4.1.1 Impurity neutral transport

Fig. (4.1) shows schematically a jet of impurity neutrals injected into tokamak confined plasma through a puffing valve and cross- sections by a magnetic flux surface of shells where impurity ions of different charges are mostly localized. The valve outlet is tangential to the magnetic field and defines the last closed flux surface (LCFS). Neutrals are assumed to move with the speed $V_0$ in the direction $x$ across the magnetic surfaces towards the plasma core. The neutral jet has a square cross-section in the $(y, z)$-plane, $|y| \leq b, |z| \leq b$, with a constant side half-width $b$. The neutral density $n_0$ is homogeneous inside the jet cross-section and vanishes outside it. Under as-

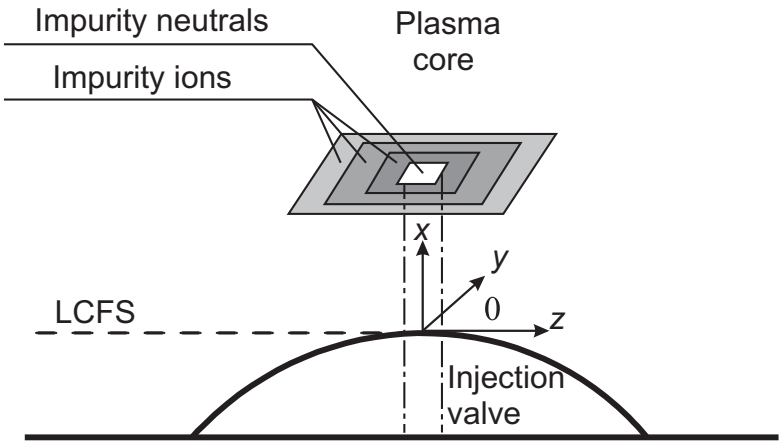


Figure 4.1: Impurity injection scheme and cross-sections of neutral jet and shells of ions with different charges by a flux surface.

sumptions above the variation of $n_0$ with time $t$ and coordinate $x$ is described by the continuity equation (2.1):

$$\frac{\partial n_0}{\partial t} + V_0 \frac{\partial n_0}{\partial x} = -k^0_{ion} n_e n_0 \tag{4.1}$$

where $k^0_{ion}$ is the ionization rate coefficient. The electron density $n_e$ is disturbed by the presence of impurity ions generated by ionization of neutrals and is determined from the quasi-neutrality condition, Eq. (2.2).

The ionization rate coefficient decreases by several orders of magnitudes with the decrease of the electron temperature below $30\,eV$, and the effects of plasma cooling due to energy losses on ionization and radiation of impurity have to be taken into account. However, such low temperatures are achieved at so high injection intensities for those $n_e$ is increased already by many times. In this chapter we consider the behavior of neutral and charged impurity in situations where the increase of $n_e$ may be of importance for impurity spreading but the effects due to reduction of $T_e$ are still negligible. Conditions under which this description has to be complemented by thermal balances of electrons and main plasma ions are discussed below.

### 4.1.2 Charged impurity transport in shell approximation

Impurity ions of low enough charges under consideration disappear due to ionization before they spread from the injection position over the whole magnetic surface. This means that their life-time is noticeably less than the characteristic time required for the transport along the magnetic field. It is

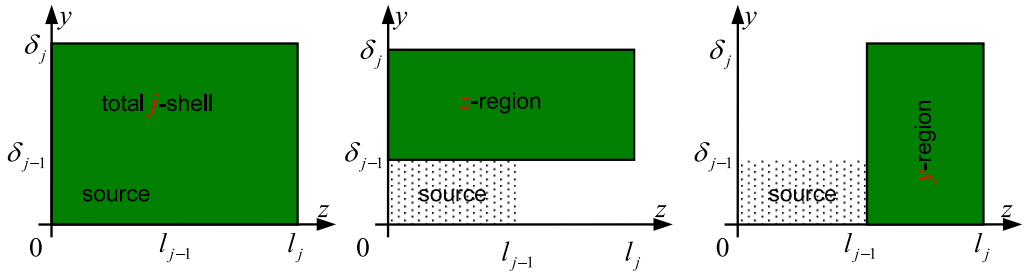


Figure 4.2: Regions in the impurity ion shell cross-section used by the integration of transport equations.

expected that during such times effects from the radial transport across the flux surfaces, $x$-direction in Fig. (4.1), are weak. Therefore, we do not treat this transport contributions explicitly but replace them in Eqs. (2.3-2.5) with loss terms characterized by a frequency $\nu_x$. We analyse the impact of the $\nu_x$ absolute level on the results further.

For any particular charge state $j$ one can subdivide the whole magnetic surface into the source region, $|y| \leq \delta_{s,j}$, $|z| \leq l_{s,j}$, where the $j$-ions are generated by the ionization of the $(j-1)$-ones, and the decay zone, $|y| > \delta_{s,j}$, $|z| > l_{s,j}$, where their density $n_j$ drops due to the ionization into the $(j+1)$-state. In the present shell model this decay is assumed as an exponential one with non-stationary characteristic decay lengths $\delta_{d,j}(t)$ and $l_{d,j}(t)$ in the $y$ and $z$ directions, correspondingly. The source region of the $j$-ions coincides with the total localization zone of the $(j-1)$-ones and the recurrent relations $\delta_j \equiv \delta_{s,j} + \delta_{d,j} \approx \delta_{s,j+1}$ and $l_j \equiv l_{s,j} + l_{d,j} \approx l_{s,j+1}$ hold. Inside the source region $n_j$ is assumed to be homogeneous and is a function of time, $n_{s,j}(t)$. The parallel component of the flux density is zero at the symmetry plane $z = 0$ and increases linearly with $z$ inside the source region to the value $\Gamma_{s,j}(t)$ at the boundary of the decay region. Otherwise, $\Gamma_{z,j}$ varies similarly to $n_j$. The impurity temperature $T_j$ is homogeneous within the whole $j$-shell.

To get equations describing the time evolution of the parameters $n_{s,j}$, $l_{d,j}$, $\delta_{d,j}$, $\Gamma_{s,j}$ and $T_j$ we select three regions: the total plane, $0 \leq (|y|, |z|) < \infty$, the $y$-region $0 \leq |y| < \infty$, $l_{s,j} \leq |z| < \infty$, and the $z$-region $\delta_{s,j} \leq |y| < \infty$, $0 \leq |z| < \infty$, see Fig. (4.2). With the assumed above form of the solution

profiles, the integration of Eq. (2.3) over these regions gives, respectively:

$$\begin{aligned} d\left(n_{s,j}l_j\delta_j\right)/dt &= k_{ion}^{j-1}n_e n_{s,j-1}l_{j-1}\delta_{j-1} - \nu_I^j n_{s,j}l_j\delta_j & (4.2)\\ d\left(n_{s,j}l_{d,j}\delta_j\right)/dt &= \left(\Gamma_{s,j} - \nu_I^j n_{s,j}l_{d,j}\right)\delta_j & (4.3)\\ d\left(n_{s,j}l_j\delta_{d,j}\right)/dt &= \left(D_y/\delta_{d,j} - \nu_I^j\delta_{d,j}\right)n_{s,j}l_j & (4.4)\end{aligned}$$

the integration of Eq. (2.4) over the total plane of magnetic surface in question provides:

$$\begin{aligned} & d\left[\Gamma_{s,j}\left(l_{s,j}/2 + l_{d,j}\right)\delta_j\right]/dt = k_{ion}^{j-1}n_e\Gamma_{s,j-1}l_{s,j}\delta_{s,j}/2 \\ & + \left(n_{s,j}T_j + \int_0^\infty jeE_z n_j dz\right)\frac{\delta_j}{m_I} \\ & - \left(k_{ij}n_i + \nu_I^j\right)\Gamma_{s,j}\left(l_{s,j}/2 + l_{d,j}\right)\delta_j \qquad (4.5)\end{aligned}$$

and the same procedure for Eq. (2.5) by using Eq. (4.2) results in:

$$\begin{aligned} dT_j/dt &= k_{ion}^{j-1}n_e\left(n_{s,j-1}/n_{s,j}\right)\left(T_{j-1} - T_j\right)\left(l_{s,j}/l_j\right)\left(\delta_{s,j}/\delta_j\right) \\ &\quad + 2k_{ij}n_i\left(T_i - T_j\right) + 2k_{ej}n_e\left(T_e - T_j\right) \qquad (4.6)\end{aligned}$$

with $\nu_I^j \equiv k_{ion}^j n_e + \nu_x$ where the latter frequency characterises radial transport. To deduce these equations the $j$-ions are assumed to make the dominant impurity contribution to the electron density in their shell, i.e. $n_e \approx n_i + jn_j$ there. This allows to compute the work of the electric field, the third term on the r.h.s. of Eq. (4.5). With $E_z$ defined from Eq. (2.6) in the assumption of non-modified electron, $T_e$, and main ion, $T_i$, temperatures, we proceed from the integration over $z$ to the integration over $n_j$, decaying from $n_{s,j}$ in the source to zero in the distant plasma:

$$\int_0^\infty jeE_z n_j dz = -T_e\int_{n_{s,j}}^0 \frac{j^2 n_j}{n_i + jn_j}dn_j = T_e\left[jn_{s,j} - n_i\ln\left(1 + \frac{jn_{s,j}}{n_i}\right)\right] \quad (4.7)$$

## 4.2 Numerical approach for solving of partial differential equation systems with interlaced variables

Eq. (4.1) is approximated by finite differences with steps $\tau$ and $h$ in time and in the $x$-direction, respectively. With the initial condition $n_0\left(0,x\right) = 0$ and $n_0\left(t,0\right)$ prescribed by the impurity injection rate, an implicit scheme:

$$n_0\left(t,x\right) = \frac{n_0\left(t-\tau,x\right)/\tau + V_0 n_0\left(t,x-h\right)/h}{1/\tau + V_0/h + k_{ion}^0 n_e\left(t,x-h\right)} \quad (4.8)$$

is used to obtain the neutral density as a function of $t$ and $x$. Since the neutral velocity $V_0$ is finite, one has to take additionally into account that the relations (4.8) are relevant in the existence domain $x \leq V_0 t$ and $n_0(t,x) = 0$ beyond that.

In the system of ordinary differential equations (4.2-4.6) the dependent variables $n_{s,j}$, $\Gamma_{s,j}$, $T_j$, $l_{d,j}$ and $\delta_{d,j}$ are interlaced in a complex implicit way both in the rhs and in the time derivatives. This system can be written in a generic form:

$$\frac{d}{dt}\overrightarrow{Y}(\overrightarrow{X}) = \overrightarrow{F}(t, \overrightarrow{X}) \tag{4.9}$$

where $\overrightarrow{Y}$ and $\overrightarrow{F}$ are non-linear vector functions of the solution vector $\overrightarrow{X}$ with the dimensionality $5j_{max}$. Due to the non-linearity of $\overrightarrow{Y}(\overrightarrow{X})$ a numerical integration of such a system is not straightforward and to do this we proceed to the variation of the solution vector after a time step $\tau$, $\overrightarrow{\zeta} = \overrightarrow{X}(t) - \overrightarrow{X}(t-\tau)$. By assuming $\overrightarrow{\zeta}$ small, we get in a linear with respect to $\tau$ approximation:

$$\frac{d\overrightarrow{Y}}{dt} = \frac{\partial\overrightarrow{X}}{\partial t} \cdot \frac{\partial\overrightarrow{Y}}{\partial\overrightarrow{X}} \approx \frac{\overrightarrow{\zeta}}{\tau} \cdot \frac{\partial\overrightarrow{Y}}{\partial\overrightarrow{X}}(t-\tau),$$
$$\overrightarrow{F}(t) \approx \overrightarrow{F}(t-\tau) + \tau \cdot \frac{\partial\overrightarrow{F}}{\partial t}(t-\tau) + \overrightarrow{\zeta} \cdot \frac{\partial\overrightarrow{F}}{\partial\overrightarrow{X}}(t-\tau)$$

By substituting these expansions into the set of Eqs. (4.9), one can reduce it to the system of linear algebraic equations for $\overrightarrow{\zeta}$:

$$\overrightarrow{\zeta} \cdot \frac{\partial}{\partial\overrightarrow{X}}\left(\frac{\overrightarrow{Y}}{\tau} - \overrightarrow{F}\right) \approx \overrightarrow{F} + \tau\frac{\partial\overrightarrow{F}}{\partial t} \tag{4.10}$$

where the vectors $\overrightarrow{Y}$ and $\overrightarrow{F}$ and their partial derivatives are calculated at the time moment $t-\tau$. For the case in question, these derivatives have been found in an analytical form after a cumbersome but straightforward algebra. This noticeably saves computational time. The system of Eqs. (4.10) can be solved by a standard method, e.g., Gauss or iteration ones, see, e.g., Ref. [91] (p. 53).

As initial conditions we assume zero densities for all impurity charge states inside the plasma. Calculations are started from the radial position at the outlet of the valve where the density of impurity neutrals, $n_0(t, x = 0)$, is given by the injection intensity. Then, for $x = 0$ the system of Eqs. (4.2-4.6) is solved, by using the quasi-neutrality condition (2.2), to find the time evolution of the parameters $n_{s,j}$, $\Gamma_{s,j}$, $T_j$, $l_{d,j}$ and $\delta_{d,j}$. After this, Eqs. (2.2), (4.2-4.6), and (4.8) are applied to get the time dependence of all parameters

at $x = h$. The procedure is repeated consequently for larger $x$. As a result, the penetration process of neutral and low ionized impurity into the plasma is described self-consistently.

To find a stability criteria for the numerical scheme used in Eq. (4.8) we have applied a standard von Neumann's approach [92] by considering spatial perturbations in the form $\exp(2\pi ix/\lambda)$. This results in the following constraint:

$$k^0_{ion} n_e \left(2 + k^0_{ion} n_e \tau\right) + 2\left[1 + \cos\left(2\pi h/\lambda\right)\right]\left(1 + k^0_{ion} n_e \tau + V_0 \tau/h\right) V_0/h > 0$$

This is valid for any $\tau$, $h$ and perturbation wave length $\lambda$, i.e., the scheme (4.8) is absolutely stable. To analyse the stability of the used approach for solve the system of Eqs. (4.9) one has to calculate the determinant of the transition matrix relating $\overrightarrow{X}(t+\tau)$ and $\overrightarrow{X}(t)$. This will provide a polynomial equation of a high order for $\tau$ which have to be solved numerically. Such procedure would extremely overcomplicate the approach. Therefore we look for an appropriate time step by comparing solutions for $\tau$ and $2\tau$. The requirement of a 1%-accuracy results in $\tau \leq 10^{-10}\, s$ for the problem in question.

## 4.3 Results of calculations and discussion

Here the results of calculations performed for the conditions of argon seeding experiments in tokamaks TEXTOR, JT-60 and JET [38, 93–96]. are presented.

### 4.3.1 Spreading of impurity ions on magnetic surfaces

First, let us consider the spreading of ionized argon over a magnetic surface with the following plasma parameters before impurity sinjection: $n_i = n_e = 6 \cdot 10^{18}\, m^{-3}$, $T_i = T_e = 150\, eV$. These parameters are representative for the range of plasma densities of $0.4 - 1 \cdot 10^{19}\, m^{-3}$ and temperatures of $100 - 200\, eV$ typical at LCFS in experiments with argon injection mentioned above [38, 93–96] performed on tokamaks with quite different dimensions, design and operational conditions (of course, this similarity of conditions may be a simple coincidence). The neutral argon jet has the half-width $b = 0.005\, m$ and the neutral density at radial position in question is of $n_0 = 1.8 \cdot 10^{19}\, m^{-3}$. The poloidal transport of impurity ions is characterized by the particle diffusivity $D_y = 1\, m^2 s^{-1}$. This is a typical level of radial anomalous diffusivity in the L confinement mode; under H-mode conditions a value by an order of magnitude smaller is normally expected [97]. In addition to the great uncertainties of experimentally measured impurity

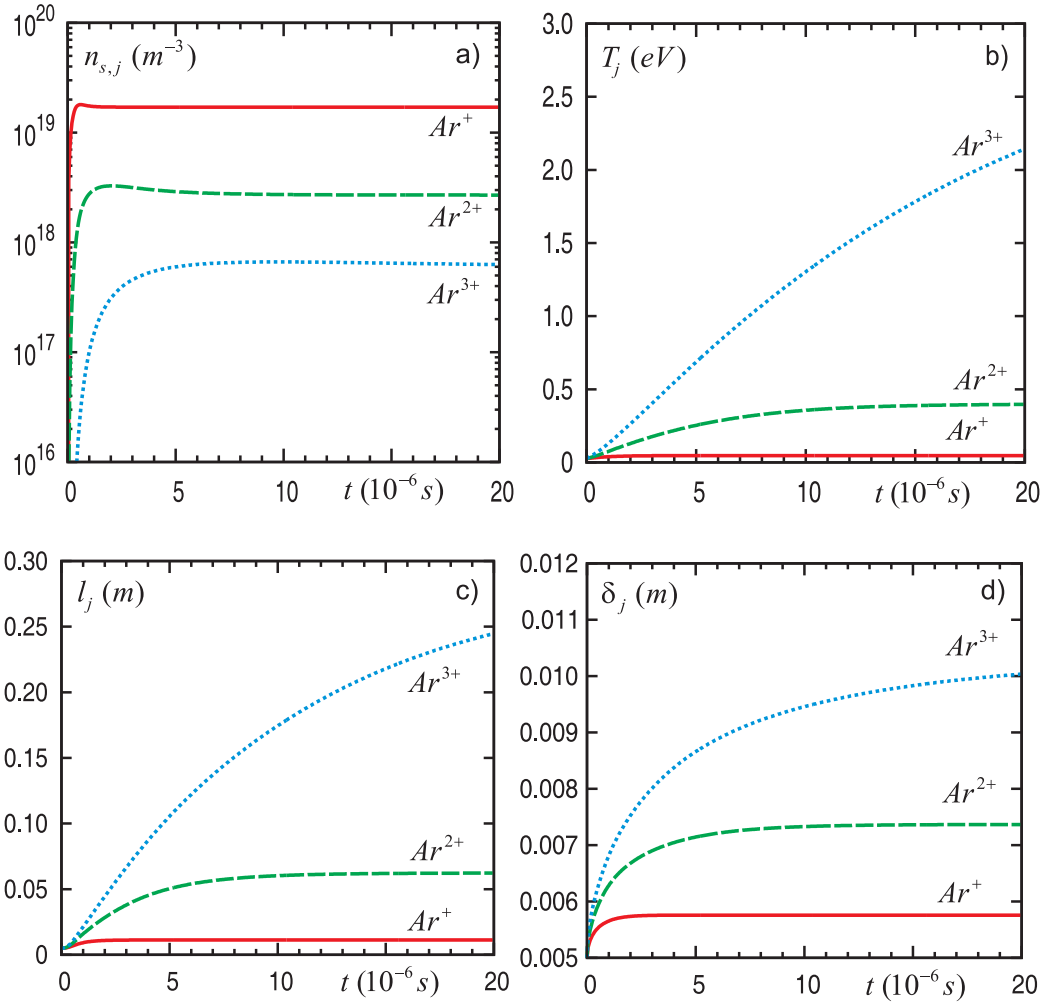


Figure 4.3: Time evolution of the densities (a), temperatures (b), half-lengths (c) and half-widths (d) of the shell cross-sections for different argon ions.

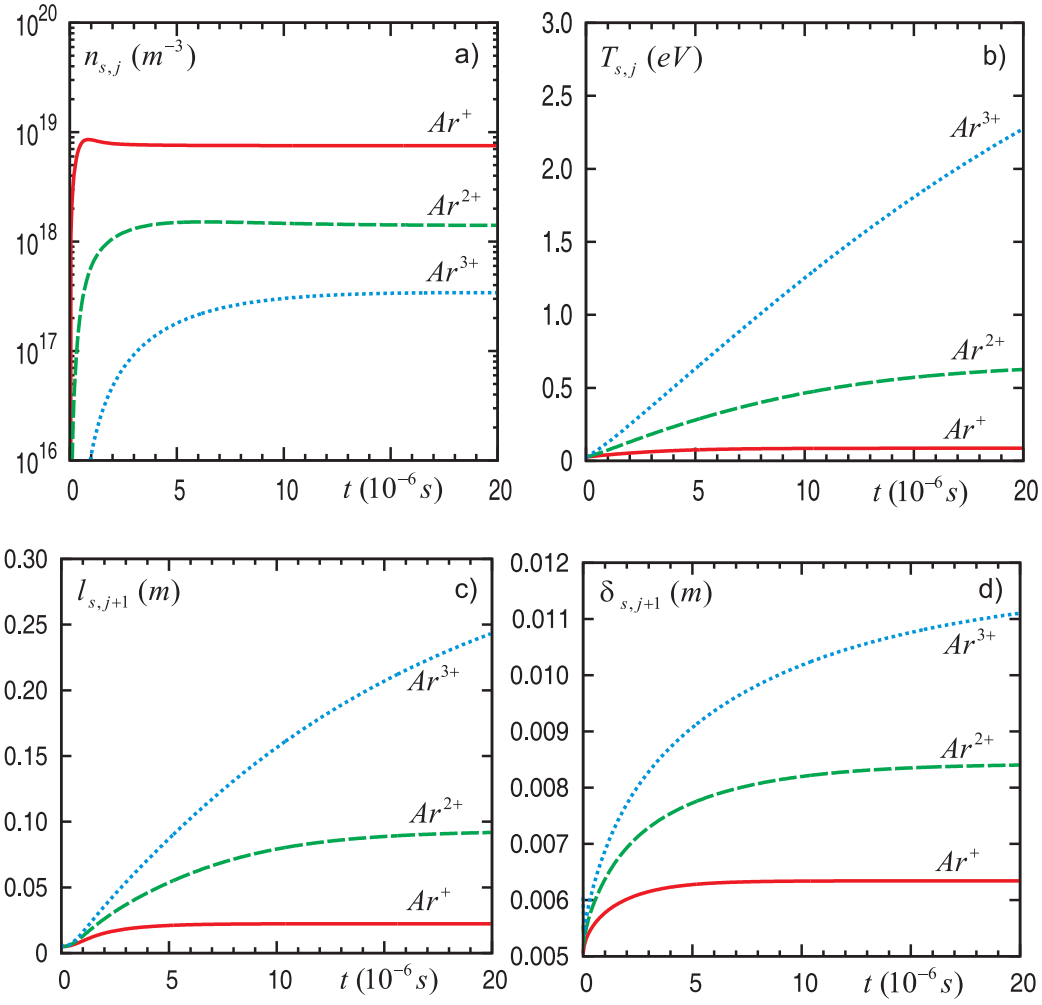


Figure 4.4: Time evolution of the densities (a), temperatures (b), half-lengths (c) and half-widths (d) of the shell cross-sections for different argon ions computed by neglecting the modification of $n_e$ in the presence of impurity.

transport characteristics one can also question the applicability of these data for the poloidal direction. Nevertheless, the particular choice of $D_y$ above does not affect most results of calculations since these are very insensitive to the $D_y$ magnitude in a very broad range up to $20\,m^2s^{-1}$, see next section. To account for the radial transport we apply $\nu_x = 2 \cdot 10^3\,s^{-1}$ estimated for the maximum transport level in the L-mode. An extreme roughness of this estimate is again excused by the weak dependence of the results on $\nu_x$ in a range up to $10^5\,s^{-1}$, see Fig. (4.7).

Fig. (4.3) shows the calculated parameters for 1, 2, 3-times ionized argon particles and the dimensions of their shells as functions of time: the characteristic densities $n_{s,j}$ (a) and temperatures $T_j$ (b), the half-widths of the impurity spread along the magnetic field, $l_j$, (c), and in the poloidal direction, $\delta_j$, (d). One can see that the density of each $j$-charge state is significantly lower than that for the $(j-1)$-one and it spreads over a larger volume. With increasing charge it needs more and more time to achieve stationary states.

One can see in Fig. (4.3) that in the shell of singly charged argon ions their density and, thus, the electron one exceeds significantly the unperturbed level of the plasma density. Thus, it is crucially important to consider the modification in $n_e$ by analysing the penetration of seeded impurities into the plasma. The equilibrium impurity ion densities are determined by the balance between generation and loss due to ionization processes and is achieved within several ionization times of $1/(k^j_{ion} n_e)$.

At the initial stage of the impurity spreading process, when $T_j \approx T_{j-1}$, the rate of the $T_j$ rise due to Coulomb collisions with the background plasma particles is of $2\,(k_{ij} n_i + k_{ej} n_e)$. The stationary value of the temperature (see Appendix):

$$T^{t\to\infty}_{s,j} = \frac{T_{j-1}\nu^j_I/2 + T_i k_{ij} n_i + T_e k_{ej} n_e}{\nu^j_I/2 + k_{ij} n_i + k_{ej} n_e} \tag{4.11}$$

is, however, determined not only by the temperatures of the main plasma components but also by $T_{j-1}$ and the frequency $\nu^j_I$, characterizing the vanishing of impurity particles. This is especially fast for ions of low charges, and their stationary temperatures are significantly less than $T_{i,e}$. This fact has to be taken into account in diagnostic applications, by determining the temperature of the main ions from Doppler broadening of impurity spectral lines. With increasing ion charge the ionization rate coefficient and, hence, $\nu^j_I$ decrease, while the Coulomb collision frequencies rise as $j^2$. Therefore, the higher charge states can be warmed up to temperatures close to those of the main plasma components. For example, under conditions in question the calculated stationary temperatures for the species $Ar^{4+} \div Ar^{7+}$ are 13, 33, 83 and $130\,eV$, correspondingly.

The approaching of the impurity ion shell extension along the magnetic field, $l_j$, to its stationary level is slower than that of $n_{s,j}$ but faster than in the case of $T_j$. This is explained by the fact that both the gradient of impurity ion pressure, proportional to $T_j$, and the electric field, controlled by $n_{s,j}$, accelerate ions away from their source region and control the shell spreading along field lines. Stationary values of the shell lengths are determined by the balance between these forces and friction due to Coulomb collisions with the main ions.

The initial rate of the increase in $\delta_{d,j}$ is governed by the diffusivity $D_y$ and, therefore, is the same for all charges. The approaching of the shell width in the direction $y$, $\delta_j$, to its final value is controlled by the ionization frequency $k_{ion}^j n_e$. For $j = 1$ the electron density is essentially increased by $n_1$ and the time evolution of $\delta_1$ mimics that of $n_{s,1}$. For larger $j$ the perturbation in $n_e$ is much weaker. In stationary states $\delta_{d,j} = \sqrt{D_y/\nu_I^j}$, as it follows from Eq. (4.4), see Appendix.

For comparison, the results of calculations without taking into account the change in the electron density, i.e. with $n_e(t) \equiv n_i$, are shown in Fig. (4.4). One can see that in the case of singly charged ions the neglection of the electron density perturbation leads to noticeable overestimation of the shell dimensions and temperature and underestimation of the ion density. The higher the ion charge, the smaller the effect from the distortion in $n_e$ although in the case of impurity ion density it is significant for all $j$ under consideration.

### 4.3.2 Stationary characteristics of impurity ions

The consideration above has shown that the characteristic duration of transient processes in the low charge impurity states in question does not exceed a hundred of $\mu s$. This duration is controlled by the ionization time $1/\left(k_{ion}^j n_e\right)$ and, thus, depends on the plasma conditions and impurity species. Nonetheless, it is normally too short for many phenomena in plasmas, e.g., global energy confinement. For those only the impurity parameters in stationary states could be of interest. (The reduction of described above model to the stationary case is given in Appendix.) Here we consider the variation of stationary values with the impurity neutral density $n_0$ and characteristics of perpendicular transport, $D_y$ and $\nu_x$, introduced before as free parameters into the model. Rise of $n_0$ leads to increasing densities of the charged impurity and electrons, and, thus, to the decrease of the ionization and heat transfer times. This results in even smaller durations of transient processes in the impurity shells.

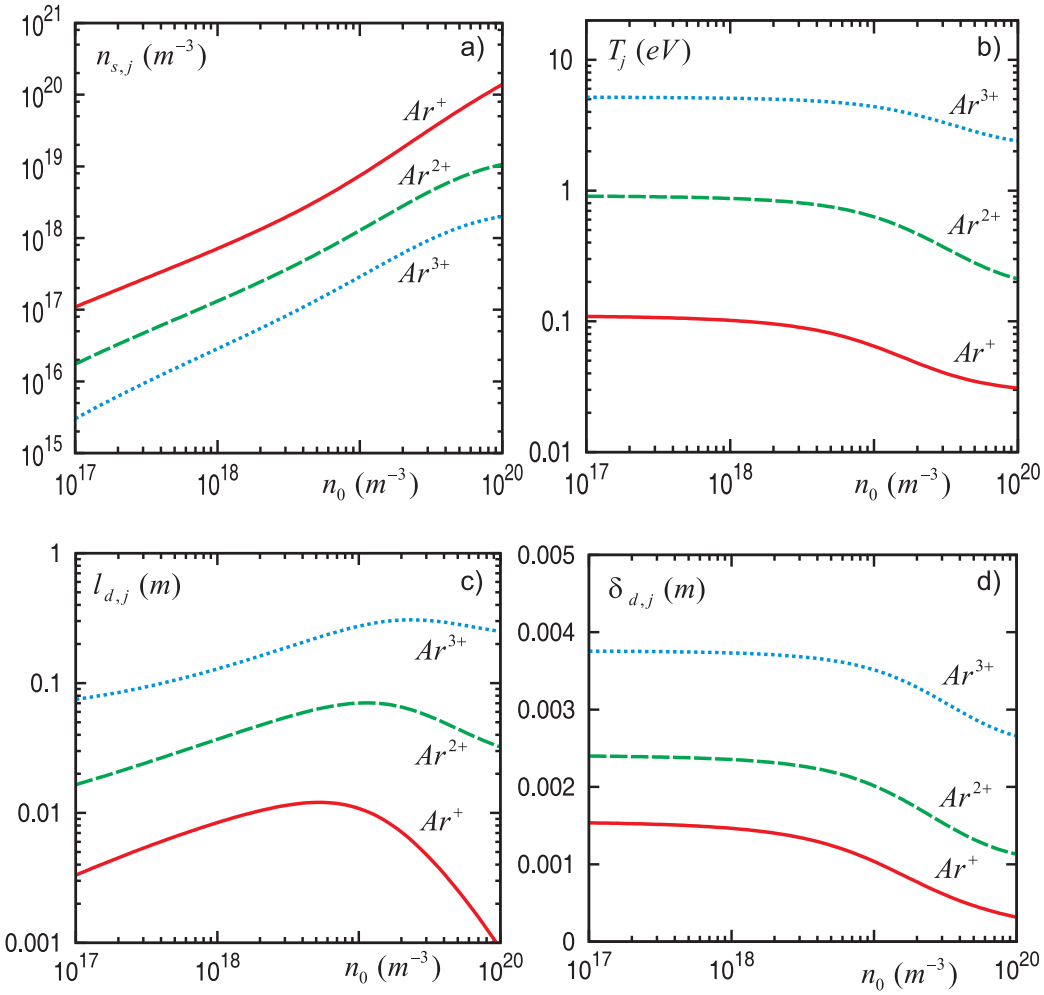


Figure 4.5: Variation with the neutral density $n_0$ of the densities (a), temperatures (b), density decay lengths (c) and widths (d) for different argon ions.

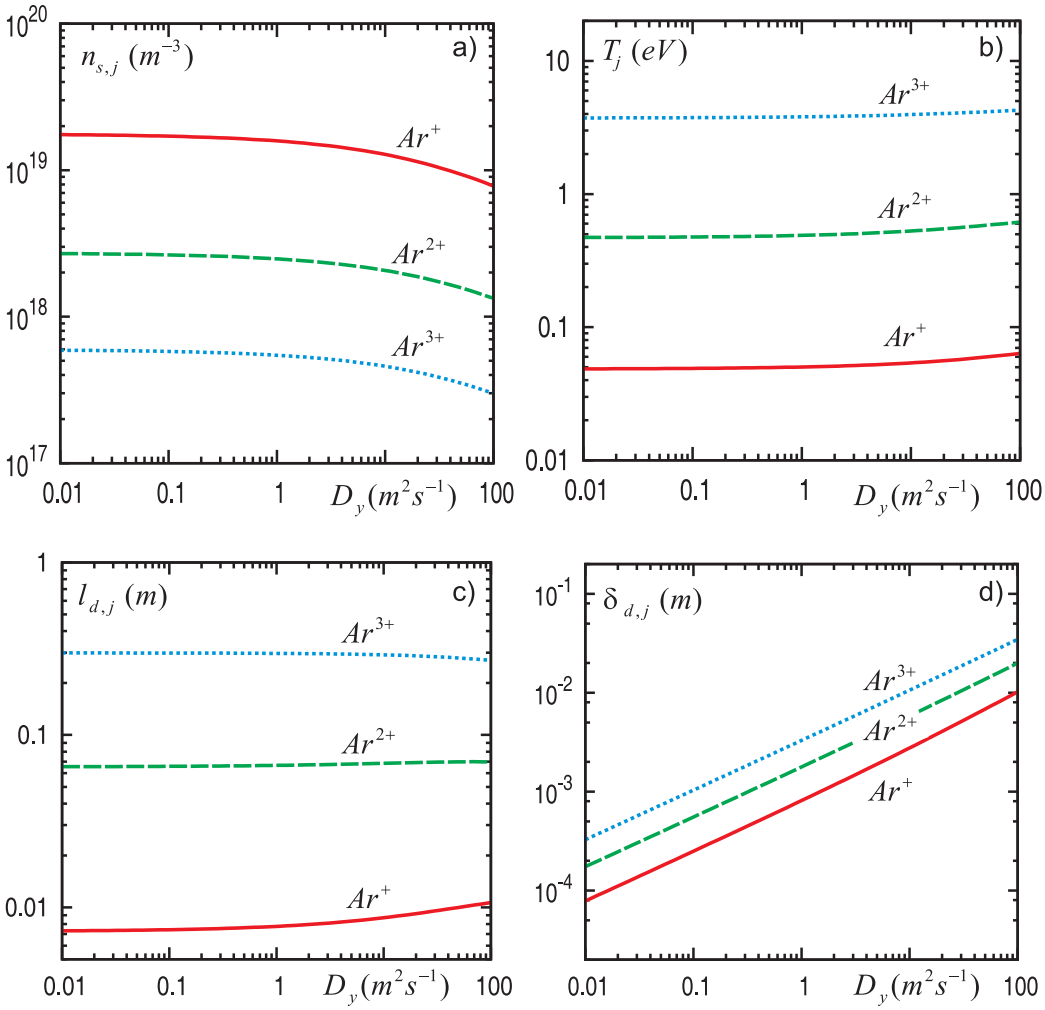


Figure 4.6: Variation with the diffusivity across the field lines, $D_y$, of the densities (a), temperatures (b), density decay lengths (c) and widths (d) for different argon ions.

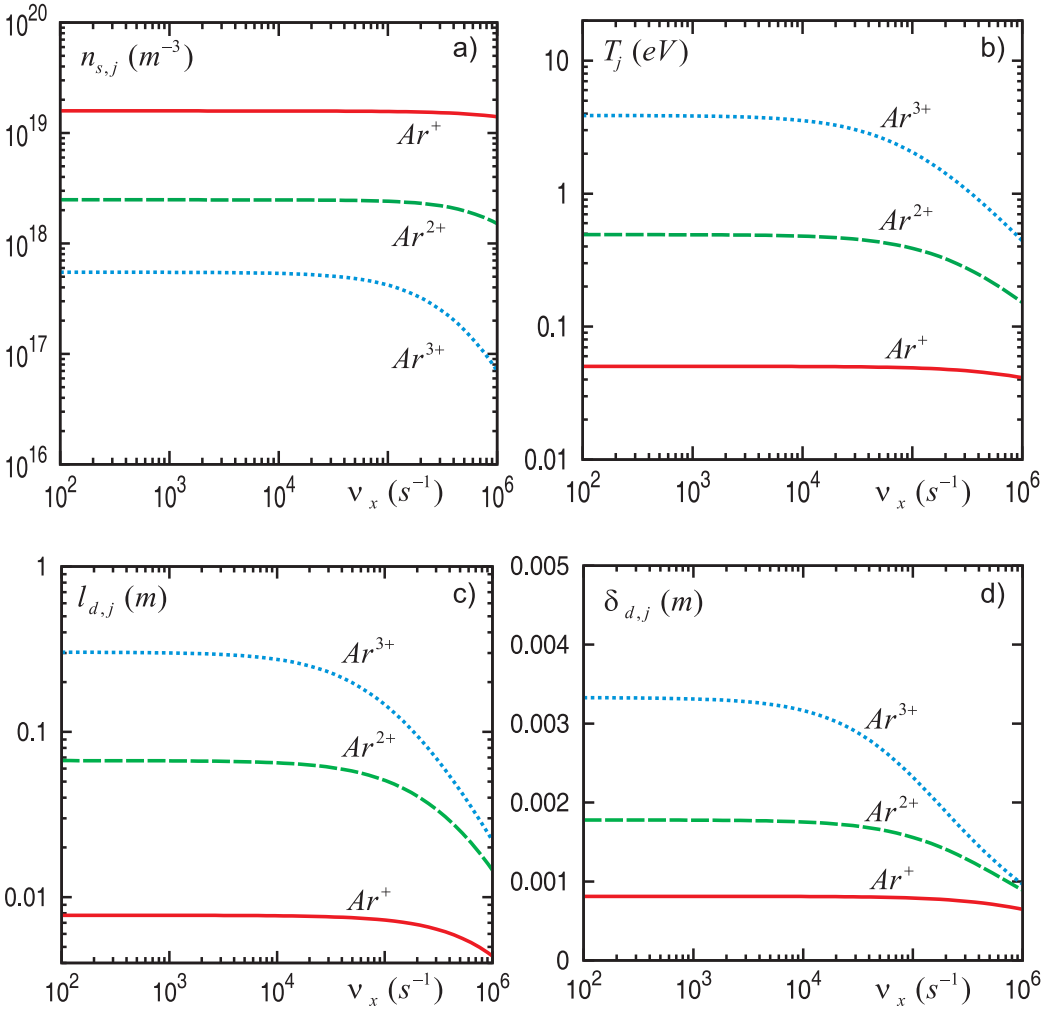


Figure 4.7: Variation with the radial transport frequency $\nu_x$ of the densities (a), temperatures (b), density decay lengths (c) and widths (d) for different argon ions.

Fig. (4.5) shows the characteristic impurity densities $n_{s,j}$ and temperatures $T_j$ in diverse shells, the $e$-folding length of the impurity density profiles both along, $l_{d,j}$, and across, $\delta_{d,j}$, the magnetic field, achieved in steady states. Plasma density and temperature before injection are assumed the same as considered above, $D_y = 1\,m^2 s^{-1}$ and $\nu_x = 2 \cdot 10^3\,s^{-1}$. The impurity ion densities increase monotonously with the neutral density. In the range $n_0 \lesssim 10^{19}\,m^{-3}$ the electron density is weakly perturbed by the presence of impurity. This explains the behavior of stationary $T_j$, given by Eq. (4.11), and $\delta_{d,j}$, which are nearly constant since dependences on the neutral density in these parameters are introduced only through $\nu_I^j \sim n_e$. The increase of the parallel shell extensions $l_{d,j}$ with $n_0$ is due to the drugging force from the electric field that grows up linearly with $n_{s,j}$ for $jn_{s,j} \leq n_i$.

For neutral densities larger $10^{19}\,m^{-3}$ shell dimensions $l_{d,j}$ and $\delta_{d,j}$ start to decrease with increasing $n_0$. Impurity ions disappear closer to the injection position since $\nu_I^j$ increases with the growing $n_e$ but the level of the electric field, pushing ions away, saturates. The diminution of the decay region area leads to even stronger rise of $n_{s,j}$ with $n_0$. Most obviously it is seen in the behavior of the first charge state that has the largest ionization rate coefficient and in whose shell the electron density is most strongly enhanced.

The motion of impurity ions on magnetic surfaces across field lines, in the direction $y$ in the present geometry, is a complex matter which has been studied in sufficient details in the trace impurity limit only. In such a case the perpendicular impurity transport in tokamak is governed by collisions with background ions and is described in the framework of the so called neoclassical theory [12] (p. 168). Under conditions in question, with impurity ion densities noticeably exceeding that of the main ions, this problem is still unexplored. In the present chapter this transport channel is assumed to be purely diffusive and characterized by the coefficient $D_y$. The sensitivity of results to the $D_y$-magnitude at fixed value of $\nu_x = 2 \cdot 10^3\,s^{-1}$ has been studied and is demonstrated in Fig. (4.6). One can see that $\delta_{d,j} \sim \sqrt{D_y}$, as expected, but all other parameters change very weakly for $D_y \lesssim 10\,m^2 s^{-1}$. For larger $D_y$ the densities $n_{s,j}$ are reducing because the same amount of ions produced by ionization of neutrals is absorbed in a broader shell. For singly charged ions this leads to the increase of the life-time since the electron density in their shell reduces down to the unperturbed level. Therefore, these particles are heated up by coulomb collisions with the main plasma components to higher temperatures and spread at larger distances along the magnetic field.

### 4.3.3 Role of impurity transport in the radial direction

The loss of impurity ions and their momentum with the transport in the radial direction $x$ perpendicular to magnetic flux surfaces has been taken above into account by introducing the frequency $\nu_x$. Fig. (4.7) demonstrates the dependence of impurity characteristics on $\nu_x$ found in the steady state for the reference parameters $n_0 = 1.8 \cdot 10^{19}\, m^{-3}$, $D_y = 1\, m^2 s^{-1}$. One can see that a noticeable dependence appears for $\nu_x$ exceeding $10^5\, s^{-1}$ and is the stronger the higher ion charge. This is explained by the fact that $\nu_x$ comes into play as a part of $\nu_I^j \equiv k_{ion}^j n_e + \nu_x$ only. The higher the charge, the smaller $k_{ion}^j n_e$ and, thus, at a lower $\nu_x$ its effect becomes visible. The increase of $\nu_x$ leads to the diminution of impurity ion life-time and, as a consequence, their densities, temperatures and shell dimensions achieve lower levels.

However, even for smaller $\nu_x$ one can not describe the process of impurity penetration into the plasma core by ignoring the radial transport totally. Consider argon impurity neutrals moving in the direction $x$ with the thermal velocity at a room temperature, $V_0 \approx 250\, m s^{-1}$. Fig. (4.8) displays the time evolution of the neutral density profile computed from Eq. (4.1) for the injection conditions discussed in the previous subsection, where the electron density is enhanced up to $2.5 \cdot 10^{19}\, m^{-3}$ in the presence of impurity ions. One can see that the penetration depth of argon atoms in the radial direction $x$ into the plasma, $h_0$, is of $V_0 / \left(k_{ion}^0 n_e\right) \approx 10^{-4}\, m$. This is by an order of magnitude smaller than the distance which singly charged ions diffuse radially during their life-time, $\sqrt{D_x / \nu_{ion}^1} \approx 10^{-3}\, m$, estimated with $D_x = 1\, m^2 s^{-1}$.

Thus, in the main part of the shell occupied by singly charged impurity ions the source term in Eq. (2.3) owing to ionization of neutrals is small in comparison with the divergence of the radial flux component. Nonetheless, the shell approximation Eq. (4.2) remains applicable since, by deriving this, Eq. (2.3) was integrated over the whole shell interior **including** the source region. To apply this, one has to define properly the frequency $\nu_x$ involved in $\nu_I^j$. For this purpose we construct a plausible shape of the radial profiles of the impurity ion densities by taking into account the following. Outside the LCFS charged particles escape to the wall and this implies at $x = 0$ a positive $e$-folding length for the density, $\lambda = dx / d \ln n_j$. Inside the source region, $x \leq h_{s,j}$, impurity density $n_j$ increases linearly but decays exponentially beyond this, $n_j \left(x \geq h_{s,j}\right) \sim \exp\left[-\left(x - h_{s,j}\right) / h_{d,j}\right]$. For such a profile shape one gets:

$$\nu_x \equiv \Gamma_{x,j}\left(x = 0\right) / \int_0^\infty n_j dx = \frac{D_x}{\lambda h_j + h_{s,j}\left(h_{s,j}/2 + h_{d,j}\right)} \tag{4.12}$$

where $h_j \equiv h_{s,j} + h_{d,j}$. An equation for the time evolution of the $e$-folding

length $h_{d,j}$ we obtain by integrating Eq. (2.3) over the shell volume **excluding** the source region, i.e. for $x \geq h_{s,j}$. This results in:

$$\frac{dh_{d,j}}{dt} \approx \frac{D_x}{h_{d,j}} - \left(k_{ion}^{j} n_e + \nu_*\right) h_{d,j} \tag{4.13}$$

with $\nu_* = d \ln\left(n_{s,j} l_j \delta_j\right)/dt$. Fig. (4.9) demonstrates the time evolution of $h_j$ for argon ions found from Eqs. (4.13) with $n_{s,j}(t)$, $l_j(t)$ and $\delta_j(t)$ shown in Fig. (4.3), and $D_x = 1\, m^2 s^{-1}$.

In stationary states the radial decay lengths approach to the values $\sqrt{D_x/(k_{ion}^{j} n_e)}$ predicted in [90]. With these asymptotic and the estimate $\lambda \approx \sqrt{D_x L_c / c_j}$, see Ref. [82] (p. 399), where $c_j = \sqrt{T_j/m_I}$ is the ion sound velocity and $L_c$ the connection length to the wall, we get from Eq. (4.12) $\nu_x \leq \sqrt{k_{ion}^{j} n_e c_j / L_c}$, a value independent of $D_x$. With a typical for JET $L_c = 30\, m$ one obtains for the plasma parameters in question the frequency $\nu_x$ is below $4 \cdot 10^4\ s^{-1}$, $3 \cdot 10^4\ s^{-1}$ and $2 \cdot 10^4\ s^{-1}$ for $Ar^+$, $Ar^{2+}$ and $Ar^{3+}$ ions, respectively. These values are in the range where the results of "shell" model are weakly dependent on $\nu_x$, see Fig. (4.7). Thus, the crudeness of our treatment of the radial transport should not introduce a large error.

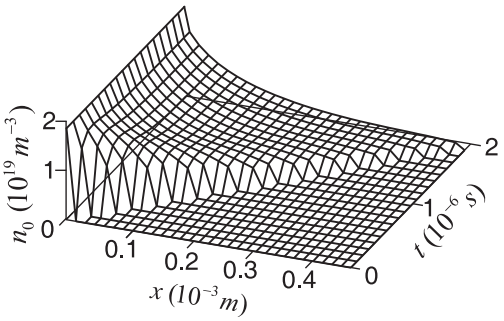


Figure 4.8: Time evolution of the radial profile of neutral argon density.

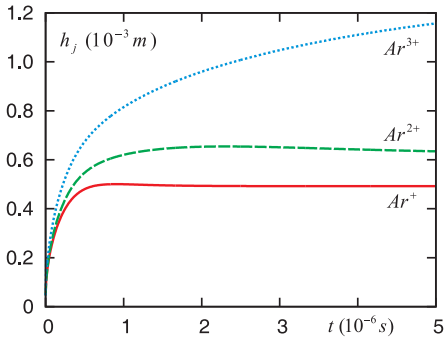


Figure 4.9: Time evolution of the penetration depth for different argon ions.

## 4.4 Conditions for applicability of unperturbed temperature approximation

If the impurity neutral density exceeds a certain level, the present model becomes inapplicable since it does not consider the reduction of the electron

temperature due to losses of energy on impurity radiation. This is of importance for ionization rate coefficients, electric field, friction with electrons, etc. Conditions where the impurity injection starts to affect significantly the local plasma temperature can be estimated by balancing the heat flux transported with electron heat conduction into the impurity cloud, $Q_e$, and the radiation loss term $Q_{rad}$. To estimate $Q_e$ we assume a relative temperature change between the injection position and the distant plasma of 20%. On the one hand, such a variation is still tolerable; on the other hand, according to results obtained in section 3.2.1, if the temperature variation exceeds this level it becomes very sensitive to the change of $n_0$ value, see Fig. (3.2). For edge plasma parameters in question the $Q_e = 1.2 \cdot 10^7\, W m^{-2}$, see Fig. (3.3). Singly charged ions make the dominant contribution both to the total impurity and electron densities, and $Q_{rad} \approx L_1 n_{s,1}^2\,(b + l_{d,1})$, where the cooling rate $L_1 \approx 3 \cdot 10^{-19}\, W m^3$ [98]. With $l_{d,1} \approx 0.01\, m$, see Fig. (4.5c), the heat balance $Q_e \approx Q_{rad}$ provides the value $n_{s,1} = 5.4 \cdot 10^{19}\, m^{-3}$, which is approached at roughly the same level of $n_0$, see Fig. (4.5a). Thus, the plasma cooling effects and temperature reduction in impurity cloud are still insignificant under the conditions where the electron density exceeds its unperturbed level already by an order of magnitude. Unfortunately, there is still a lack of measurements of local plasma parameters at the position of argon injection and we can not compare the found critical $n_0$ with experimental data. Nevertheless, such a comparison done in the previous chapter for the case of $CH_4$ puffing led to a good agreement between theory and experiment.

Since $Q_e \sim \sqrt{\kappa_{||} T}$, see Eq. (3.27), the level of $n_0$, admissible before a significant local cooling takes place, increases fast with the edge temperature. Therefore, one can expect that the present model is relevant for higher injection rates in the H confinement mode than in the L one. In ITER with a hotter edge than in present devices the applicability range will be even broader and argon influxes up to $10^{21} - 10^{22}\, s^{-1}$ can be treated in the framework of model approximations.

For more intensive impurity influxes, as e.g. by massive gas injection [49, 55], one has to consider the effects of main plasma components heat transport in the vicinity of the impurity cloud. This is done in the next chapter.

## 4.5 Conclusions

The spreading of impurity, locally injected into a hot magnetized plasma, under the conditions where in the vicinity of the injection position the impurity ion density can noticeably exceed the density of background plasma ions

but the effects of plasma cooling due to impurity radiation are still unimportant, is considered. The model elaborated in this chapter supposes that impurity particles of different charges are mostly localized inside nested shells whose dimensions grow in time. It is assumed that the densities of each impurity ion species and their flux component parallel to the magnetic field decay exponentially from the source region, where these particles are generated by ionization of lower charged ones, and the temperature is homogeneous. Under such assumptions about solutions fluid equations for continuity of impurity ions, their momentum and energy are integrated over the shell interior. As a result, a system of non-linear ordinary differential equations, describing the time evolution of the characteristic impurity ion densities, their $e$-folding length along and across the magnetic field, and temperatures, is derived. An approach based on the reduction of ordinary differential equations to a system of linear algebraic equations for the variations of the dependent variables after the time step is elaborated.

Calculations have been performed for the conditions at the plasma edge typical for experiments with argon impurity seeding in tokamaks. First, both the dynamics of impurity spreading at the last closed flux surface and characteristics of final stationary states have been studied. The distances covered by impurity ions of different charges both along and across the magnetic field from the injection position till ionization distinct noticeably. That is of importance by reconstructing impurity transport properties from experimentally measured patterns of the impurity emission. Moreover, even in stationary state the temperatures of low charged impurity species differ strongly from those of the main plasma components but are approaching to them with increasing charge. This is necessary to keep in mind by applying plasma diagnostics based on injection of light impurities.

With increasing injection intensity both the impurity ion density and shell expansion along the magnetic field increase. The latter is determined by the rise of the electric field and impurity pressure pulling impurity ions away from the injection position. However, if the density of singly charged impurity becomes comparable with that of the unperturbed plasma the increase in the electron density results in a noticeable reduction of the impurity ion life-time before ionization into higher charge state and shell dimensions, both along and across the magnetic field, begin to decrease. This is accompanied by an even faster growth of the impurity ion densities, while their temperatures achieve lower values.

For typical plasma parameters in experiments with impurity seeding and injection intensities in question perpendicular transport does not affect noticeably the processes of impurity spreading along field lines and heating and the characteristics of impurity species are determined mostly by their

life-time before ionization into higher charge states. Due to the increase of electron density in the presence of impurity the penetration depth of neutrals is much less than that of ions. Therefore, in the main part of the ion shell the radial diffusion dominates over the source from ionization. Nonetheless, the shell approximation elaborated here remains applicable with a proper definition of the transport frequency $\nu_x$. An equation for the time evolution of the shell radial thickness is derived and solved.

The model can be directly applied to calculate the time-dependent three-dimensional patterns of radiation from low ionized impurity species by taking into account the modifications in the background plasma density. This allows to estimate the radiation loads on the injection valves and other wall elements. With known constraints on such loads one would be in position to predict the necessary number of inlet valves.

The present model is an important but intermediate step in the development of approaches to describe the spreading of impurities from local sources. The effect of local plasma cooling will be studied in the next chapters.

# Chapter 5

# The impact of plasma cooling on impurity spreading

## 5.1 Model

### 5.1.1 Heat transfer in main plasma components

Here we extend our previous consideration of impurity spreading to the case of higher impurity influxes where both plasma density, through ionization of impurity, and plasma temperature, through heat losses on radiation and Coulomb collisions, are disturbed. Before impurity injection, in the reference state, this temperature is homogeneous and equal to $T_e^{ref}$. Impurity cloud is localized strongly in comparison with the whole square of magnetic surface, heat sink and causes heat fluxes into it. In this very preliminary study we neglect the inertia of the main plasma components assuming the temperatures of the main ions to be equal the electron one, that however varies on the magnetic surface and evolves in time $T_e = T_e(t, y, z)$. The role of the main ions will be thoroughly considered in the next chapter. By neglecting inertia, heat convection is supposed to be small in comparison with the heat conductivity. Heat sink due to impurity injection may be powerful enough to significantly cool the surface far away from the cloud. The difference in temperatures with the magnetic surfaces nearby causes radial heat transfer on the surface in question. Under these assumptions $T_e(t, y, z)$ is governed by the heat transfer equation:

$$\frac{3}{2}n_e\frac{\partial T_e}{\partial t} - \frac{\partial}{\partial y}\left(\kappa_{e,y}\frac{\partial T_e}{\partial y}\right) - \frac{\partial}{\partial z}\left(\kappa_{e,z}\frac{\partial T_e}{\partial z}\right) = \frac{3}{2}\nu_x n_e\left(T_e^{ref} - T_e\right) - R \quad (5.1)$$

Here the parallel heat conductivity, $\kappa_{e,z} = A_e T_e^{5/2}$, is taken as reduced Spitzer-Härm one, see chapter (3), the perpendicular one, $\kappa_{e,y}$, is assumed to

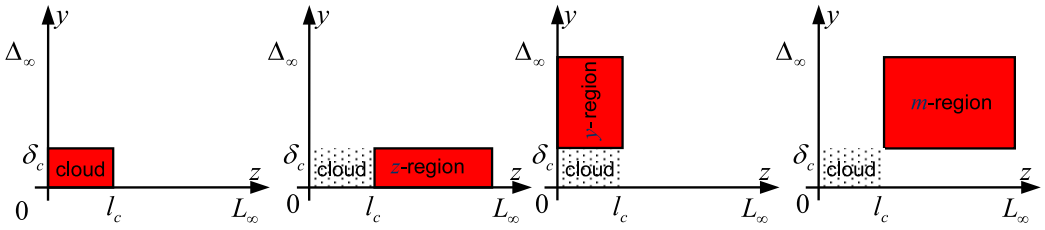


Figure 5.1: Regions on the magnetic surface used by integration of the main plasma heat transport equations.

be constant. Heat sink due to radiation of impurity and Coulomb collisions between electrons and impurity ions:

$$R = n_e n_0 L_0 + \sum_{j=1}^{3} n_e n_j \left[ L_j + 3k_{ej}(T_e - T_j) \right] \tag{5.2}$$

with $L_j$ being cooling rates and $k_{ej}$ friction coefficient due to coulomb collisions between electrons and impurity ions, see chapter (2).

The electron density is determined by quasi-neutrality, Eq. (2.2), the densities and temperatures of impurity ions – by the model from the previous chapter.

### 5.1.2 Integrated heat balance

To integrate Eq. (5.1) we subdivide the magnetic surface in question on four regions represented in Fig. (5.1) and involve assumptions concerning piece-wise profile of the electron temperature. In this work we concentrate on the case of local cooling which means that the total length and width occupied by impurity shells, $l_c = b + \sum_{j=1}^{3} l_j$ and $\delta_c = b + \sum_{j=1}^{3} \delta_j$, are much smaller than the connection length and the poloidal width of the magnetic surface, $L_\infty$ and $\Delta_\infty$. From this point of view, the impurity cloud-region is characterized by the electron temperature $T_{e,c}$ varying with time only. In thin $z$-region, $0 \le |y| \le \delta_c$ and $l_c \le |z| \le L_\infty$, the parallel heat transport is dominated, and we neglect the temperature dependence in the $y$-direction and temperature decreases towards $z$ axis from $T_{e,L}$, far from the cloud, to $T_{e,c}$, on its boundary, according to the parabolic law:

$$T_e(z) = T_{e,L} - (T_{e,L} - T_{e,c}) \left( \frac{L_\infty - z}{L_\infty - l_c} \right)^2 \tag{5.3}$$

In the same manner, in the short $y$-region, $\delta_c \le |y| \le \Delta_\infty$ and $0 \le |z| \le l_c$, the transport in the $y$-direction is dominated and we neglect the temperature

dependence in parallel direction. The parabolic decrease from $T_\Delta$ to the cloud temperature $T_{e,c}$ is assumed:

$$T_e(y) = T_{e,\Delta} - (T_{e,\Delta} - T_{e,c}) \left( \frac{\Delta_\infty - y}{\Delta_\infty - \delta_c} \right)^2 \tag{5.4}$$

In the $m$-region, $l_c \leq z \leq L_\infty$ and $\delta_c \leq y \leq \Delta_\infty$, we use bi-parabolic approximation of the temperature decreasing from $T_{e,S}$, far away from the cloud, to temperature values in the $y$- and $z$- regions:

$$T_e(y,z) = T_e(y, L_\infty) - [T_e(y, L_\infty) - T_e(y, l_c)] \left( \frac{L_\infty - z}{L_\infty - l_c} \right)^2 \tag{5.5}$$

with

$$T_e(y, L_\infty) = T_S - (T_S - T_L) \left( \frac{\Delta_\infty - y}{\Delta_\infty - \delta_c} \right)^2$$

As one can see, the approximation above satisfies the condition of zero heat flux at the stagnation point ($y = \Delta_\infty, z = L_\infty$). By using involved profile one can calculate the values of the heat fluxes ion the boundaries between introduced regions. By integrating the divergence $\partial(\kappa_{e,z}\partial T_e/\partial z)/\partial z$ over $z$-region one gets the density of the parallel heat flux coming into the impurity cloud through the boundary $z = l_c$:

$$q^c_{e,z} = -\frac{A_e}{L_\infty - l_c} \int_{l_c}^{L_\infty} T_e^{5/2} \frac{\partial T_e}{\partial z} dz = \frac{A_e}{L_\infty - l_c} \frac{2}{7} \int_{T_{e,c}}^{T_{e,L}} dT^{7/2} = \frac{2}{7} A_e \frac{T_{e,L}^{7/2} - T_{e,c}^{7/2}}{L_\infty - l_c} \tag{5.6}$$

Integration of the divergence $\partial(\kappa_{e,y}\partial T_e/\partial y)/\partial y$ over $y$-region gives the density of the perpendicular heat flux coming into the impurity cloud through the boundary $y = \delta_c$:

$$q^c_{e,y} = \frac{2\kappa_{e,y}}{\Delta_\infty - \delta_c} (T_{e,\Delta} - T_{e,c}) \tag{5.7}$$

In the same manner, by integrating over $m$-region one obtains the densities of the heat exchange fluxes at the boundaries between $m - z$ and $m - y$ regions, respectively:

$$q^{ex}_{e,z} = \frac{2}{7} \frac{A_e}{L_\infty - l_c} \left[ \left( \frac{2}{3} T_{e,S} + \frac{1}{3} T_{e,L} \right)^{7/2} - \left( \frac{2}{3} T_{e,\Delta} + \frac{1}{3} T_{e,c} \right)^{7/2} \right] \tag{5.8}$$

$$q^{ex}_{e,y} = \frac{\kappa_y}{\Delta_\infty - \delta_c} \left[ \frac{2}{3} T_{e,S} + \frac{1}{3} T_{e,\Delta} - \left( \frac{2}{3} T_{e,L} + \frac{1}{3} T_{e,c} \right) \right] \tag{5.9}$$

where one can recognize the mean values arising by averaging parabolic dependencies.

Integration of Eq. (5.1) over impurity cloud, $z$-, $y$- and $m$- regions by using expressions for heat flux densities in Eqs. (5.6-5.9) gives four heat balances, respectively:

$$n_{e,c}\frac{dT_{e,c}}{dt} = \nu_x n_{e,c}\left(T^{ref} - T_{e,c}\right) + \frac{2}{3}\left(\frac{q^z_{e,c}}{l_c} + \frac{q^y_{e,c}}{\delta_c} - R\right) \tag{5.10}$$

with characteristic electron density in the impurity cloud, $n_{e,c} = n_i + \sum_{j=1}^{3} j n_j$,

$$n_e\frac{dT_{e,z}}{dt} = \nu_x n_e\left(T^{ref}_e - T_{e,z}\right) + \frac{2}{3}\left(\frac{q^{ex}_{e,y}}{\delta_c} - \frac{q^c_{e,z}}{L_\infty - l_c}\right) \tag{5.11}$$

with $T_{e,z} = \left(2T_{e,L} + T_{e,c}\right)/3$,

$$n_e\frac{dT_{e,y}}{dt} = \nu_x n_e\left(T^{ref}_e - T_{e,y}\right) + \frac{2}{3}\left(\frac{q^{ex}_{e,z}}{l_c} - \frac{q^y_{e,c}}{\Delta_\infty - \delta_c}\right) \tag{5.12}$$

with $T_{e,y} = (2T_{e,\Delta} + T_{e,c})/3$,

$$n_e\frac{dT_{e,m}}{dt} = \nu_x n_e\left(T^{ref}_e - T_{e,m}\right) - \frac{2}{3}\left(\frac{q^{ex}_{e,z}}{L_\infty - l_c} + \frac{q^{ex}_{e,y}}{\Delta_\infty - \delta_c}\right) \tag{5.13}$$

with $T_{e,m} = \left(4T_{e,S} + 2T_{e,L} + 2T_{e,\Delta} + T_{e,c}\right)/9$

By discretizing the time derivatives in the form $dT_{e,\beta}/dt \approx \left(T_{e,\beta} - T^-_{e,\beta}\right)/\tau$ with $T^-_{e,\beta}$ being the temperature at the previous time step $\tau$, one can obtain absolutely stable implicit scheme for solving numerically:

$$T_{e,\beta} = \frac{T^-_{e,\beta} + \tau\left(\nu_x T^{ref}_e + F_\beta\right)}{1 + \tau\nu_x} \tag{5.14}$$

where $\beta = (c, z, y, m)$ and $F_\beta$ are the corresponding last terms in r.h.s. of Eqs. (5.10-5.13). A convergent solution for the vector of dependent variables, $\overrightarrow{f}$, from the set of Eqs. (4.10), describing impurity spreading and (5.14), describing plasma cooling, is obtained at each time step by using a relaxation procedure, see Refs. [99] or [91] (p. 60):

$$\overrightarrow{f_{p+1}} = \overrightarrow{f_p}\cdot(1 - \alpha_{mix}) + \overrightarrow{\lambda}\cdot\alpha_{mix} \tag{5.15}$$

where $\overrightarrow{f_p}$ is the approximation of the solution after $p$ iterations with the first iteration $\overrightarrow{f_1}$ assumed equal to the set of variables at the previous time step, and $\overrightarrow{\lambda}$ found by solving Eqs. (4.10) and (5.14) with the coefficients calculated with $\overrightarrow{f_p}$. The mixing parameter $\alpha_{mix} \le 1$ is chosen to minimize the number of iterations needed for convergence.

## 5.2 Results of calculations and discussion

### 5.2.1 The impact of plasma cooling on impurity spreading

Calculations were performed for argon seeded discharges in JET [55] with the plasma density $n_e = 1.6 \cdot 10^{19}\, m^{-3}$ and temperature $T_e^{ref} = 300\, eV$ on the magnetic surface in question before injection, and the density of injected neutral impurity, $n_0 = 1.6 \cdot 10^{19}\, m^{-3}$.

First, consider the main plasma components. After injection, the electron density, see Fig. (5.2a), rises due to ionization of impurity and fast (tens of $\mu$s) overcomes the level where heat losses, growing with the electron density, become significant. Plasma in impurity cloud (solid curve) cools down up to several $eV$ and due to large electron conductivity decreases the temperature in thin $z$-stripe of magnetic surface (dashed curve). Perpendicular heat conductivity practically can not compete with the cooling of the plasma at the magnetic surface, as it is seen from the temperature evolution on $y$ and $m$ regions (dot-dashed curve). One has to draw two important conclusions from the temperature behavior on the magnetic surface: (i) local impurity source significantly cools the magnetic surface, (ii) the temperature far away from the impurity cloud does not approach to the temperature in it. Presented results give a new look on interpretation of the results of the radiation power reconstruction [55, 100] where the approximation of toroidal symmetry has been used. Our calculations show that during impurity injection magnetic surface is cooled down not homogeneously.

Impurity spread under cooling of the main plasma is in a qualitative agreement with our considerations in the previous chapter. It is seen in Fig. (5.3d) that intensive ionization in the beginning of injection preserves the cloud from spread in poloidal $y$-direction until cooling. Due to high temperature of the plasma, impurity ions are ionized into higher charge states faster than diffuse perpendicular to the magnetic field. When the cloud cools, ionization coefficient drops and perpendicular to the magnetic field ions spread diffusively as $\sqrt{D_y t}$. Spread of the cloud along the magnetic field, shown in Fig. (5.3c) is governed by competition between (i) electric field and ion pressure gradient on the one side and (ii) friction force on the other side. During intensive ionization at the beginning of injection the former forces stretch the cloud; when the plasma cools down, the friction force hampers its spread. Heating up of impurity ions, see Fig. (5.3b), in the beginning is replaced by electron cooling, impurity ion temperature drops close to the electron one.

One has to note that the total impurity cloud length and width are much

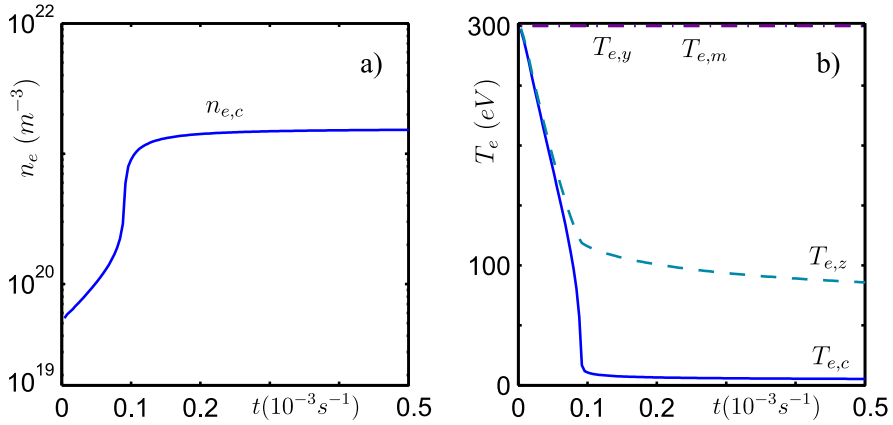


Figure 5.2: Time evolution of plasma density in the impurity cloud (a) and electron temperature in different regions of magnetic surface (b). Neutral injection density is constant, $n_0 = 1.6 \cdot 10^{19}\, m^{-3}$.

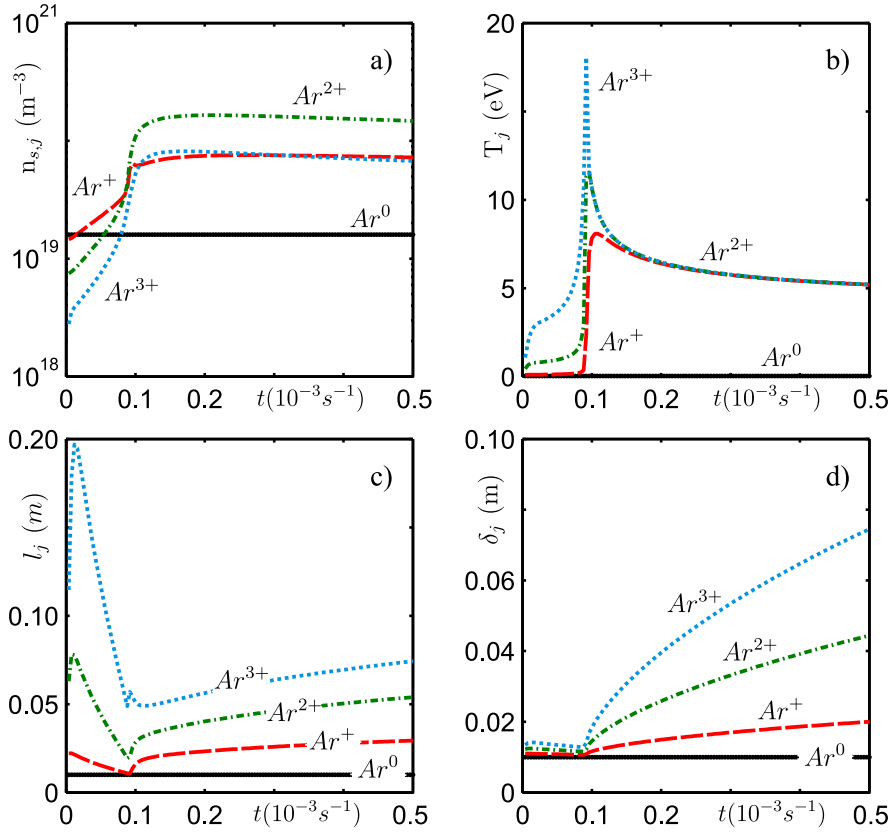


Figure 5.3: Time evolution of the densities (a), temperatures (b), half-lengths (c) and half-widths (d) of the shell cross-sections for different argon ions computed with modification of $n_e$ and $T_e$. Neutral injection density is constant, $n_0 = 1.6 \cdot 10^{19}\, m^{-3}$.

smaller than the connection length $L_\infty = 9.3\,m$ and poloidal width $\Delta_\infty = 4\,m$ of the magnetic surface in question on JET machine, e.i. our assumption of local impurity spreading is valid, but the cooling affects, with varying degree, the plasma over the whole magnetic surface.

### 5.2.2 Unstationary neutral injection

The situation is drastically changes if the neutral injection is unstationary. In real experiments fast-injection valves have the finite time of opening $\geq 400\,\mu s$ [101–105]. We approximated roughly the time-dependence of neutral impurity density, $n_0(t)$, by the square sinus pulse with the duration of $5\,ms$. The peak value of the density is chosen equal to $3.2 \cdot 10^{19}\,m^{-3}$ to inject the same amount of particles as in calculations of the previous section. Time evolution of the electron density in the impurity cloud and electron temperatures in different regions of magnetic surface are shown in Fig. (5.4) and respective effect of cooling on the impurity spreading parameters – in Fig. (5.5). There is a sharp contrast with Figs. (5.2) and (5.3) from the previous section. Here all transition processes occur slower following the neutral impurity density pulse. Dependence of the impurity transport parameters is determined by duration of the neutral pulse, but cooling of the main plasma to cold dense state, see Fig. (5.4b), occurs during the heat transfer times. ECE-diagnostics on JET shows, however, that the process of transition to cooled state occurs during a time by an order of magnitude longer. The question why temperature drops so fast is still unclear. In this chapter we present only preliminary results of plasma cooling, and thorough parameter study satisfying the real injection pulses is out of the scope of the present work. This discrepancy should be revealed in future developments by consideration of the radial transport through 3D modeling of both neutral and charged impurity.

### 5.2.3 Effect of radial transport on local plasma cooling by impurity spreading

To show the role of radial heat transport we change here the characteristic frequency $\nu_x$ being a free parameter in our model and assumed in calculations of previous two sections equal to $10\,s^{-1}$. It is worth to note that the frequency $\nu_x$ in Eqs. (4.2-4.5), characterizing radial transport of impurity particles, can differ from that in Eqs. (4.6) and (5.10-5.13). However, in present calculations it was found that the variation of particle radial transport itself does not change significantly time-dependent plasma characteristics shown in Figs. (5.2-5.7), as it was also in the previous chapter,

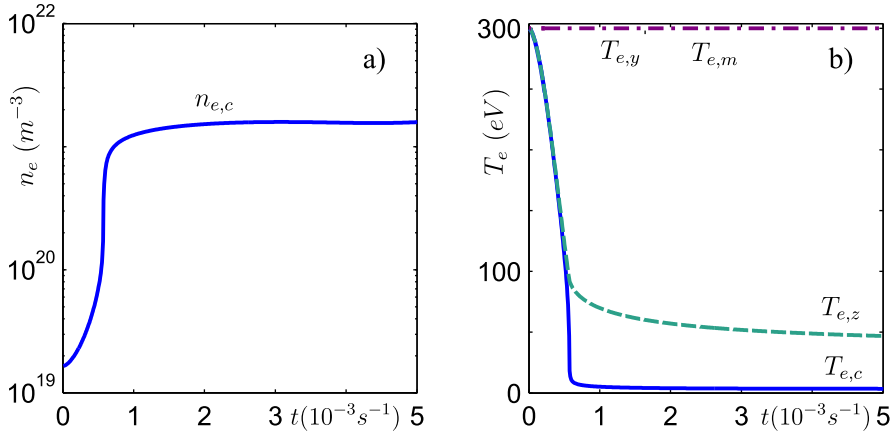


Figure 5.4: Time evolution of plasma density in the impurity cloud (a) and electron temperature in different regions of magnetic surface (b). Neutral injection density is changing in time, and $\nu_x = 10\,s^{-1}$.

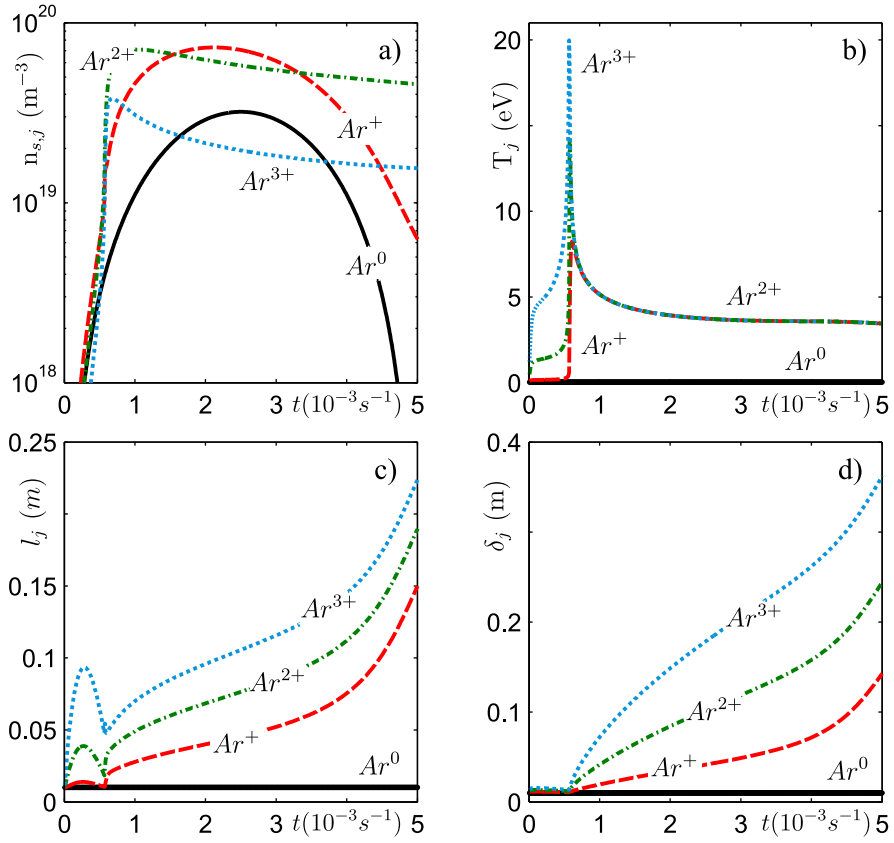


Figure 5.5: Times evolution of the densities (a), temperatures (b), half-lengths (c) and half-widths (d) of the shell cross-sections for different argon ions computed with modification of $n_e$ and $T_e$. Neutral injection density is changing in time, and $\nu_x = 10\,s^{-1}$.

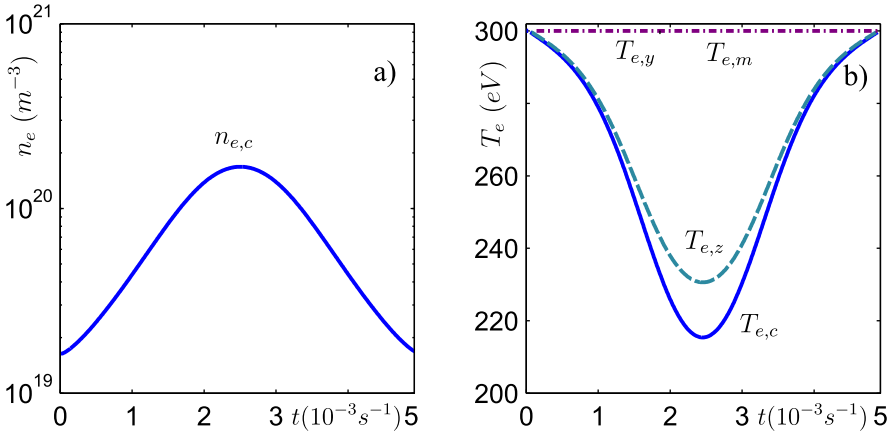


Figure 5.6: Time evolution of plasma density in the impurity cloud (a) and electron temperature in different regions of magnetic surface (b). Neutral density is changing in time, and $\nu_x = 10^4\ s^{-1}$.

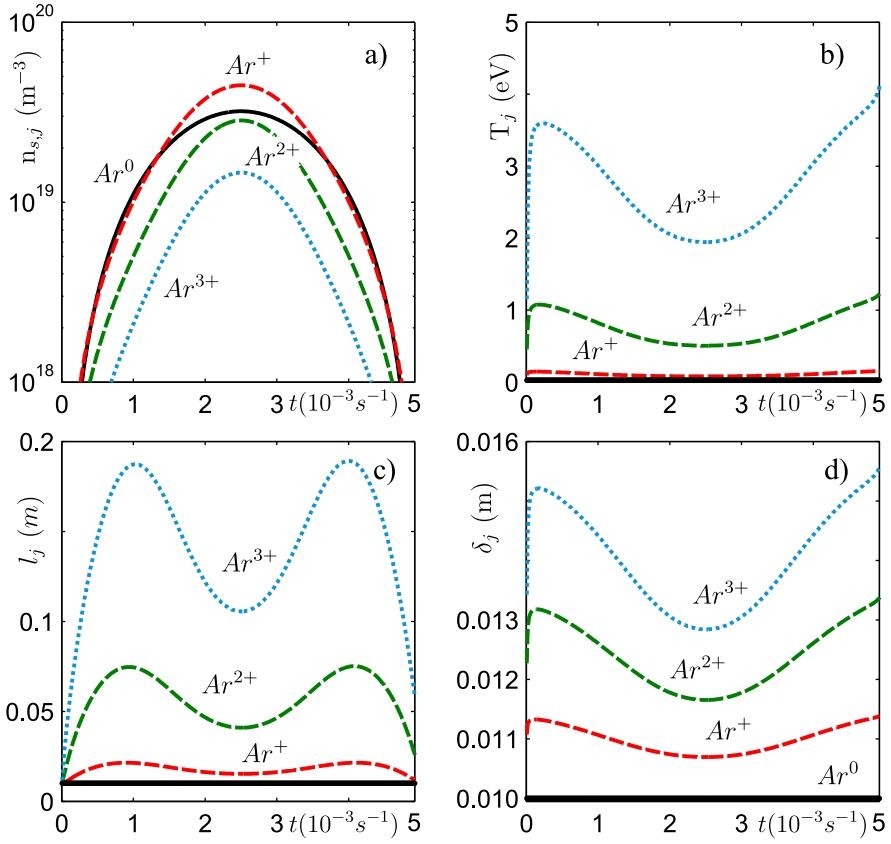


Figure 5.7: Times evolution of the densities (a), temperatures (b), half-lengths (c) and half-widths (d) of the shell cross-sections for different argon ions computed with modification of $n_e$ and $T_e$. Neutral injection density is changing in time, and $\nu_x = 10^4\ s^{-1}$.

see Fig. (4.7). Thus, in calculations of this chapter it was assumed equal to the heat transport frequency. Time evolution of the electron density in the impurity cloud, electron temperatures in different regions of magnetic surface and impurity spreading parameters under conditions of plasma cooling with initial plasma parameters and injection density from the previous section and heat transport frequency $\nu_x = 10^4\, s^{-1}$ in Figs. (5.6) and (5.7), respectively. One can see that radial heat transport plays an important role in transition to cold dense state. On the one hand, charge state higher one, which ionization frequencies strongly depend on the electron temperature, are not accumulated on the magnetic surface in question, and friction force hampers impurity spreading over it. On the other hand, enhanced radial heat transport slows down the cooling of the plasma and can prevent the formation of long-living cold dense state. This role have to be taken into account in future developments.

## 5.3 Conclusions

The model elaborated in this chapter complements the description of impurity spreading over magnetic surface by the case of high enough neutral injection rates where the modification of both plasma density and temperature are significant. Shell approach developed in the previous chapter and the parabolic approximation of the electron temperature were used to integrate the electron heat transport equation and obtain time-evolution of characteristic temperature values in the region of interest.

Calculations have been performed for the conditions typical at the plasma edge in experiments with argon impurity seeding in tokamaks. Local intensive source of impurity significantly cools the plasma on the magnetic surface. The temperature far away from the impurity cloud does not approach to the temperature in it. Cooling of surrounding plasma hampers the spreading of the impurity through decrease in impurity pressure gradient and increase of friction force. Unstationary neutral injection strongly determines the time-dependent transport of charged impurity, but to a lesser extend influences the cooling of the plasma both in the impurity cloud and distant regions. Radial heat transport plays an important role in transition to cold dense plasma and has to be taken into account in future developments.

# Chapter 6

# A new look on formation of cold dense structures in plasmas

Compact structures with cold dense plasma offten arise in fusion devices. A prominent example of these phenomena is the development of multifaceted radiation from the edge (MARFE) close to the density limit [106], manifesting itself as a toroidally symmetric loop of cold, dense and luminous plasma at the inner edge. Instabilities caused by impurity radiation, originally considered as a possible cause for the star formation from primordial homogeneous interstellar medium [107–109], are usually suspected as a MARFE trigger [110, 111]. The mechanism of such an instability is simple: a spontaneous reduction of the temperature in some region leads to a local drop of the pressure there thus particles flow into this region; consequently the plasma density increases, radiation losses grow and the original temperature perturbation is enhanced. The usage of deliberate impurity injection, in particular for disruption mitigation purposes [49], has revealed other mechanisms of impurity influence, in particular, the cooling of the main plasma components in coulomb collisions with cold impurity ions [64]. Bifurcation with sharp increase of the electron density and decrease of the electron temperature, as the injection neutral rate overcomes a threshold level, was found by modeling of methane puff performed in chapter (3) of this work. And the model allowing to calculate the spatial scales of such cold formation was developed in chapters (4) and (5). It was found there that friction between main and impurity ions locks the latter in the vicinity of the impurity source, if the density of impurity neutrals in the source exceeds a critical level. Therefore, it is enlightening to examine the relevance of mentioned above mechanisms on non-stationary development of compact cold dense structures.

## 6.1 Model

In this chapter we apply the "shell" approach developed in previous sections to integrate the full set of non-stationary three-dimensional equations (2.2-2.11) and examine the competition between various mechanisms responsible for plasma cooling on the example of light impurities such as singly ionized lithium at the edge of a deuterium plasma in a tokamak device. As in the previous two chapters, we consider the situation where the outlet of the injection valve defines itself the last closed flux surface and impurities are spreading out in the confined region inside LCFS, see Fig. (2.1). The impact of scrape-off layer outside the LCFS is taken into account as a boundary condition. It is supposed that without impurity the plasma is homogeneous and motionless on magnetic surfaces. The impurity neutral density is assumed constant within the whole region of their localization, because it is not of the main importance for the present study.

In the initial state before impurity injection the densities and temperatures of electrons and main ions are assumed identical and homogeneous, $n_{e,i}\,(t=0,x,y,z) = n^{ref}$ and $T_{e,i}\,(t=0,x,y,z) = T^{ref}$. At the moment $t=0$ the density of impurity neutrals is enhanced instantaneously in the source area, $x \le h_0$, $|y| \le \delta_0$, $|z| \le l_0$, to a level $n_0$ maintained constant later. The plasma parameters, being perturbed in the vicinity of the impurity source, approach to the values $n^{ref}$ and $T^{ref}$ far away from it.

## 6.2 Approach to numerical solution of partial differential equation systems using "generalized" variables

In the framework of the shell model the whole space region occupied by any particular charge state $j$ of impurity is subdivided into two subregions. In the source subregion, $x \le h_{s,j}$, $|y| \le \delta_{s,j}$, $|z| \le l_{s,j}$, the $j$-ions are generated by the ionization of the $j-1$ ones and in the decay zone, $h_{s,j} < x$, $\delta_{s,j} < |y|$, $l_{s,j} < |z|$, their density $n_j$ drops due to ionization into the $j+1$ state. For impurity ions in question of low charges this behavior is formally reproduced with boundary conditions corresponding to zero $y,z$-derivatives of the densities at the source center position, $y = z = 0$, and $n_j \to 0$ far from the source, $x, |y|, |z| \to \infty$. The shape of the radial profiles is constructed by taking into account that outside the LCFS charged particles escape to the wall and at $x = 0$ a positive $e$-folding length for the density, $\lambda_j = dx/d\ln n_j$, is fixed.

An approximate solution of Eq. (2.3) satisfying these conditions and be-

ing, as well as its derivatives, continuous at the source boundary, is presumed in the form $n_j(t,x,y,z) = n_j^0(t)\,\theta_j(t,x)\,\phi_j(t,y)\,\psi_j(t,z)$ with

$$\begin{aligned}\theta_j(x \le h_{s,j}) &= 1 - a_j(x - x_j)^2 \\ \theta_j(x > h_{s,j}) &= \left[1 - a_j(h_{s,j} - x_j)^2\right] \exp\left(-\frac{x - h_{s,j}}{h_{d,j}}\right)\end{aligned} \tag{6.1}$$

$$\begin{aligned}\phi_j(y \le \delta_{s,j}) &= 1 - \frac{\delta_{s,j}}{2\delta_{d,j} + \delta_{s,j}}\left(\frac{y}{\delta_{s,j}}\right)^2 \\ \phi_j(\delta_{s,j} < y) &= \frac{\delta_{d,j}}{\delta_{d,j} + \delta_{s,j}/2} \exp\left(-\frac{y - \delta_{s,j}}{\delta_{d,j}}\right)\end{aligned} \tag{6.2}$$

$$\begin{aligned}\psi_j(z \le l_{s,j}) &= 1 - \frac{l_{s,j}}{2l_{d,j} + l_{s,j}}\left(\frac{z}{l_{s,j}}\right)^2 \\ \psi_j(l_{s,j} < z) &= \frac{l_{d,j}}{l_{d,j} + l_{s,j}/2} \exp\left(-\frac{z - l_{s,j}}{l_{d,j}}\right)\end{aligned} \tag{6.3}$$

where $x_j = h_{s,j}\left(h_{s,j}/2 + h_{d,j}\right)/\left(h_{s,j} + \lambda_j + h_{d,j}\right)$ and $a_j = 1/x_j/\left(x_j + 2\lambda_j\right)$. Here $h_{d,j}$, $\delta_{d,j}$ and $l_{d,j}$ are the functions of time determined in the model.

By constructing approximation profiles for impurity flux densities one has to take into account that $\Gamma_j = 0$ at the axis $z = 0$ and achieves its maximum at the source boundary, $z = l_{s,j}$. Therefore, $\Gamma_j(t,x,y,z) = \Gamma_j^0(t)\,\theta_j(t,x)\,\phi_j(t,y)\,\chi_j(t,z)$ with $\chi_j(0 \le z \le l_{s,j}) = z/l_{s,j}$ and $\chi_j = \psi_j$ for $l_{s,j} < z$.

The impurity ion temperature is characterized by a single averaged value $T_j$ in the whole shell occupied by $j$-ions that combines the source and decay regions: $x \le h_j \equiv h_{s,j} + h_{d,j}$, $|y| \le \delta_j \equiv \delta_{s,j} + \delta_{d,j}$, $|z| \le l_j \equiv l_{s,j} + l_{d,j}$. In this region the ions in question dominate the impurity contribution to the electron density, i. e.

$$n_e \approx n_{i,j} + j n_j \tag{6.4}$$

Since the source region of the $j$-ions coincides with the total localization shell of the $j-1$ ones, the recurrent relations $h_{s,j} \approx h_{j-1}$, $\delta_{s,j} \approx \delta_{j-1}$ and $l_{s,j} \approx l_{j-1}$ hold. The temperatures of electrons and main ions, and the density of the latter are approximated by step functions with spatially homogeneous but time dependent values $T_{e,j}$, $T_{i,j}$ and $n_{i,j}$, respectively, in the decay region of $j$-ions, $h_{s,j} < x \lesssim h_j$, $\delta_{s,j} < |y| \lesssim \delta_j$ and $l_{s,j} < |y| \lesssim l_j$.

Time evolution of the parameters $h_{d,j}$, $\delta_{d,j}$, $l_{d,j}$, $n_j^0$, $\Gamma_j^0$, $T_j$, $T_{e,j}$, $T_{i,j}$ and $n_{i,j}$ determines the behavior of the plasma parameters in the whole calculation domain in the vicinity of the injection source and requires necessary amount of balance equations.

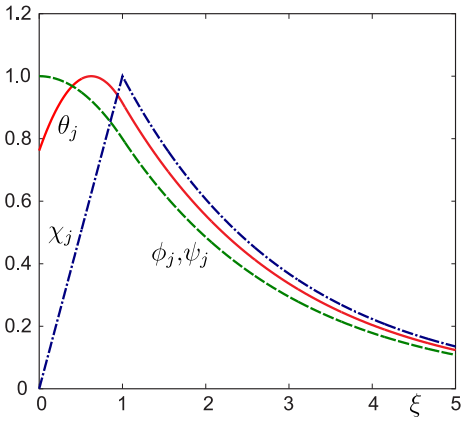


Figure 6.1: The functions $\theta_j$, $\phi_j$, $\psi_j$, and $\chi_j$ versus the dimensionless coordinate $\xi$ equal to $x/h_{s,j}$, $y/\delta_{s,j}$, and $z/l_{s,j}$, correspondingly, for $h_{d,j}/h_{s,j} = \delta_{d,j}/\delta_{s,j} = l_{d,j}/l_{s,j} = 2$.

By integrating Eqs. (2.5-2.10) with described above approximation profiles over the region we will not here try to avoid the interlacement of the parameters above. Instead, the system of ordinary differential equations (ODEs) for "generalized" variables is deduced. Let us start with $h_{d,j}$, $\delta_{d,j}$, $l_{d,j}$, and $n_j^0$. The solution in the form of assumed above approximation profiles is substituted into Eq. (2.5) and both sides of the latter are integrated over four regions in the $(x, y, z)$-space: the total shell, $0 \le x, |y|, |z| < \infty$, the $x$-region $h_{s,j} \le x, 0 \le |y|, |z| < \infty$, the $y$-region $0 \le x, \delta_{s,j} \le |y| < \infty$, $0 \le |z| < \infty$, and the $z$-region $0 \le x, |y| < \infty$, $l_{s,j} \le |z| < \infty$. This procedure results in the following ODEs:

$$dN_{w,j}/dt = N_{w,j-1}k_{ion}^{j-1}n_{ew,j-1} - N_{w,j}\left(k_{ion}^{j}n_{ew,j} + k_j\right) \quad (6.5)$$

$$dN_{x,j}/dt = \left(D_x/h_{d,j}^2 - k_{ion}^{j}n_{ex,j}\right)N_{x,j} \quad (6.6)$$

$$dN_{y,j}/dt = \left(D_x/\delta_{d,j}^2 - k_{ion}^{j}n_{ey,j} + \nu_j\right)N_{y,j} \quad (6.7)$$

$$dN_{z,j}/dt = G_j/l_{s,j}/\left(0.5 + I_{z11}\right)/m_I - \left(k_{ion}^{j}n_{ez,j} + \nu_j\right)N_{z,j} \quad (6.8)$$

where $N_{w,j} = n_j^0 h_{s,j}\delta_{s,j}l_{s,j}I_{x1}I_{y1}I_{z1}$, $N_{x,j} = N_{w,j}I_{x11}/I_{x1}$, $N_{y,j} = N_{w,j}I_{y11}/I_{y1}$, $N_{z,j} = N_{w,j}I_{z11}/I_{z1}$ are the whole numbers of $j$-ions in the regions in question with $I_{x1} = I_{x01} + I_{x11}$, $I_{y1} = I_{y01} + I_{y11}$, $I_{z1} = I_{z01} + I_{z11}$, $\xi_x = h_{d,j}/h_{s,j}$, $\xi_y = \delta_{d,j}/\delta_{s,j}$, $\xi_z = l_{d,j}/l_{s,j}$, $I_{x01} = 1 - a_j[h_{s,j}^2/3 - x_j(h_{s,j} - x_j)]$, $I_{x11} = \xi_x\left[1 - a_j\left(h_{s,j} - x_j\right)^2\right]$, $I_{y01} = 1 - \delta_{s,j}/\left(6\delta_j\right)$, $I_{y11} = 2\xi_y^2/\left(1 + 2\xi_y\right)$, $I_{z01} = 1 - l_{s,j}/\left(6l_j\right)$, $I_{z11} = 2\xi_z^2/\left(1 + 2\xi_z\right)$, $n_{ew,j} = n_{i,j} + n_j^0 I_{x2}I_{y2}I_{z2}/(I_{x1}I_{y1}I_{z1})$, $n_{ex,j} = n_{i,j} + n_j^0 I_{x12}I_{y2}I_{z2}/\left(I_{x11}I_{y1}I_{z1}\right)$, $n_{ey,j} = n_{i,j} + n_j^0 I_{x2}I_{y12}I_{z2}/\left(I_{x1}I_{y11}I_{z1}\right)$, $n_{ez,j} = n_{i,j} + n_j^0 I_{x2}I_{y2}I_{z12}/\left(I_{x1}I_{y1}I_{z11}\right)$, $I_{x2} = I_{x02} + I_{x12}$, $I_{y2} = I_{y02} + I_{y12}$, $I_{z2} = I_{z02} + I_{z12}$, $I_{x02} = 2I_{x01} - 1 + a_j^2\left[\left(h_{s,j} - x_j\right)^5 - x_j^5\right]/\left(5h_{s,j}\right)$, $I_{x12} = I_{x11}^2/2/\xi_x$, $I_{y02} = 1 - 2/\left(1 + 2\xi_y\right)/3 + 1/\left(1 + 2\xi_y\right)^2/5$, $I_{y11} = 2\xi_y^2/\left(1 + 2\xi_y\right)$, $I_{z02} = 1 - 2/\left(1 + 2\xi_z\right)/3 + 1/\left(1 + 2\xi_z\right)^2/5$, $I_{z11} = 2\xi_z^2/\left(1 + 2\xi_z\right)$. The frequency $\nu_j = 2D_x a_j x_j/h_{s,j}/\left(I_{x01} + I_{x11}\right)$ characterizes the loss of the $j$-ions through the LCFS.

Thus, the original dependent variables of the "shell" model, $h_{d,j}$, $\delta_{d,j}$, $l_{d,j}$, and $n_j^0$, can be explicitly expressed through $N_{w,j}$, $N_{x,j}$,$N_{y,j}$ and $N_{x,j}$. After

cumbersome algebra with the definitions above one gets:

$$h_{d,j} = \frac{h_{s,j}}{(h_{s,j}+2\lambda_j)\,(N_{w,j}/N_{x,j}-1)}\Bigg(h_{s,j}/3+\lambda_j + \sqrt{(h_{s,j}/3+\lambda_j)^2+(h_{s,j}+2\lambda_j)\,(h_{s,j}/6+\lambda_j)\,(N_{w,j}/N_{x,j}-1)}\Bigg) \quad (6.9)$$

$$l_{d,j} = \frac{l_{s,j}}{2}\frac{1+\sqrt{(4N_{w,j}/N_{z,j}-1)/3}}{N_{w,j}/N_{z,j}-1} \quad (6.10)$$

$$\delta_{d,j} = \frac{\delta_{s,j}}{2}\frac{1+\sqrt{(4N_{w,j}/N_{y,j}-1)/3}}{N_{w,j}/N_{y,j}-1} \quad (6.11)$$

In Eq. (6.8) $G_j \equiv m\Gamma_j^0 h_{s,j}\delta_{s,j}l_{s,j}I_{x1}I_{y1}\,(1/2+I_{z11})$ is the total parallel momentum of impurity $j$-ions. The integral of Eq. (2.4) over the whole shell, with Eq. (2.6) taken into account, provides the equation for time evolution of $G_j$:

$$dG_j/dt = f_j N_{z,j} - \nu_G^j G_j \quad (6.12)$$

where $f_j \approx \left(T_j + jT_e\left[1-n_{i,j}/(jn_j^0)\ln\left(1+jn_j^0/n_{i,j}\right)\right]\right)/l_{s,j}/\left(I_{z01}+I_{z11}\right)$ is the effective force per one $j$-ion due to the pressure gradient and electric field, and $\nu_G^j = k_{ij}n_{i,j}+k_{ion}^1 n_{e\Gamma}+D_x/\lambda_j/h_{s,j}/I_{x1}$, with $n_{e\Gamma} = n_{i,j}+n_j^0 I_{x2}I_{y2}/I_{x1}/I_{y1}\cdot\left(1/2+a_j h_{s,j}^2/3+I_{z12}\right)/\left(1/2+I_{z11}\right)$, characterizes the diminishing of momentum by friction and ionization. The integration of Eq. (2.5) over the whole $(y,z)$-plane results in the following equation for the time evolution of the characteristic temperature of impurity $j$-ions:

$$\begin{aligned} dT_j/dt &= \left(T_{j-1}-T_j\right)k_{ion}^{j-1}n_{ew,j-1}N_{w,j-1}/N_{w,j} \\ &\quad +2k_{ij}n_{i,j}\left(T_{i,j}-T_j\right)+2k_{ej}n_{ew,j}\left(T_{e,j}-T_j\right) \end{aligned} \quad (6.13)$$

Equations for the parameters $T_{e,j}$, $T_{i,j}$ and $n_{i,j}$ are formulated below for $j=1$ only. Although this is a limitation of the present model, such a reduced description is of direct relevance for such important impurities as helium ($He$) and lithium ($Li$). Both species are used in fusion for diagnostic purposes. In addition, helium is a product of thermonuclear reactions and lithium is utilized as a plasma facing material. The $j=2$ ions of helium are completely stripped and spread out over the whole magnetic surfaces. The ionization energy of doubly charged lithium ions is of $122.5eV$ and at the plasma edge with an electron temperature of several tens of $eVs$ they disappear very slowly and also have enough time for spreading out over the magnetic surfaces. Moreover, as it was seen in chapter (4), even for argon impurity, whose charge states with $j \geq 2$ have much lower ionization energies, these do not contribute visibly to $n_e$ up to extremely high injection rates

being unrealistic for many applications. As one can presume from the results of stationary analysis for singly charged carbon ions, see chapter (3), and estimates done for argon in chapter (4), even higher impurity densities are necessary to change $T_e$, $T_i$ and $n_i$ noticeably.

For the temperatures of the main plasma components in the shell of singly charged impurity ions we have got the following equations:

$$\begin{aligned} 1.5N_{i,1}dT_{i,1}/dt &= 3n_{i,1}[k_{ei}\left(N_{i,1}+N_{w,1}\right)\left(T_{e,1}-T_{i,1}\right) \\ &\quad +k_{i1}N_{w,1}(T_1-T_{i,1})] + Q_{i,1} \end{aligned} \tag{6.14}$$

$$\begin{aligned} &1.5\left(N_{i,1}+N_{w,1}\right)dT_{e,1}/dt \\ &= 3n_{i,1}k_{ei}\left(N_{i,1}+N_{w,1}\right)\left(T_{i,1}-T_{e,1}\right) \\ &+3n_{ew,1}k_{e1}N_{w,1}\left(T_1-T_{e,1}\right) \\ &-n_{e,0}N_0\left[k^0_{ion}\left(I_0+1.5T_{e,1}\right)+L_0\right] \\ &-n_{ew,1}N_{w,1}\left[k^1_{ion}\left(I_1+1.5T_{e,1}\right)+L_1\right]+Q_{e,1} \end{aligned} \tag{6.15}$$

where $N_0 = n_0h_0\delta_0l_0$, $N_{i,1} = n_{i,1}h_1\delta_1l_1$ and $n_{e,0} = n_{i,1} + n^0_1I_{x01}I_{y01}I_{z01}$; $Q_{i,1}$ and $Q_{e,1}$ are the total heat influxes into the shell of singly charged impurity ions transported from distant plasma regions by the heat conductions of the main ions and electrons, respectively. These are evaluated according to the approach developed in chapter (3), see Eq. (3.25). The density of the main ions in the shell in question is governed by the time evolution equation:

$$dN_{i,1}/dt = h_1\delta_1\Gamma_{i,1} + \nu_{i\perp}\left(n^{ref}h_1\delta_1l_1 - N_{i,1}\right) \tag{6.16}$$

Here the r.h.s. gives the particle supply due to flows both parallel, the first term, and perpendicular, the second one, to the magnetic field from the distant plasma where the unperturbed density $n^{ref}$ is maintained. The parallel flux density $\Gamma_{i,1}$ is assessed according to Ref. [113]; the frequency $\nu_{i\perp}$, characterizing the perpendicular transport induced by the deviation of $n_i$ from $n^{ref}$ beyond the $j = 1$ shell, is adopted as a free parameter. We have found that in a wide range of physically reasonable values of $\nu_{i\perp}$, up to $10^5$ $s^{-1}$, the results of calculations are very insensitive to its absolute magnitude.

## 6.3 Results of calculations and discussion

### 6.3.1 The roles of different mechanisms in impurity impact on plasma

Eqs. (6.6-6.16) of the "shell" model have been applied to study the time dynamics of the spreading of singly charged lithium ions at the edge of a

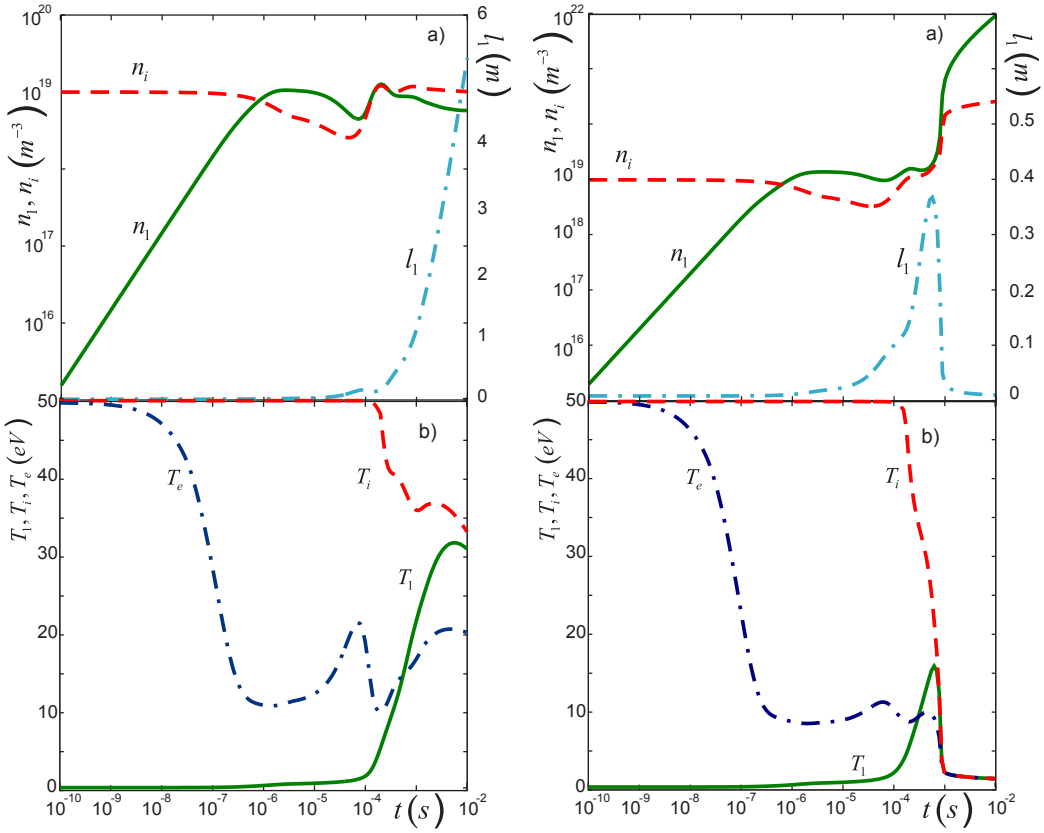


Figure 6.2: Time evolution of the densities of $Li^+$ ions (solid curve) and main deuterons (dashed curve), the parallel extension of the $Li^+$ shell (dash-dotted curve) (a) and of the temperatures of the $Li^+$ ions (solid curve), the main ions (dashed curve), and electrons (dashed-dotted curve) (b) computed for the density of lithium atoms $n_0 = 0.75 \cdot 10^{19}\, m^{-3}$ (from the left) and $n_0 = 10^{19}\, m^{-3}$ (from the right).

deuterium plasma in a tokamak device. In the initial state before impurity injection the identical densities and temperatures of electrons and deuterons are equal $n^{ref} = 10^{19}\, m^{-3}$ and $T^{ref} = 50\, eV$, respectively. During injection the parameters of the main plasma components far from the impurity source are assumed approaching to their unperturbed levels $n^{ref}$ and $T^{ref}$. For the perpendicular diffusivity components we adopted $D_{x,y} = 1 m^2\, s^{-1}$. The ionization and cooling rates of lithium atoms and ions have been taken from Refs. [114, 115]. Fig. (6.2) shows the time evolution of the parameters $l_1$, $n_1^0$, $n_i$, $T_1$, $T_e$ and $T_i$ in the shell of singly charged lithium ions. Calculations have been done for two close magnitudes of the impurity atom density $n_0$ by assuming that lithium atoms are localized in the source region with the dimensions $h_0 = 0.01\, m$, $\delta_0 = l_0 = 0.02\, m$ and have a temperature $T_0$ of

$0.03\,eV$.

For $n_0 = 0.75 \cdot 10^{19}\,m^{-3}$, see the left Fig. (6.2), the initial transient cooling of electrons, mostly due to energy losses on ionization and radiation of impurity atoms, is not supported by the main ions. Finally, owing to heating in collisions with the main ions, remaining hot, $T_e$ relaxes to a level comparable with the initial one. Both excitation of impurity ions and coulomb collisions with them are not efficient to preserve electron cooling because $n_1$ is limited at a low enough level: in collisions with the main ions the impurity ones are heated up and their pressure gradient and the electric field dissolve them on a distance $l_1$ of several meters along the magnetic field. In the case of a slightly higher $n_0 = 10^{19}\,m^{-3}$, see the right Fig. (6.2), a compact bubble of very dense and cold plasma, with a dimension $l_1$ of several centimeters along the magnetic field, develops. Impurity ions are confined in this structure by the friction with the main ones and their density $n_1$ and, thus, $n_e$ exceed the initial plasma density $n^{ref}$ by two orders of magnitude. The final state can not be, however, consistently described in the framework of the present model because it does not account for recombination processes being important under such conditions.

### 6.3.2 A new look on formation of cold dense structures

Normally, condensation phenomena like that demonstrated in the right Fig. (6.2) are thought to be triggered by electron energy losses on excitation of impurity and radiated away. Our present model includes in addition to this loss channel also coulomb collisions between different plasma components. This allows to analyse which mechanisms are of the most importance for the condensation phenomena and structure development. Figure (6.3) displays the time evolution of parameters computed under different assumptions for $n_0 = 1.5 \cdot 10^{19}\,m^{-3}$. One can see that in all cases there is an initial significant cooling of electrons and main ions. However, if coulomb collisions between the main and impurity ions are switched off, both $T_i$ and $T_e$ recover significantly and a compact cloud of cold dense plasma does not arise. In the case with collisions but without radiation losses the initial cooling state is dragged on but finally a condensation develops.

Thus, coulomb collisions between ion components are vitally important for the formation of structures with cold dense plasma. Radiation losses alone can lead only to a transient drop in the electron temperature recovering later to a level comparable with the unperturbed one. These findings offer a new look on condensation instabilities and structure formation triggered in hot plasmas in the presence of impurities, differing principally from the standard explanation exploiting the effect of radiation losses [108–111, 116]. Ion-ion

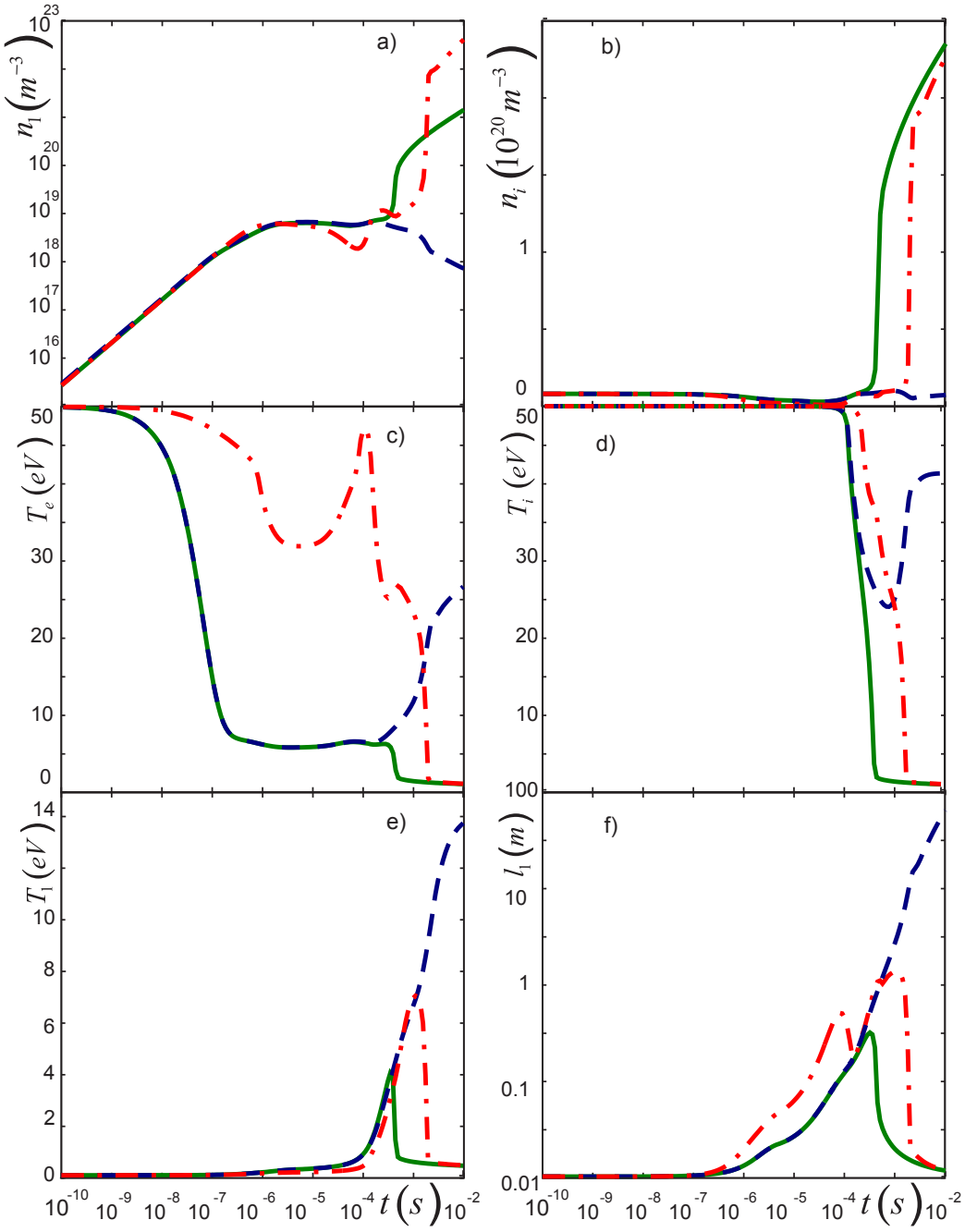


Figure 6.3: Time evolution of the densities of $Li^+$ impurity (a) and main (b) ions, the temperatures of electrons (c), deuterons (d) and $Li^+$ particles (e), and the extension of $Li^+$ shell along the magnetic field (f) computed for $n_0 = 1.5 \cdot 10^{19}\,m^{-3}$, with all cooling mechanisms included (solid curves), without coulomb collisions between main and impurity ions (dashed curves) and without radiation energy losses (dash-dotted curves).

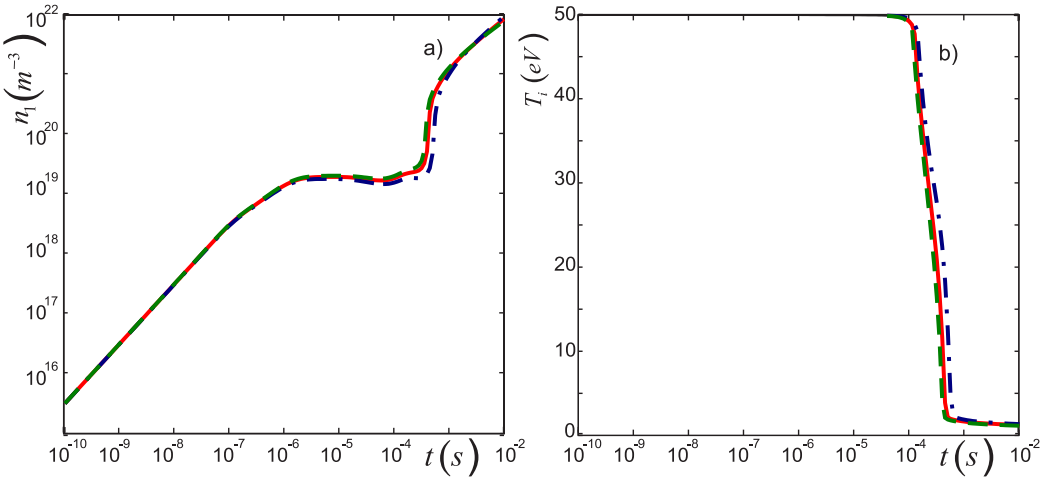


Figure 6.4: Time evolution of the density of $Li^+$ impurity (a) and the temperature of the main ions (b) computed for $n_0 = 1.5 \cdot 10^{19}\, m^{-3}$, with different magnitudes of the perpendicular diffusivities $D_x = D_y$: 1 (solid curves), 0.3 (dashed curves) and $3\, m^2 s^{-1}$ (dash-dotted curves).

coulomb collisions reduce the temperature of the main ions, the collision frequency rises as ${T_i}^{-1.5}$, and $T_i$ drops further. This mechanism is enforced by the confinement of impurity ions near the entrance position due to friction with the main ones that counteracts a dispersion of impurity by their pressure gradient and electric field. In addition also $n_i$ grows up because a flow of the main ions towards the source is generated since the temperature reduction there results in a plasma pressure drop.

In the present study the transport perpendicular to the magnetic field is assumed to be purely diffusive and characterized by the same diffusivities in both perpendicular directions, $D_x = D_y = 1\, m^2 s^{-1}$. To study how critical is this assumption for the results, these parameters have been varied by an order of magnitude, in the range $0.3 - 3\, m^2 s^{-1}$. Figure (6.4) demonstrates the time evolution of the characteristic density of singly charged impurity, $n_1^0$, and of the temperature of the main ions in the shell of $Li^+$ particles, computed with $n_0 = 1.5 \cdot 10^{19}\, m^{-3}$ for three values of $D_x = D_y$. One can see that the results are hardly distinguishable for $D_{x,y} \lesssim 1\, m^2 s^{-1}$ and a moderate delay in the development of the dense cold structure becomes visible if $D_x$ and $D_y$ are enhanced up to $3 m^2 s^{-1}$. This behavior is explained by the fact that the singly charged lithium ions have a relatively short life time and the motion along the magnetic field dominates the evolution of their density and, through coulomb collisions, of the main ion temperature. A higher level of impurity perpendicular transport is normally unrealistic in fusion devices.

### 6.3.3 Criterion for formation of cold dense structures

We have stressed above that the formation of plasma structures discussed in this study can not be directly applied to MARFE phenomenon. It is nonetheless instructive to analyse the relative importance of electron cooling through impurity radiation and cooling of the main ions by coulomb collisions with impurities under the conditions typical for MARFE development. To make the results more transparent, constraints typical for a radiation instability analysis are imposed. We neglect in Eqs. (2.7-2.10) the contributions from perpendicular transport, the energy loss on neutral radiation, the electron-ion heat exchange and the contribution of impurity ions to the electron density, i.e. $n \equiv n_e = n_i$ is assumed henceforth. Instead of Eqs. (2.6) and (2.8) the pressure constancy along the magnetic field is adopted:

$$n\left(T_e + T_i\right) = const. \tag{6.17}$$

This follows from the sum of Eqs. (2.6) and (2.8) where non-stationary and non-linear terms, $\partial_t \Gamma_i$ and $\partial_z \left(\Gamma_i^2/n_i\right)$, respectively, are omitted. (The latter allows to exclude acoustic waves being inessential for the present consideration). Assume that electron and ion temperatures, equal to $T^{ref}$ in the initial stationary state, spontaneously get small perturbations $\widetilde{T}_{e,i} = \widehat{T}_{e,i} \exp\left(\gamma t - ikz\right)$ with a certain wave vector $k$ along the magnetic field. Under these assumptions and for cold impurity ions, $T_1 \ll T^{ref}$, heat transport equations for the main plasma components, Eqs. (2.9) and (2.10), provide a system of equations for the initial perturbation amplitudes $\widehat{T}_{e,i}$:

$$\gamma\left(2\widehat{T}_i + 0.5\widehat{T}_e\right) + \frac{k^2\kappa_{iz}}{n}\widehat{T}_i = \frac{3m_i k_{i1} n_1}{m_I}\left(\widehat{T}_i + 0.5\widehat{T}_e\right) \tag{6.18}$$

$$\gamma\left(2\widehat{T}_e + 0.5\widehat{T}_i\right) + \frac{k^2\kappa_{ez}}{n}\widehat{T}_e = n_1\left[\left(\frac{L_1}{2T^{ref}} - \frac{dL_1}{dT^{ref}}\right)\widehat{T}_e + \frac{L_1}{2T^{ref}}\widehat{T}_i\right] \tag{6.19}$$

The requirement for existence of non-trivial solutions provides an equation for the perturbation growth rate $\gamma$. Consider two limit cases: (i) collision ion cooling is dominant, i.e. $\widehat{T}_e \ll \widehat{T}_i$ and (ii) radiation electron cooling prevails, i.e. $\widehat{T}_i \ll \widehat{T}_e$. In the former one Eq. (6.18) results in:

$$\gamma = \frac{3m_i}{2m}k_{i1}n_1 - \frac{k^2\kappa_{iz}}{n} \tag{6.20}$$

and in the latter one Eq.(6.19) leads to the simplest expression for the increment of radiation instability which is known from the literature:

$$\gamma = \left(\frac{L_1}{2T^{ref}} - \frac{dL_1}{dT^{ref}}\right)\frac{n_1}{2} - \frac{k^2\kappa_{ez}}{2n} \tag{6.21}$$

The condition for the instability threshold, $\gamma = 0$, provides a critical level of the parameter $\eta = n_1 n/k^2$. For an ion collision cooling instability this is:

$$\eta_{coll} = \frac{m\kappa_{iz}}{3m_i k_{i1}} \tag{6.22}$$

and for electron radiation cooling one:

$$\eta_{\rm rad} = \frac{\kappa_{ez}}{0.5L_1/T^{ref} - dL_1/dT^{ref}} \tag{6.23}$$

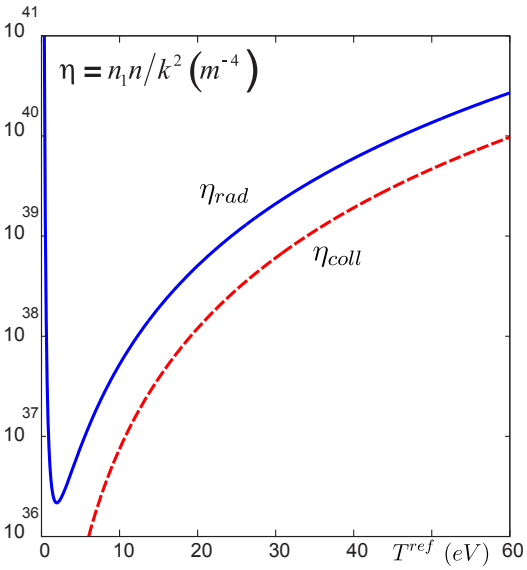


Figure 6.5: Critical parameter $\eta$ for the development of thermal instabilities due to electron cooling with carbon impurity radiation (solid) and cooling of the main ions by coulomb collisions with impurities (dashed).

For certain background plasma and impurity species $\eta_{coll}$ and $\eta_{\rm rad}$ are functions of the temperature $T^{ref}$ only. Figure (6.5) demonstrates these dependences for carbon impurity in a deuterium plasma, a typical situation for tokamak devices [110], with the cooling rate, $L_1$, computed by using data from Ref. [117]. One can see that for the conditions usual for MARFE development, with the edge temperature below $50eV$, an ion collision instability develops at $\eta$ at least several times smaller than the critical value for electron radiation instability. Thus also by studying the MARFE development one has to take ion-ion collisions into account. For impurity ions with the charge $j$ higher than one the cooling rate does not differ significantly from $L_1$ but the friction coefficient increases as $j^2$. Therefore, the conclusion above holds if impurity ions of higher charges are taken into account.

## 6.4 Conclusions

Usually, radiating impurity particles enter the plasma as neutrals with a temperature significantly lower than those of background plasma components. The cooling of electrons through impurity radiation losses considered

normally as the main cause of cold dense structures formation through radiation instability. Coulomb collisions with impurity ions, generated by the ionization of neutrals, however, provide an effective channel to reduce the temperature of the plasma main ions. This offers an independent self-sustaining mechanism for the structure formation since the collision frequency increases non-linearly, as $T_i^{-1.5}$, with decreasing ion temperature.

The friction between main and impurity ions, induced by collisions, counteracts the forces dispersing impurity ions from their source. These forces arise due to the impurity pressure gradient and electric field. The former comes up since there is a maximum in the impurity ion density at the source center, the latter – because, owing to plasma quasi-neutrality, the electron density also has a maximum there. With reducing $T_i$ and increasing friction the impurity cloud shrinks, the impurity ion density grows, collisions are intensified and $T_i$ drops further. Also the radiation energy losses increase further decreasing the electron temperature. As a result a region with high densities and low temperatures of all plasma components arises. In this chapter it was demonstrated that such a phenomenon, however, happens if the impurity neutral density exceeds some critical level. Below this level the forces, dispersing impurity ions, win the competition. Thus, coulomb collisions between main and impurity ion species which, on the one hand, cool down the main ions and, on the other hand, confine impurity ions near the source. This mechanism is efficient even if the impurity radiation, considered usually as the most important cause of condensation instabilities, is completely switched off in the calculations. On the contrary, without ion-ion coulomb collisions the radiation losses result only in a transient cooling of electrons with a later recovery of their temperature to a level comparable with the initial one.

The proposed mechanism of cold dense structure formation may be of relevance for both laboratory plasmas and in interstellar medium.

# Chapter 7

# Summary & Outlook

## 7.1 Main results of this work

Self-consistently modeling of plasma response to impurity spreading from intense localized source is performed in this work. A number of approaches is developed, that describe in fluid approximation the behavior of electrons, main plasma ions, injected neutral and ionized impurity of various charges and take into account the plasma quasi-neutrality, coulomb collisions between charged particles, radiation losses and sinks of particles to bounding material surfaces. The range of applicability is determined for each of the approaches. Calculations, performed by using developed models for the conditions of fusion experiments with impurity seeded plasma, illuminated a number of effects summarized below.

It is well known that injection of impurities into the plasma of fusion devices may significantly change the global plasma behavior, e.g., through the radiation from the plasma core and modification of transport properties. However, noticeable changes in plasma characteristics were shown to happen also locally close to the injection position, by calculating the magnitudes and spatial scales of this modifications.

The spreading of charged impurity along the magnetic field is demonstrated to be determined, on the one hand, by the competition between the electric force and the pressure gradient and, on the other hand, the friction with the main ions and finite, due to perpendicular transport, lifetime on the field line.

The temperature of impurity ions, gained through heat exchange between charged particles exceeds significantly the temperature of impurity neutrals. Different impurity charge states are heated up to different temperatures. Even in stationary state the temperature of low charged impurity species

differs strongly from those of the main plasma components, but approaching to them with increasing charge. This should be taken into account by applying plasma diagnostics based on injection of light impurities.

Heating of the impurity ions by collisions with the main ones is important for impurity transport along magnetic field, since it enhances strongly the impurity pressure gradient. Produced force, pushing impurity ions away from the injection source can overcome the drugging force from the parallel electric field created by enhanced electron density.

Significant increase of the electron density occurs at low enough impurity injection rates where the reduction of plasma temperature can be still neglected.

It was found that even at high injection rates the cooling of magnetic surface occurs not homogeneously. The toroidal symmetry in plasmas, modified by local impurity source, is broken. This is of importance for reconstruction of both plasma parameters from experimentally measured patterns of impurity emissions and properties of the impurity transport in the vicinity of impurity source by measurements in a distant plasma.

Change in time of injection rate, taking place normally due to limited opening time of injection valve and in-vessel geometry, plays a significant role in time evolution of impurity spreading and corresponding bifurcation in plasma behavior.

With increasing injection intensity both the impurity ion density and the area occupied by low charged ions increase. However, at a certain neutral injection rate there is a bifurcation to cold dense plasma caused mostly by cooling of main ions in coulomb collisions with impurity. The bifurcation results in thermal instability and required conditions were examined in this work. This mechanism is found to be efficient even if the impurity radiation, considered usually as the most important cause of condensation instabilities, is completely switched off in calculations. Thus, it was shown that a standard explanation of the formation of cold dense structures in plasmas through radiation instability has to be complemented by taking into account the role of collisions between main and impurity ions. This result is of importance not only for fusion, but also for interstellar media.

The sets of equations arising by development of physical models in question represent systems of partial differential equations with non-linearly interrelated parameters. To obtain the approximate solutions new numerical approaches were developed in this work.

## 7.2 Future developments

Impurity spreading phenomena is restricted in this work by considering of low enough impurity charge states. For higher charge states recombination processes becomes of importance giving non-linear input into impurity particle transport equation. Moreover, higher charge states penetrating deeper into the plasma cause global changes in plasma behavior. For account of these effects, developed approach can be coupled with a one-dimensional code describing time-dependent transport of particles and energy across magnetic surfaces in the presence of impurities, e.g. RITM [65].

Perpendicular transport of particles and energy was shown to play an important role in phenomena described in this work. Characteristic rates are used as free parameters in developed models and coupling with codes describing global plasma changes would help to estimate them more firmly.

Otherwise, with convective transfer of particles and energy and proper boundary conditions far away from the impurity source taken into account, the shell approach used in this work can be extended for the case where higher charge states fill the magnetic surfaces and complete time-dependent three-dimensional modeling can be performed.

The model can be directly applied for calculation of convection and radiation fluxes in the near-wall region and modeling of local impacts onto the wall. This allows to estimate the radiation loads on the injection valves and other wall elements. Complemented by conductive heat transport inside plasma facing material the model can be extended to self-consistent description of interaction between plasma and wall components under conditions of intensive impurity sources.

# Appendix A

## A.1 Condition of zero parallel current

The pressure gradient $\nabla P$ disturbed in the impurity cloud induces a perturbation in the perpendicular diamagnetic currents, $\mathbf{j}_\perp$. From the force balance, $\nabla P = \mathbf{j} \times \mathbf{B}$, we get:

$$|j_\perp| \approx \frac{n_I T_e}{l_0 B}$$

Through the plasma quasi-neutrality, $\nabla \cdot \mathbf{j} = \mathbf{0}$, this violates zero parallel current condition, $j_z \equiv e\left(\Gamma_i + \Gamma_I - \Gamma_e\right) = 0$, so that:

$$|\ j_z| \approx l_c \frac{\left|\widetilde{j}_\perp\right|}{l_0} \approx \frac{n_I T_e l_c}{l_0^2 B}$$

With the estimate $\Gamma_I \approx n_I \sqrt{T_e/m_I}$ one finds:

$$\frac{|\ j_z|}{e\Gamma_I} \approx \frac{\sqrt{T_e m_I} l_c}{eBl_0^2} = \frac{\rho_I l_c}{l_0^2}$$

where $\rho_I$ is the Larmor radius of singly ionized impurity ions. For the conditions of experiments modeled in this paper and a magnetic field $B \gtrsim 1T$, we obtain $|\ j_z| \leq 0.1 e\Gamma_I$. Thus, by estimating $\Gamma_e$ from the assumption $j_z = 0$, one does not make a large error.

## A.2 Calculation of the heat flux into the cloud

Here for concreteness we derive Eq. (3.27) for $q_e$. With the assumed relation between temperatures, Eq. (3.26), the pressure balance, Eq. (3.7),

gives:

$$n = \frac{n^\infty}{\psi}\frac{T_i^\infty + T_e^\infty}{T_e + \tau T_e^\infty}$$

where $\psi = 1 + \left(T_i^\infty - T_i^c\right) / \left(T_e^\infty - T_e^c\right)$
and $\tau = \left(T_i^c - T_i^\infty T_e^c / T_e^\infty\right) / \left(T_e^\infty - T_e^c + T_i^\infty - T_i^c\right)$.
Under the assumptions made in the beginning of section (3.1.3), beyond the impurity cloud, $z < z_* - l_c^-$, Eq. (3.8) takes the form:

$$\frac{dq_e}{dz} = 1.5\left(T_e^\infty - T_e\right)\nu_\perp^e n$$

By multiplying both hands of Eq. (3.25) by $2q_e dz = 2\kappa_{||}^e dT_e$, one can make a transition from the integration over $z$ to the integration over $T_e$:

$$dq_e^2 = -3A_e n_\infty \nu_\perp^e \frac{T_i^\infty + T_e^\infty}{\psi}\left(T_e\right)^{2.5}\frac{T_e^\infty - T_e}{T_e + \tau T_e^\infty}dT_e$$

where the electron heat conductivity is taken in the form $\kappa_{||}^e = A_{||}^e T_e^{2.5}$ [59].

The heat flux density $q_e$ changes from zero in the distant plasma, where $T_e = T_e^\infty$, to the value $q_e^c$ at the boundary of the impurity cloud, where $T_e = T_e^c$. Thus:

$$\left(q_e^c\right)^2 = B_e \int\limits_{T_e^c}^{T_e^\infty} \frac{1 - T_e/T_e^\infty}{T_e/T_e^\infty + \tau}\left(\frac{T_e}{T_e^\infty}\right)^{2.5} d\frac{T_e}{T_e^\infty} = 2B_e \int\limits_{\Theta}^{1} \frac{1-\theta^2}{\theta^2 + \tau}\theta^6 d\theta$$

with $B_e = 3A_{||}^e n_\infty \nu_\perp^e \left(T_e^\infty\right)^{3.5}\left(T_i^\infty + T_e^\infty\right)/\psi$, $\Theta_e = \sqrt{T_e^c/T_e^\infty}$, and $\theta = \sqrt{T_e/T_e^\infty}$. As a result of integration, see e.g. Ref. [118], we get $q_e^c = \sqrt{2B_e\Psi_e}$, where

$$\Psi_e = (1+\tau)\left(\frac{1-\Theta_e^5}{5} - \tau\frac{1-\Theta_e^3}{3} + \tau^2\left(1-\Theta_e\right) - |\tau|^{2.5}\varphi\right) - \frac{1-\Theta_e^7}{7}$$

with

$$\varphi\left(\tau > 0\right) = \arctan\frac{1}{\sqrt{\tau}} - \arctan\frac{\Theta_e}{\sqrt{\tau}}$$

in the case of $T_e^\infty > T_i^\infty$, and

$$\varphi\left(\tau < 0\right) = \frac{1}{2}\ln\frac{\left(1+\sqrt{-\tau}\right)\left(\Theta_e - \sqrt{-\tau}\right)}{\left(1-\sqrt{-\tau}\right)\left(\Theta_e + \sqrt{-\tau}\right)}$$

for $T_e^\infty < T_i^\infty$. Note that both cases $\tau = -1$ and $\tau = -T_e^c/T_e^\infty$, leading in the latter expression to singularities, correspond to the condition $T_e^c = T_e^\infty$

and, thus, $q_e^c = 0$. Finally:

$$q_e^c = \sqrt{\frac{6A_{\|}^e \nu_{\perp}^e n_\infty \left(T_i^\infty + T_e^\infty\right) \left(T_e^\infty\right)^{3.5}}{1 + \left(T_i^\infty - T_i^c\right) / \left(T_e^\infty - T_e^c\right)}} \Psi_e$$

A similar derivation can be done for $q_i^c$.

## A.3 Reduction of time-dependent model to stationary case

By neglecting time derivatives in Eqs. (4.2-4.6) one obtains:

$$k_{ion}^{j-1} n_e n_{s,j-1} l_{j-1} \delta_{j-1} = \nu_I^j n_{s,j} l_j \delta_j \tag{A.1}$$

$$\Gamma_{s,j} = \nu_I^j n_{s,j} l_{d,j} \tag{A.2}$$

$$D_y / \delta_{d,j} = \nu_I^j \delta_{d,j} \tag{A.3}$$

$$\begin{aligned} &k_{ion}^{j-1} n_e \Gamma_{s,j-1} l_{s,j} \delta_{s,j}/2 - \left(k_{ij} n_i + \nu_I^j\right) \Gamma_{s,j} \left(l_{s,j}/2 + l_{d,j}\right) \delta_j \\ &+ \left(n_{s,j} T_j + T_e \left[j n_{s,j} - n_i \ln\left(1 + \frac{j n_{s,j}}{n_i}\right)\right]\right) \frac{\delta_j}{m_I} = 0 \end{aligned} \tag{A.4}$$

$$\begin{aligned} &k_{ion}^{j-1} n_e \left(n_{s,j-1}/n_{s,j}\right) \left(T_{j-1} - T_j\right) \left(l_{s,j}/l_j\right) \left(\delta_{s,j}/\delta_j\right) \\ &+2k_{ij} n_i \left(T_i - T_j\right) + 2k_{ej} n_e \left(T_e - T_j\right) = 0 \end{aligned} \tag{A.5}$$

which gives stationary solutions for the shell widths $\delta_j$ and temperatures $T_j$ and interrelation for the shell lengths $l_j$:

$$T_j = \frac{T_{j-1}\nu_I^j + 2\left(k_{ej} n_e T_e + k_{ij} n_i T_i\right)}{\nu_I^j + 2\left(k_{ej} n_e + k_{ij} n_i\right)} \tag{A.6}$$

$$\delta_j = \delta_{j-1} + \sqrt{D_y / \nu_I^j} \tag{A.7}$$

$$l_j = l_{j-1} + \Gamma_{s,j} / \left(n_{s,j} \nu_I^j\right) \tag{A.8}$$

By substituting the latter in Eq. (A.4) one obtains the quadratic equation for $\Gamma_{s,j}$:

$$\left(\frac{\Gamma_{s,j}}{n_{s,j}}\right)^2 + \frac{l_{j-1}\nu_I^j}{2n_{s,j}} - \frac{\nu_I^j}{k_{ij} n_i} C_j = 0 \tag{A.9}$$

where $C_j = \frac{T_j}{m_I} + \frac{T_e}{m_I}\left(j - \frac{n_i}{n_{s,j}} \ln \frac{n_e}{n_i}\right) + \frac{k_{ion}^{j-1} n_e \Gamma_{s,j-1}}{n_{s,j}} \frac{l_{j-1}\delta_{j-1}}{\delta_j}$. From its two roots one has to chose the solution possessing physical meaning:

$$\Gamma_j = \frac{n_{s,j}}{4}\left(\sqrt{\left(l_{j-1}\nu_I^j\right)^2 + 16 C_j \frac{\nu_I^j}{k_{ij} n_i}} - l_{j-1}\nu_I^j\right) \tag{A.10}$$

Substitution of calculated $\Gamma_{s,j}$ and $l_j$ into Eq. (A.1) gives the equation for $n_{s,j}$

$$\left(n_{s,j}\nu_I^j l_{j-1} + \Gamma_{s,j}\right)\left(\delta_{j-1} + \sqrt{D_y/\nu_I^j}\right) = k_{ion}^{j-1} n_e n_{s,j-1} l_{j-1}\delta_{j-1} \tag{A.11}$$

which is solved by bisection.

# Bibliography


[1] J. Sheffield "World population growth and the role of annual energy use per capita" *Techn. Forecast. and Soc. Change* **59** (1998) 55-87 http://dx.doi.org/10.1016/S0040-1625(97)00071-1

[2] L. Miranda "On the forecasting of the challenging world future scenarios" *Techn. Forecast. and Soc. Change* **78** (2011) 1445-1470 http://dx.doi.org/10.1016/j.techfore.2011.04.001

[3] J. Bogo "Lone star energy: why Texas will resist the call for a unified grid" *Pop. Mechanics*, 18 Dec 2009 http://www.popularmechanics.com/science/energy/solar-wind/4333893

[4] J. McCall "Superconductor electricity pipelines: an optimal long-haul transmission solution" *Alt. Energy eMag.*, Sep 2009 http://www.altenergymag.com/emagazine/2009/08/superconductor-electricity-pipelines-an-optimal-long-haul-transmission-solution/1371

[5] J. Ongena and G. Van Oost "Energy for future centuries. Prospects for fusion power as a future energy source." *Fus. Sci. and Tech.* **57** 2T (2010) 3-15

[6] M. Bunn and O. Heinonen "Preventing the next Fukushima" *Science* **333** (2011) 1580-1581 http://dx.doi.org/10.1126/science.1209668

[7] J. Wood *Nuclear Power*, The Institution of Engineering and Technology, London, 2007, chapter 3

[8] T. J. Dolan *Fusion research: principles, experiment and technology*, Pergamon Press, 2000, chapter 4

[9] E. R. Rebhan and G. Van Oost "Thermonuclear Burn Criteria for D-T Plasmas" *Fus. Sci. Tec.* **49** 2T (2006) 16-26

[10] G. Goncharov "From the Archive of the President, Russian Federation (USSR Council of Ministers Resolution)" *Phys.-Usp.* **44** (2001) 859-861 http://dx.doi.org/10.1070/PU2001v044n08ABEH001074

[11] "Fusion for the Future: ITER" *The Astronomist*, May 11, 2012 http://theastronomist.fieldofscience.com/2012/05/fusion-for-future-iter.html

[12] J. Wesson (ed.) *Tokamaks*, $3^{rd}$ ed., Oxford: Clarendon Press, 2004

[13] L. D. Horton "Physics issues for DEMO" *Fus. Sci. and Tech.* **53** 2T (2008) 468-473

[14] J. Jacquinot and the JET team "Deuterium-tritium operation in magnetic confinement experiments: results and underlying physics" *Plasma Phys. Control. Fusion* **41** (1999) A13-A46 http://dx.doi.org/10.1088/0741-3335/41/3A/002

[15] M. J. Loughlin "Neutron profile measurements for trace tritium experiments" *Rev. Sci. Instrum.* **70** (1999) 1123-1125 http://dx.doi.org/10.1063/1.1149330

[16] J. W. Coenen *et al* 2011 "Analysis of tungsten melt-layer motion and splashing under tokamak conditions at TEXTOR" *Nucl. Fusion* **51** 083008 (11pp) http://dx.doi.org/10.1088/0029-5515/51/8/083008

[17] M. Z. Tokar *et al* 2012 "Tokamak plasma response to droplet spraying from melted plasma-facing components" *Nucl. Fusion* **52** 013013 (6pp) http://dx.doi.org/10.1088/0029-5515/52/1/013013

[18] D. E. Post *et al* "Steady-state radiative cooling rates for low-density, high-temperature plasmas" *Atomic Data and Nuclear Data Tables* **20** (1977) 397-439 http://dx.doi.org/10.1016/0092-640X(77)90026-2

[19] G. S. Voronov "A practical formula for ionization rate coefficients of atoms and ions by electron impact: $Z = 1 - 28$" *Atomic Data and Nuclear Data Tables* **65** (1997) 1-35 http://dx.doi.org/10.1006/adnd.1997.0732

[20] G. M. McCracken and P. E. Stott "Plasma-surface interactions in tokamaks" *Nucl. Fusion* **19** (1979) 889-981 http://dx.doi.org/10.1088/0029-5515/19/7/004

[21] D. M. Meade "Effect of high-Z impurities on the ignition and Lawson conditions for a thermonuclear reactor" *Nucl. Fusion* **14** (1974) 289-291 http://dx.doi.org/10.1088/0029-5515/14/2/017

[22] V. A. Vershkov and S. V. Mirnov "Role of impurities in current tokamak experiments" *Nucl. Fusion* **17** (1974) 383-395 http://dx.doi.org/10.1088/0029-5515/14/3/012

[23] V. I. Gervids and V. I. Kogan "Dependence of the radiation losses of a thermonuclear plasma on the atomic number of the impurity and the temperature" *JETP Lett.* **21** (1975) 150-151 http://www.jetpletters.ac.ru/ps/1465/article_22319.shtml

[24] R. V. Jensen *et al* "Calculations of impurity radiation and its effects on tokamak experiments" *Nucl. Fusion* **17** (1977) 1187-1196 http://dx.doi.org/10.1088/0029-5515/17/6/007

[25] R. J. Hawryluk *et al* "The effect of current profile evolution on plasma-limiter interaction and the energy confinement time" *Nucl. Fusion* **19** (1979) 1307-1317 http://dx.doi.org/10.1088/0029-5515/19/10/002

[26] M. Z. Tokar *et al* "Nature of high-Z impurity accumulation in tokamaks" *Nucl. Fusion* **37** (1997) 1691-1708 http://dx.doi.org/10.1088/0029-5515/37/12/I03

[27] Y. Shimomura "Possibility of heavy-impurity control by light-impurity radiation in a large tokamak" *Nucl. Fusion* **17** (1977) 626-628 http://dx.doi.org/10.1088/0029-5515/17/3/021

[28] U. Samm *et al* "Radiative edges under control by impurity fluxes" *Plasma Phys. Control. Fusion* **35** (1993) B167-B175 http://dx.doi.org/10.1088/0741-3335/35/SB/013

[29] V. A. Evtikhin *et al* "Lithium divertor concept and results of supporting experiments" *Plasma Phys. Control. Fusion* **44** (2002) 955-977 http://dx.doi.org/10.1088/0741-3335/44/6/322

[30] S. Mirnov "Plasma-wall interactions and plasma behaviour in fusion devices with liquid lithium plasma facing components" *J. Nucl. Mater.* **390–391** (2009) 876-885 http://dx.doi.org/10.1016/j.jnucmat.2009.01.228

[31] G. Mazzitelli *et al* "FTU results with a liquid lithium divertor" *Nucl. Fusion* **51** (2011) 073006 (7pp) http://dx.doi.org/10.1088/0029-5515/51/7/073006

[32] G. M. McCracken *et al* "A study of detached plasmas in the DITE tokamak" *J. Nucl. Mater.* **145–147** (1987) 181-185 http://dx.doi.org/10.1016/0022-3115(87)90323-0

[33] U. Samm *et al* "Influence of impurity radiation losses on plasma edge properties in TEXTOR" *J. Nucl. Mater.* **176–177** (1990) 273-277 http://dx.doi.org/10.1016/0022-3115(90)90059-V

[34] F. Alladio *et al* "The regime of enhanced particle recycling in high density tokamak discharges in the Frascati torus" *Phys. Lett. A* **90** (1982) 405-409 http://dx.doi.org/10.1016/0375-9601(82)90796-4

[35] K. McCormick *et al* "Edge density measurements with a fast Li beam probe in tokamak and stellarator experiments" *Fusion Eng. Des.* **34–35** (1997) 125-134 http://dx.doi.org/10.1016/S0920-3796(96)00685-0

[36] P. Wienhold *et al* "Investigation of carbon transport in the scrape-off layer of TEXTOR-94" *J. Nucl. Mater.* **290–293** (2001) 362-366 http://dx.doi.org/10.1016/S0022-3115(00)00573-0

[37] ITER Physics Expert Group "ITER physics basis. Chapter 1: Overview and summary" *Nucl. Fusion* **39** (1999) 2137-2638 http://dx.doi.org/10.1088/0029-5515/39/12/301

[38] H. Takenaga *et al* "Compatibility of advanced tokamak plasma with high density and high radiation loss operation in JT-60U" *Nucl. Fusion* **45** (2005) 1618-1627 http://dx.doi.org/10.1088/0029-5515/45/12/017

[39] A. Kallenbach *et al* "Non-boronized compared with boronized operation of ASDEX Upgrade with full-tungsten plasma facing components" *Nucl. Fusion* **49** (2009) 045007 (10pp) http://dx.doi.org/10.1088/0029-5515/49/4/045007

[40] G. P. Maddison "Moderation of divertor heat loads by fuelling and impurity seeding in well-confined ELMy H-mode plasmas on JET" *et al Nucl. Fusion* **51** (2011) 042001 (6pp) http://dx.doi.org/10.1088/0029-5515/51/4/042001

[41] S. Moradi *et al* "Modeling of energy confinement improvement in high power JET discharges with neon seeding" *Plasma Phys. Control. Fusion* **54** (2012) 015004 (11pp) http://dx.doi.org/10.1088/0741-3335/54/1/015004

[42] L. Delgado-Aparicio *et al* "Impurity transport studies in NSTX neutral beam heated H-mode plasmas" *Nucl. Fusion* **49** (2009) 085028 (10pp) http://dx.doi.org/10.1088/0029-5515/49/8/085028

[43] J. E. Rice *et al* "Transport of injected impurities in Heliotron E" *Nucl. Fusion* **24** (1984) 1205-1211 http://dx.doi.org/10.1088/0029-5515/24/9/010

[44] Wendelstein VII-A Team and NI Group "Impurity transport in the Wendelstein VII-A stellarator" *Nucl. Fusion* **25** (1985) 1593-1609 http://dx.doi.org/10.1088/0029-5515/25/11/006

[45] Y. Nakamura *et al* "Impurity behaviour in LHD long pulse discharges" *Plasma Phys. Control. Fusion* **44** (2002) 2121-2134 http://dx.doi.org/10.1088/0741-3335/44/10/304

[46] P.C. De Vries *et al* "Survey of disruption causes at JET" *Nucl. Fusion* **51** (2011) 053018 (12pp) http://dx.doi.org/10.1088/0029-5515/51/5/053018

[47] B. Pegourie and J.-M. Picchiottino "Pellet ablation theory and experiments" *Plasma Phys. Control. Fusion* **35** (1993) B157-B166 http://dx.doi.org/10.1088/0741-3335/35/SB/012

[48] D. G. Whyte *et al* "Mitigation of tokamak disruptions using high-pressure gas injection" *Phys. Rev. Lett.* **89** (2002) 055001 (4pp) http://dx.doi.org/10.1103/PhysRevLett.89.055001

[49] R. S. Granetz *et al* "Gas jet disruption mitigation studies on Alcator C-Mod and DIII-D" *Nucl. Fusion* **47** (2007) 1086-1091 http://dx.doi.org/10.1088/0029-5515/47/9/003

[50] M. Lehnen *et al* "Disruption Mitigation by massive gas injection in JET" *Proc. of the* $23^{rd}$ *IAEA Fusion Energy Conference*, Daejon, Rep. of Korea, 11-16 October 2010, EXS/P2-13 http://www-pub.iaea.org/mtcd/meetings/PDFplus/2010/cn180/cn180_papers/exs_p2-13.pdf

[51] M. Bakhtiari *et al* "Using mixed gases for massive gas injection disruption mitigation on Alcator C-Mod" *Nucl. Fusion* **51** (2011) 063007 (9pp) http://dx.doi.org/10.1088/0029-5515/51/6/063007

[52] M. Sugihara *et al* "Disruption scenarios, their mitigation and operation window in ITER" *Nucl. Fusion* **47** (2007) 337-352 http://dx.doi.org/10.1088/0029-5515/47/4/012

[53] D. G. Whyte *et al* "Disruption mitigation with high-pressure noble gas injection" *J. Nucl. Mater.* **313–316** (2003) 1239-1246 http://dx.doi.org/10.1016/S0022-3115(02)01525-8

[54] D. Kh. Morozov *et al* "Mechanisms of disruptions caused by noble gas injection into tokamak plasmas" *Nucl. Fusion* **45** (2005) 882-887 http://dx.doi.org/10.1088/0029-5515/45/8/015

[55] M. Lehnen *et al* "Disruption mitigation by massive gas injection in JET" *Nucl. Fusion* **51** (2011) 123010 (12pp) http://dx.doi.org/10.1088/0029-5515/51/12/123010

[56] B. Pégourié *et al* "Supersonic gas injection on Tore Supra" *J. Nucl. Mater.* **313–316** (2003) 539-542 http://dx.doi.org/10.1016/S0022-3115(02)01462-9

[57] P. T. Lang *et al* "Impact of a pulsed supersonic deuterium gas jet on the ELM behaviour in ASDEX Upgrade" *Plasma Phys. Control. Fusion* **47** (2005) 1495-1516 http://dx.doi.org/10.1088/0741-3335/47/9/009

[58] M. Z. Tokar and S. Moradi "Optimization of isotope composition of fusion plasmas" *Nucl. Fusion* **51** (2011) 063013 (9pp) http://dx.doi.org/10.1088/0029-5515/51/6/063013

[59] S. I. Braginskii "Transport Processes in a Plasma" in *Reviews of Plasma Physics*, ed. M. A. Leontovich, New York: Consultants Bureau, **1** (1965) 205-311

[60] K-U. Riemann "Review article: the Bohm criterion and sheath formation" *J. Phys. D: Appl. Phys.* **24** (1991) 493-518 http://dx.doi.org/10.1088/0022-3727/24/4/001

[61] M. Z. Tokar "Fluid approximation of the Bohm criterion for plasmas of several ion species" *Contrib. Plasma Phys.* **34** (1994) 139-144 http://dx.doi.org/10.1002/ctpp.2150340208

[62] D. G. Whyte *et al* "Energy balance, radiation and stability during rapid plasma termination via impurity pellet injections on DIII-D" *Proc. of* $24^{th}$ *European Conference on Controlled Fusion and Plasma Physics*, June 914, 1996, Berchtesgaden, Germany http://www.osti.gov/bridge/servlets/purl/513523-3yAR1V

[63] B. V. Kuteev *et al* "Emergency discharge quench or rampdown by a noble gas pellet" *Nucl. Fusion* **35** (1995) 1167-1172 http://dx.doi.org/10.1088/0029-5515/35/10/I02

[64] E. O. Baronova and V. V. Vikhrev "Modeling of Plasma parameters during high pressure gas injection with a three temperature model" *Contrib. Plasma Phys.* **50** (2010) 313-318 http://dx.doi.org/10.1002/ctpp.201010051

[65] M. Z. Tokar "Modelling of detachment in a limiter tokamak as a nonlinear phenomenon caused by impurity radiation" *Plasma Phys. Control. Fusion* **36** (1994) 1819-1843 http://dx.doi.org/10.1088/0741-3335/36/11/009

[66] A. Savtchkov *Mitigation of disruptions in a tokamak by means of large gas injection*, PhD thesis, Forschungszentrum Jülich, 2003 (85pp), chapter 6

[67] V. Rozhansky *et al* "Penetration of supersonic gas jets into a tokamak" *Nucl. Fusion* **46** (2006) 367-382 http://dx.doi.org/10.1088/0029-5515/46/2/019

[68] P. C. Stangeby and J. D. Elder "Calculation of observable quantities using a divertor impurity interpretive code, DIVIMP" *J. Nucl. Mater.* **196–198** (1992) 258-263 http://dx.doi.org/10.1016/S0022-3115(06)80042-5

[69] D. Reiser, D. Reiter and M. Z. Tokar "Improved kinetic test particle model for impurity transport in tokamaks" *Nucl. Fusion* **38** (1998) 165-177 http://dx.doi.org/10.1088/0029-5515/38/2/302

[70] D. Naujoks *et al* "Material transport by erosion and redeposition on surface probes in the scrape-off layer of JET" *Nucl. Fusion* **33** (1993) 581-590 http://dx.doi.org/10.1088/0029-5515/33/4/I05

[71] A. J. Kirschner *et al* "Modelling of carbon transport in fusion devices: evidence of enhanced re-erosion of in-situ re-deposited carbon" *J. Nucl. Mater.* **328** (2004) 62-66 http://dx.doi.org/10.1016/j.jnucmat.2004.03.011

[72] B. J. Braams *Computational studies in tokamak equilibrium and transport*, PhD Thesis, Rijksuniversiteit Utrecht, 1986 (217pp)

[73] D. Reiter *et al* "The EIRENE and B2-EIRENE codes" *Fusion Sci. and Tech.* **47** (2005) 172-186

[74] R. Schneider *et al* "B2-EIRENE simulation of ASDEX and ASDEX-Upgrade scrape-off layer plasmas" *J. Nucl. Mater.* **196–198** (1992) 810-815 http://dx.doi.org/10.1016/S0022-3115(06)80147-9

[75] T. D. Rognlien *et al* "2-D fluid transport simulations of gaseous/radiative divertors" *Contrib. Plasma Phys.* **34** (1994) 362-367 http://dx.doi.org/10.1002/ctpp.2150340241

[76] R. Zagórski, H. Gerhauser and H. A. Claassen "Numerical Simulation of the TEXTOR Edge Plasma Including Drifts and Impurities" *Contrib. Plasma Phys.* **38** (1998) 61-66 http://dx.doi.org/10.1002/ctpp.2150380110

[77] I. S. Landman *et al* "Modeling of wall and SOL processes and contamination of ITER plasma after impurity injection with the tokamak code TOKES" *Fusion Eng. Design* **85** (2010) 1366-1370 http://dx.doi.org/10.1016/j.fusengdes.2010.03.044

[78] I. S. Landman *et al* "Two-dimensional modeling of disruption mitigation by gas injection" *Fusion Eng. Design* **86** (2011) 1616-1619 http://dx.doi.org/10.1016/j.fusengdes.2010.12.017

[79] S. Pestchanyi *et al* "Verification of TOKES simulations against the MGI experiments in JET" (2012) in press, corrected proof http://dx.doi.org/10.1016/j.fusengdes.2012.02.107

[80] Y. Feng *et al* "A 3D Monte Carlo code for plasma transport in island divertors" *J. Nucl. Mater.* **241–243** (1997) 930-934 http://dx.doi.org/10.1016/S0022-3115(97)80168-7

[81] S. I. Krasheninnikov "On scrape off layer plasma transport" *Phys. Lett. A* **283** (2001) 368-370 http://dx.doi.org/10.1016/S0375-9601(01)00252-3

[82] P. C. Stangeby *The plasma boundary of magnetic fusion devices*, London: IOP Publishing, 2000

[83] S. Chapman "Thermal diffusion in ionized gases" *Proc. Phys. Soc.*, London, Sect. A **A72** (1958) 353-362 http://dx.doi.org/10.1088/0370-1328/72/3/305

[84] M. Z. Tokar *et al* "Modelling of plasma behaviour in the vicinity of intensive impurity sources" *Plasma Phys. Control. Fusion* **52** (2010) 075003 (10pp) http://dx.doi.org/10.1088/0741-3335/52/7/075003

[85] E. M. Epperlein and R. W. Short "Nonlocal heat transport effects on the filamentation of light in plasmas" *Phys. Fluids B* **4** (1992) 2211-2216 http://dx.doi.org/10.1063/1.860025

[86] R. W. Harvey *et al* "Electron dynamics associated with stochastic magnetic and ambipolar electric fields" *Phys. Rev. Lett.* **47** (1981) 102-105 http://dx.doi.org/10.1103/PhysRevLett.47.102

[87] M. Z. Tokar *et al* "Numerical solution of momentum balance equations for plasmas with two ion species" *J. Comp. Phys.* **230** (2011) 2696-2705 http://dx.doi.org/10.1016/j.jcp.2011.01.013

[88] G. M. McCracken *et al* "Studies of fuelling rates of $CO$, $CH_4$ and oxygen in the TEXTOR tokamak" *J. Nucl. Mater.* **196–198** (1992) 199-203 http://dx.doi.org/10.1016/S0022-3115(06)80031-0

[89] R. K. Janev and D. Reiter "Collision processes of $CH_y$ and $CH_y^+$ hydrocarbons with plasma electrons and protons" *Phys. Plasmas* **9** (2002) 4071-4081 http://dx.doi.org/10.1063/1.1500735

[90] M. Z. Tokar "Effect of radial particle transport on radiation from light impurities" *Nucl. Fusion* (1994) **34** 853-861 http://dx.doi.org/10.1088/0029-5515/34/6/I08

[91] S. Jardin *Computational methods in plasma physics*, Boca Raton: CRC Press, 2000 (340pp)

[92] D. Potter *Computational Physics* London: John Wiley & Sons, 1973

[93] G. M. D. Hogeweij *et al* "Confinement and transport in EC heated RI-mode discharges in TEXTOR-94" *Proc. of the* $28^{th}$ *EPS Conference on Contr. Fusion and Plasma Phys.*, Funchal, 18-22 June 2001, ECA Vol. **25A** 1381-1384 http://www.cfn.ist.utl.pt/EPS2001/CD/pdfs/P4.013.pdf

[94] S. Jachmich *et al* "Influence of impurity seeding on ELM behaviour and edge pedestal in ELMy H-Mode discharges" *Proc. of the* $28^{th}$ *EPS Conference on Contr. Fusion and Plasma Phys.*, Funchal, 18-22 June 2001, ECA Vol. **25A** 977-980 http://www.cfn.ist.utl.pt/EPS2001/CD/pdfs/P3.013.pdf

[95] H. Kubo *et al* "High radiation and high density experiments in JT-60U" *Nuclear Fusion* **41** (2001) 227-233 http://dx.doi.org/10.1088/0029-5515/41/2/310

[96] P. Dumortier *et al* "Confinement properties of high density impurity seeded ELMy H-mode discharges at low and high triangularity on JET" *Plasma Phys. Control. Fusion* **44** (2002) 1845-1861 http://dx.doi.org/10.1088/0741-3335/44/9/304

[97] G. D. Porter *et al* "Characterization of the separatrix plasma parameters in DIII-D" *Phys. Plasmas* **5** (1998) 1410-1423 http://dx.doi.org/10.1063/1.872830

[98] Atomic Data and Analysis Structure http://www.adas.ac.uk/

[99] D. M. Young, Jr. *Iterative methods for solving partial difference equations of elliptic type*, PhD Thesis, Harvard University Cambridge, Mass, 1950 (74pp)

[100] A. Huber *et al* "Radiation loads onto plasma-facing components of JET during transient events –Experimental results and implications for ITER" *J. Nucl. Mater.* **415** (2011) S821S827 http://dx.doi.org/10.1016/j.jnucmat.2010.10.061

[101] J. Marshall "Performance of a hydromagnetic plasma gun" *Phys. Fluids* **3** (1960) 134-135 http://dx.doi.org/10.1063/1.1705989

[102] B. Novak and S. Pekarek "A fast acting allmetal gas valve for plasma research" *Rev. Sci. Instrum.* **41** (1970) 369-373 http://dx.doi.org/10.1063/1.1684519

[103] M. G. Haines "A review of the dense Z-pinch" *Plasma Phys. Control. Fusion* **53** (2011) 093001 (168pp) doi:10.1088/0741-3335/53/9/093001

[104] T. C. Jernigan *et al* "Massive gas injection systems for disruption mitigation on the DIII-D tokamak" $21^{st}$ *IEEE/NPSS symposium on fusion engineering*, Knoxville, Tennessee, USA, Sept 26-29, 2005, 11_ 17 www.telegrid.enea.it/Conferenze/SOFE05/DATA/11_17.PDF

[105] K. H. Finken, M. Lehnen and S. A. Bozhenkov "A new disruption mitigation valve (DMV) and gas flow in guiding tubes of different diameter" *Nucl. Fusion* **51** (2011) 033007 (12pp) doi:10.1088/0029-5515/51/3/033007

[106] M. Greenwald "Density limits in toroidal plasmas" *Plasma Phys. Control. Fusion* **44** (2002) R27-R80 http://dx.doi.org/10.1088/0741-3335/44/8/201

[107] A. Brandenburg, M. J. Korpi and A. J. Mee "Thermal Instability in shearing and periodic turbulence" *Astrophys. J.* **654** (2007) 945-954 http://dx.doi.org/10.1086/509143

[108] E. N. Parker *Astrophys. J.* "Instability of thermal fields" **117** (1953) 431-436 http://articles.adsabs.harvard.edu/full/1953ApJ...117..431P

[109] G. B. Field "Thermal instability" *Astrophys. J.* **142** 531-567 (1965) http://articles.adsabs.harvard.edu/full/1965ApJ...142..531F

[110] B. Lipschultz *et al* "Marfe: an edge plasma phenomenon" *Nucl. Fusion* **24** (1984) 977-988 http://dx.doi.org/10.1088/0029-5515/24/8/002

[111] J. F. Drake "Marfes: Radiative condensation in tokamak edge plasma" *Phys. Fluids* **30** (1987) 2429-2433 http://dx.doi.org/10.1063/1.866133

[112] M. Z. Tokar "Localized recycling as a trigger of MARFE" *J. Nucl. Mater.* **266–269** (1999) 958-962 http://dx.doi.org/10.1016/S0022-3115(98)00680-1

[113] M. Z. Tokar *et al* "A model for particle and heat losses by type I edge localized modes" *Plasma Phys. Control. Fusion* **49** (2007) 395-403 http://dx.doi.org/10.1088/0741-3335/49/4/004

[114] K. L. Bell *et al* "Recommended data on the electron impact ionization of light atoms and ions" *J. Phys. Chem. Ref. Data* **12** (1983) 891-916 http://dx.doi.org/10.1063/1.555700

[115] J. Schweinzer *et al* "Database for inelastic collisions of lithium atoms with electrons, protons, and multiply charged ions" *Atomic Data and Nuclear Data Tables* **72** (1999) 239-273 http://dx.doi.org/10.1006/adnd.1999.0815

[116] W. M. Stacey "Thermal stability of the tokamak plasma edge" *Plasma Phys. Control. Fusion* **39** (1997) 1245 http://dx.doi.org/10.1088/0741-3335/39/8/006

[117] Y. Itikawa "Electron-impact cross sections and rate coefficients for excitations of carbon and oxygen ions" *Atomic Data and Nuclear Data Tables* **33** (1985) 149-193 http://dx.doi.org/10.1016/0092-640X(85)90025-7

[118] H. B. Dwight, *Tables of integrals and other mathematical data*, New York: The Macmillan Company, 1961, p. 31

# List of publications 2009-2012

## Articles

"Time-dependent shell model for spreading of impurities locally injected into hot plasmas" M. Koltunov and M. Z. Tokar *Plasma Phys. Control. Fusion* **54** (2012) 025003 (11pp)
http://dx.doi.org/10.1088/0741-3335/54/2/025003

"Modeling of non-stationary local response on impurity penetration in plasma" M. Z. Tokar and M. Koltunov *Phys. Plasmas* **19** (2012) 042502 (9pp) http://dx.doi.org/10.1063/1.3701555

"Proposed mechanism for the formation of cold dense structures in plasmas" M. Z. Tokar and M. Koltunov *Phys. Rev. E* **85** (2012) 046412 (6pp) http://dx.doi.org/10.1103/PhysRevE.85.046412

"Modification of local plasma parameters by impurity injection" M. Koltunov and M. Z. Tokar *Plasma Phys. Control. Fusion* **53** (2011) 065015 (18pp) http://dx.doi.org/10.1088/0741-3335/53/6/065015

"Numerical realization of a shell model for impurity spreading in plasmas" M. Z. Tokar and M. Koltunov *AIP Conf. Proc.* **1389** 1660-1663 http://dx.doi.org/10.1063/1.3636928

"Modelling of plasma behaviour in the vicinity of intensive impurity sources" M. Z. Tokar, R. Ding and M. Koltunov *Plasma Phys. Control. Fusion* **52** (2010) 75003 (10pp)
http://dx.doi.org/10.1088/0741-3335/52/7/075003

## Conferences

Poster "Shell model for spreading of impurities injected locally into fusion plasmas" M. Koltunov and M. Z. Tokar *Proc. 14th European Fusion Theory Conference* (Frascati, Italy, September 26-29, 2011)
http://www.fusione.enea.it/EVENTS/eventifiles/EFTC14-2011/Posters/PRESENTAZIONI_POSTER/MKoltunov.pdf

Poster "A model for modification of local plasma parameters induced by impurity injection" M. Koltunov, M. Z. Tokar, D. Borodin, R. Ding, A. Kirschner and M. Lehnen *Proc. 37th European Physical Society Conference on Plasma Physics* **34A**, 2010, P2.164 (Dublin, Ireland, June 21-25, 2010) http://ocs.ciemat.es/EPS2010ABS/pdf/P2.164.pdf

## GRK 1203 Workshops

Talk "Time-dependent shell model for spreading of impurities locally injected into hot plasmas" M. Koltunov and M. Z. Tokar Graduirtenkolleg 1203 Workshop (Bad Breisig, Germany, October 6-7, 2011)

Talk "Modification of local plasma parameters by impurity injection" M. Koltunov and M. Z. Tokar Deutsche Physicalische Gesellschaft Annual Spring Meeting (Kiel, Germany, March 28-31, 2011)

Talk "A model for modification of local plasma parameters induced by impurity injection" M. Koltunov and M. Z. Tokar Graduirtenkolleg 1203 Workshop (Bad Honef, September 20-21, 2010)

Poster "Modelling of massive gas injection in tokamaks" M. Koltunov, M. Z. Tokar and M. Lehnen Deutsche Physicalische Gesellschaft Annual Spring Meeting (Hannover, Germany, March 8-12, 2010)

## Other publications (referenced)

Article "Studies of influence of hydrocarbon injection on local plasma conditions and resulting carbon transport" R. Ding, A. Kirschner, M. Z. Tokar, M. Koltunov, D. Borodin, S. Brezinsek, A. Kreter, J. L. Chen, J. G. Li and G.-N. Luo *J. Nucl. Mater.* **415** (2011) S270-S273 http://dx.doi.org/10.1016/j.jnucmat.2010.09.037

Paper "Disruption mitigation by massive gas injection in JET" M. Lehnen, A. Alonso, G. Arnoux, N. Baumgarten, S. A. Bozhenkov, S. Brezinsek, M. Brix, T. Eich, S. N. Gerasimov, A. Huber, S. Jachmich, U. Kruezi, P. D. Morgan, V. V. Plyusnin, C. Reux, V. Riccardo, G. Sergienko, M. F. Stamp, A. Thornton, M. Koltunov, M. Z. Tokar, B. Bazylev, I. Landman, S. Pestchanyi and JET EFDA contributors *Proc. 20th IAEA Fusion Energy Conf.* EXS/P2-13 (Vilamoura, Portugal, November 1-6, 2010) http://www-pub.iaea.org/mtcd/meetings/PDFplus/2010/cn180/cn180_papers/exs_p2-13.pdf

Article "Dense plasma focus wide energy range pulsed X-ray radiation investigation" A. S. Savyolov, G. Kh. Salakhutdinov, M. V. Koltunov, B. D.

Lemeshko, D. I. Yurkov, P. P. Sidorov *Applied Physics* **4** (2010) (in Russian) http://www.vimi.ru/applphys/appl-10/10-4/10-4-7e.htm

Article "Application of a plasma focus-based source for fast neutron and X-ray radiography" Ye. P. Bogolubov, M. V. Koltunov, B. D. Lemeshko, V. I. Mikerov, V. N. Samosyuk, P. P. Sidorov and D. I. Yurkov *Nuclear Instruments and Methods in Physics Research A* **605** (2009) 62 http://dx.doi.org/10.1016/j.nima.2009.01.128

# Acknowledgments

On this final page of the present work I would like to thank my colleagues for their support during the last three years of research.

I would like to express my gratitude to Prof. Dr. D. Reiter from the Research Center Jülich (FZJ) for the opportunity to work in this project.

This work was partially supported by the German Research Foundation through the Research Training Group 1203, and I would like to thank particularly Univ.-Prof. Dr. O. Willy from the Heinrich Heine University of Düsseldorf.

I would like to thank also Dr. M. Groth from Culham Science Center, Dr. S. Brezinsek and Dr. S. Wiesen from FZJ for the interest to my work during "Modelling month on JET" in November-December 2012.

I am grateful to Dr. M. Lehnen from FZJ, Dr. B. Bazylev and Dr. S. Pestchanyi from Karlsruhe Institute of Technology for many fruitful discussions of the experiment, theory and simulations during my visit to Culham Science Center.

Finally, I am kindly grateful to my supervisor Prof. Dr. M. Z. Tokar from the Research Center Jülich for his scrupulosity in upbringing of the next scientific generation. I am thankful for his passion to our work and physics of hot plasma in general, his almost Cartesian ability to call into question our ideas and create new ones, for teaching me to separate the global vision and details, the science which in concerning our theoretical studies realized a lot of times in the form: "The more complicated it initially looks, the easier it finally works".

Forschungszentrum Jülich,
Germany, July 2012
Mikhail Koltunov